UNIVERSITY OF WARMIA AND MAZURY IN OLSZTYN

Technical Sciences

20(3) 2017

PUBLISHER UWM

OLSZTYN 2017

The Technical Sciences is indexed and abstracted in BazTech (http://baztech.icm.edu.pl) and in IC Journal Master List (http://journals.indexcopernicus.com)

The Journal is available in electronic form on the web sites
http://www.uwm.edu.pl/techsci (subpage Issues)
http://wydawnictwo.uwm.edu.pl (subpage Czytelnia)

The electronic edition is the primary version of the Journal

PL ISSN 1505-4675
e-ISNN 2083-4527

Address
ul. Jana Heweliusza 14
10-718 Olsztyn-Kortowo, Poland
tel.: +48 89 523 36 61
fax: +48 89 523 34 38
e-mail: wydawca@uwm.edu.pl

Ark. wyd. 8,7, ark. druk. 7,0, nakład 85 egz.
Druk – Zakład Poligraficzny UWM w Olsztynie
zam. nr 563

Contents

Technical Sciences, 2017, 20(3), 209–225

Quarterly peer-reviewed scientific journal
ISSN 1505-4675
e-ISSN 2083-4527
TECHNICAL SCIENCES
Homepage: www.uwm.edu.pl/techsci/

ANALYSIS OF ECONOMIC AND AGRICULTURAL INDICATORS UNDER SUSTAINABLE AGRICULTURE CONDITIONS WITH THE USE OF BAYESIAN MODELLING

Katarzyna Grotkiewicz

Faculty of Production and Power Engineering
University of Agriculture in Kraków, Poland

Received 16 October 2016, accepted 24 April 2017, available online 4 May 2017

Key words: sustainable agriculture, mineral fertilization, stocking density, agri-economic indicators, Bayesian networks, model.

Abstract

Searching for relations between the level of production intensity, land efficiency and work performance, comparative analyses were carried out on international scale taking into consideration 45 countries from around the world with the use of the Statistical Yearbook (2013) and International Statistics Yearbook (2015). The research covered basic qualification criteria of sustainable agriculture, i.e. the level of mineral fertilization and stocking density as well as productivity rates, i.e. land efficiency and work performance and factors which shape them. The main aim of the research is the use of Bayesian modelling in order to predict the development of various economical and agricultural indicators and also show relationships between events basing on the theory of probability.

Introduction

Poland accession to the European Union obliged Member States to introduce assumptions of sustainable agriculture. Sustainable agriculture is one of main ideas of precise agriculture, consisting in achieving high crops with high quality at the simultaneous reduction of costs in an environmentally friendly manner. Using precise agriculture tools we decide, inter alia, on precise agri-technical treatments, suitable fertilization, crops protection or relevant

Correspondence: Katarzyna Grotkiewicz, Instytut Inżynierii Rolniczej i Informatyki, Wydział Inżynierii Produkcji i Energetyki, ul. Balicka 116B, 30-149 Kraków, e-mail: katarzyna.grotkiewicz@ur.krakow.pl

amount of sowed seeds and efficient control of machines operation (KRASOWICZ 2005). In Poland, precise agriculture consists mainly in rational fertilization. Fertilization industry development is fundamental for ensuring food safety of a country and constitutes an indispensable condition for sustainable development of the world. Contrary, both in Europe and around the world it is more often applied for combating weeds, diseases and pests (BUJAK 2009). The main task of mineral fertilization is maintenance and increase of soil fertility. Based on the national and foreign research (BAUM 2006, KOPIŃSKI, TUJAKA 2009, TILMAN et al. 2002) it may be simultaneously stated that the increase of soil fertility and crops of cultivated plants ensures sustainable organic and mineral fertilization i.e. manure, mineral fertilizers NPK and calcium fertilizers Ca. One of the reasons of reduction of organic matter content in soil is intensification of agricultural production and inventory farming. According to the Main Statistical Office (2013) in 2005–2011 livestock of pigs in Poland reduced by over 4.5 million pieces contrary to cattle when in the same period an increase of livestock by approx. 300 thousand pieces was reported.

Lower content of organic matter weakens soil ability to accumulate water, reduces also its absorption ability which results in consequence in deterioration of soil structure and lower assimilability of nutrients. Therefore, mineral fertilizers, which boost growth and development of crops, are the only source of nutrients in agriculture. However, one should remember that their irrational use, through too high fertilization doses threatens soil and water. According to the Main Statistical Office (2013) in Poland in 2005–2011 an increase of mineral fertilizers use by 267 NPK per a hectare of agricultural land was reported.

The above mentioned issues concerning sustainable agriculture do not provide a full diagnosis with regard to precise agriculture, which requires from farm owners the use of modern technological solutions at relevant management of agricultural production. Therefore, there is a need to analyse and interpret agri-economic indicators and in particular land efficiency and work performance, which are the most universal, and as a result detailed productivity rates (GROTKIEWICZ, MICHAŁEK 2009). Both these rates considerably depend on the agriculture modernity degree thus they are derivatives of the level and efficiency of scientific progress. To take the best decisions within sustainable agriculture in order to achieve high indicators of land efficiency and work performance in an environmentally friendly manner, we may model farms based on international comparison and relevant statistical methods with the use of both quality and quantity data in order to present trends in changes of productivity rates on international scale in comparison to the criteria which meet the level of sustainable agriculture which decides on the productivity level and social efficiency in agriculture with regard to cognitive and application reasons. One of the most popular and used techniques for modelling are Bayesian networks (Bayesian Networks). Bayesian networks which are also called probabilistic graphical models, chains of cause and effect, they serve as a tool for knowledge representation under uncertainty and decision making process (APOLLO, MISZEWSKA-URBAŃSKA 2014). Systems which are based on Bayesian networks have found many practical applications not only in medicine, genetics or economics but also in agriculture and forestry (KUSZ 2015, MAKSYM 2011, OIJEN et al. 2005, SVENSSONA et al. 2008, SAGRADOA et al. 2016, WANG et al. 2009).

According to literature (ACHEL 2005, SUCHETA, PRAKASH 2004, BARTNIK, KUSZ 2005), Bayesian network is a non-oriented acyclic graph which reflects relations between variables and more precisely correlations between distributions of discreet variables basing on the probability calculus. Nodes of network are variables (properties with discreet values) and the connections of nodes (arches or vectors) reflect relations between properties and their direction. Thickness of connections between nodes on the graphs which present Bayesian networks symbolizes strength between variables (OLBRYŚ 2007). Each network includes a quality part, which constitutes a set of variables (graph nodes) along with relations between them and quantity part which represents distribution of probability for these variables (LUIS, JAVIER 2007, KUSZ et al. 2006). At the same time we should bear in mind that statistical methods used for research, mainly should be supported by knowledge in order to completely use information included in the analysed data and to carry out a detailed analysis.

Objective and scope of the study

The main aim of the research is to analyse the current problems of fertilization on the background of the concept of sustainable agriculture, using modelling based on Bayesian networks.

The effect of the research will consist in obtaining information on probability distribution where each node of a network is related to conditional distribution of probability that a given component (feature, variable) is in a given state (group or the value class), preconditioned with the state of components (factors) represented by components related to them (BARTNIK et al. 2006).

Based on network topologies and the conditional probability distribution, in the work will be presented the modelling method of the farm which operates in sustainable agriculture, with a special emphasis on information that concerns the indicators of economic and agricultural performance according to the used doses of mineral and organic fertilization.

Data from the Main Statistical Office (2013) and International Statistics Yearbook (2015) which covers 45 world countries were used for the research. The analysis concerns 2010–2012.

Methodology

When searching for relations between the production intensity level, land efficiency and work performance, comparative analyses on international scale were carried out. The analysis covered the basic qualification criteria of sustainable agriculture, i.e. the level of mineral fertilization: nitrogen, phosphorus, potassium (NPK) and stocking density as well as productivity rates, i.e. land efficiency (WZ) and work performance (WP) and factors which shape them (gross national product in agriculture (PKBR), professionally active people in agriculture (LAR)).

For calculating indicators of performance of land and labour were used the following formulas:

$$W_P = \frac{\mathrm{PKB}_R}{L_{\mathrm{AR}}} \ [\mathrm{USD} \cdot \mathrm{man}^{-1}]$$

where:
W_P – work productivity [USD · man^{-1}],
PKB_R – gross national product in agriculture [USD],
L_{AR} – people professionally active in agriculture [man].

$$W_Z = \frac{\mathrm{PKB}_R}{Z_{\mathrm{UR}}} \ [\mathrm{USD} \cdot \mathrm{ha}^{-1}]$$

where:
W_Z – land productivity [USD · ha^{-1}],
PKB_R – gross national product in agriculture [USD],
Z_{UR} – area of agricultural land [ha].

A detailed methodology concerning productivity measures were presented also in the monograph ,,Scientific and technical progress in the process of modernization of Polish agriculture and rural areas" (GROTKIEWICZ et al. 2013).

Based on the collected figures of characteristics on economic and agricultural indicators, and subsequently accomplishing the objective of the project, the quantitative variables which were analyzed were then subjected to the data exploration by eliminating unusual data from the set of data, and then values have been grouped by using the method TwoStep Cluster Analysis.

Based on the undertaken statistical analysis and existing cause and effect relationship between quantitative variables the modelling process started using the Bayesian networks and also done an analysis of the conditional relationships between quantitative variables (economic and agricultural indicators), i.e. stocking density*,* NPK, WP, WZ, PKBR, LAR.

By taking into account the parametric models it was possible to obtain a posteriori probability distribution of single variable model or the cumulative distribution of conditional probabilities and thus find the most likely configuration variables, as well as to estimate the probability of the hypothesis, taking into account the specific observations.

GeNie program will be used for Bayesian analyses. This program serves for construction and testing of predictive models which base on various algorithms of Bayesian networks (JONGSAWAT i in. 2010). IBM SPSS Statistics 23 is the program which was used for analysis of basic descriptive analyses and TwoStep Clustering analysis.

Research results

Based on the review of the analysed data from 45 countries from around the world their average values were presented on maps. Data show both the stocking density and consumption of mineral fertilizers i.e. nitrogen, potassium and phosphorus.

Fig. 1. Stocking density in the worldwide countries [SD · ha^{-1} AL]

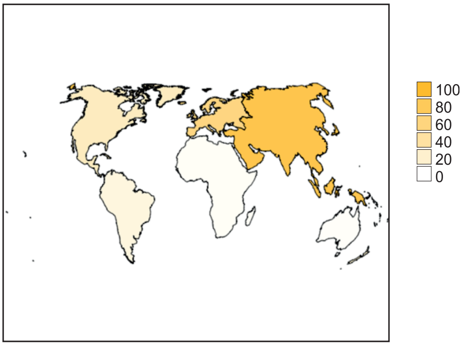

Fig. 2. Consumption of mineral nitrogen fertilizers in the world [kg · ha^{-1} AL]

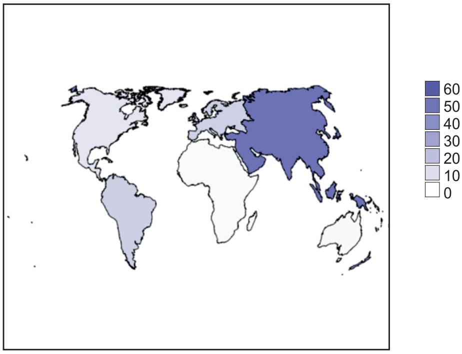

Fig. 3. Consumption of mineral phosphorus fertilizers around the world [kg · ha^{-1} AL]

Fig. 4. Consumption of mineral potassium fertilizer around the world [kg · ha^{-1} AL]

In case of European countries, which constitute the most numerous group of information in the analysed data, the situation is as presented on the European maps. Russia was excluded from analysis despite data for this country (which concern a summary region of Euroasia).

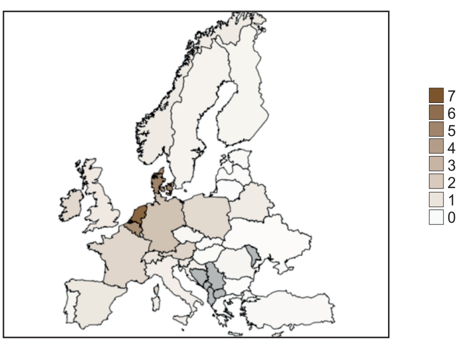

Fig. 5. Stocking density in the European countries [SD · ha^{-1} AL]

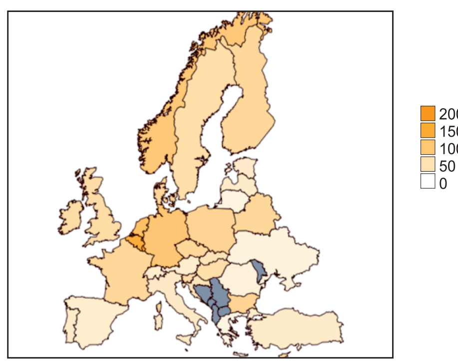

Fig. 6. Consumption of mineral nitrogen fertilizers in the European countries [kg · ha^{-1} AL]

Nitrogen is a basic crop factor. Based on the analyses from the Statistical Yearbook (2013) and International Statistics (2015) from among the analysed countries of the world the highest level of nitrogen fertilization occurs in the Republic of South Korea, Japan and China and their fertilization level per hectare of AL is respectively: 125.3 [kg · ha^{-1} AL], 96.4 [kg · ha^{-1} AL], 73.7 [kg · ha^{-1} AL]. On the other hand, the lowest demand of mineral nitrogen fertilization per one hectare of AL was reported in Australia (2.7), Republic

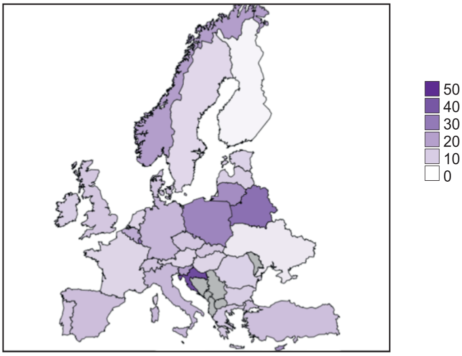

Fig. 7. Consumption of mineral phosphorus fertilizers in the European countries [kg · ha^{-1} AL]

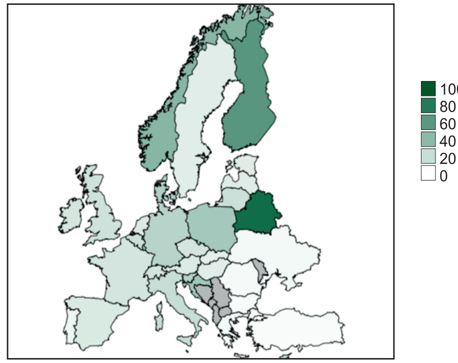

Fig. 8. Consumption of mineral potassium fertilizers in the European countries [kg · ha^{-1} AL]

of South Africa (4) and Russia (5.9). From among the European countries, countries located in the Western Europe prevail. They include: Luxembourg 165.7 [kg · ha^{-1} AL], Belgium 142.8 [kg · ha^{-1} AL] and the Netherlands 112 [kg · ha^{-1} AL]. The list of data concerning mineral nitrogen fertilization as well as remaining minerals prove high variability of the analysed countries of the World and Europe resulting from, inter alia, the area of agricultural land and the condition of soil as well as the number of people and economic reasons.

The essence of sustainable agriculture means not only the use of rational mineral fertilization but also stocking density which does not exceed 1.2 SD per one hectare of fodder surface area (MICHAŁEK et al. 2010). According to the Main Statistical Office (2013) from among 45 world countries the highest stocking density occurs in the countries with moderate climate, i.e. in the Netherlands 6.45 [SD · ha^{-1} AL], the Republic of South Korea 5.48 [SD · ha^{-1} AL] and Denmark 5.06 [SD · ha^{-1} AL], while we have a reverse situation in case of such countries as: Australia 0.07 [SD · ha^{-1} AL], Greece 0.83 [SD · ha^{-1} AL] and Bulgaria 0.12 [SD · ha^{-1} AL].

After the analysis was carried out on the data from economic and agricultural base from 45 countries of the World according to the assumed objective of this paper, the research with the use of Bayesian modelling algorithms was initiated. However, before formation of the network had begun, an exploratory review of available data including basic qualifying criteria of sustainable agriculture, i.e. the level of mineral fertilization NPK and stocking density as well as productivity rates, such as land efficiency and work performance was carried out. Necessity of carrying out the analysis of this type results from the process of data preparation for Bayesian modelling (MORZY 2007). The exploratory analysis is also justified by assumptions referring to data that may be used by Bayesian network.

Table 1

Descriptive statistics of the investigated quantity variables

Economic and agricultural indicators	*N*	Range	Minimum	Maximum	Average	Standard deviation	Skewness		Kurtosis	
	statistics	statistics	statistics	statistics	statistics	statistics	statistics	standard error	statistics	standard error
1	45	6.380	0.070	6.450	1.159	1.479	2.391	0.357	5.308	0.702
2	45	163.000	2.700	165.700	54.537	37.163	0.999	0.357	0.944	0.702
3	45	95.500	1.700	97.200	18.111	18.929	2.662	0.357	8.154	0.702
4	45	86.000	0.400	86.400	18.211	19.345	2.114	0.357	4.648	0.702
5	45	16.900	0.300	17.200	3.684	3.240	2.184	0.357	6.189	0.702
6	45	35.900	0.300	36.200	4.090	6.119	4.109	0.357	19.076	0.702
7	45	89.280	0.540	89.820	17.574	16.500	2.119	0.357	7.242	0.702
8	45	16,224.940	91.500	16,316.440	2,334.498	3,334.537	3.304	0.357	11.521	0.702

1 – Stocking density SD · ha AL^{-1}, 2 – Consumption of mineral nitrogen fertilizers, kg · ha AL^{-1}, 3 – Consumption of phosphorus mineral fertilizers, kg · ha AL^{-1}, 4 – Consumption of potassium mineral fertilizers, kg · ha AL^{-1}, 5 – gross national product in agriculture, %, 6 – professionally active people in agriculture, %, 7 – Work performance, thous PLN · mhr^{-1}, 8 – Land efficiency, thous PLN · LAR^{-1}

On the example of this analysis a uniformity of values distribution for the investigated properties was reported. Any of the variables does not have a regular distribution and the basic descriptive statistics for the investigated variables were set in Table 1.

Grouping values in the analysed variables

All analysed variables have values measured in the quantity scale. Nevertheless, Bayesian networks require properties with discreet values in the analysis. Discretization of constant values may be carried out arbitrary or analytically. Division into categories (discreet values) consists in grouping constant values and assigning to these groups values that represent them. Discreet values for variables were formed in a result of analysis which uses a two-step cluster technique (TwoStep Cluster Analysis). The advantage of this method in comparison to other grouping methods is an assumption of independence of variables which enables the analysis of variables with combined multi-normal distributions (PARK et al. 2006). For assessment of the number of clusters Schwarz's information criterion (BIC) was used. It enables adjustment of a model to data (RAFTERY 1999, GROTKIEWICZ et al. 2016). Values of Schwarz'z Bayesian criterion in case of all variables provided in the analysis indicate the best model which adjusts to data when values are divided into 3 clusters (groups). However, at such division grouping is not justified since clusters have a varied number. Majority of observations is only in one group (93.2%). Confirmation of these results was also obtained when the algorithm of hierarchical cluster analysis was used. On account of absence of natural clusters of values in data, which would serve as an element of representation of data group in the discretization process (categorization) of quantity variables, arbitrary division of values was applied for further analyses.

Due to absence of natural clusters of values in the analysed quantity variables constructed Bayesian networks will be based on discreet values which are formed from the conversion of constant values of the investigated quantity variables. Quality variables (categorial) will be formed as a result of division. New variables which have discreet values result from the application of arbitrary determined criteria of division in comparison to quantity variables. Each of quantity variables was divided into several value ranges. Arbitrary determined value ranges, which describe cluster (groups) with their borders, do not have a balanced number. It will of course affect distribution of initial probabilities in Bayesian network nodes but it will not influence the occurrence of relations and the power of relations between the network nodes.

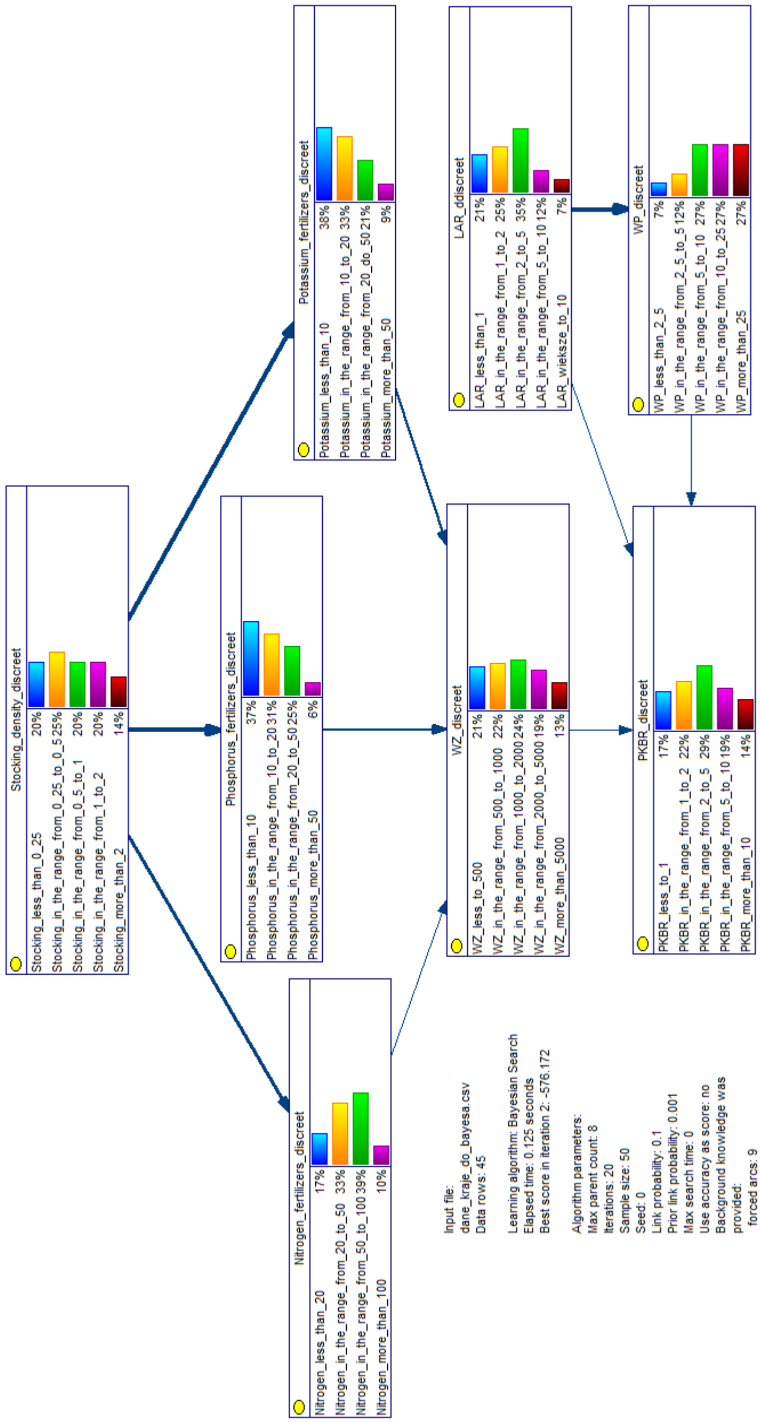

Fig. 9. Distribution of conditional probabilities for agri-economic indicators

Basing on the knowledge and experience some relations between particular indicators are already known. Before construction of network, which uses discretized variables (Stocking_density_discreet, Nitrogen_fertilizers_discreet, Potassium_fertilizers_discreet, Phosphorus_fertilizers_discreet, PKBR_discreet, LAR_discreet, WP_discreet and WZ_discreet), was initiated, it was decided to check whether there are any correlations between them. Person's correlation proved significant relations between professionally active people in agriculture and the gross national product in agriculture and work performance. Moreover, a relation between stocking density and consumption of mineral fertilizers (for all groups of fertilizers, although correlation is significant at various levels) is noticeable. Stocking density and fertilization have a significant impact on shaping the values of the indicator that describes land efficiency. The knowledge resulting from the correlation which was carried out and based on the developed methodology (GROTKIEWICZ et al. 2013, GROTKIEWICZ, KOWALCZYK 2015) was used during construction of Bayesian network as well as at the construction of bindings between nodes.

Based on the data exploration and arbitrary determined value criteria, based on the discreet values, finally for further analyses the network takes the form which was presented on the Figure 9. This network presents the system of relations between the investigated properties (discretized agri-economic indicators) and power of relations between these properties which represent basic qualification criteria of sustainable agriculture in the world agriculture. Probability of occurrence of values in a particular cluster of variables values (continuous) and its percentage value were presented in the nodes of the network in the form of a bar chart. In the description of the network, also algorithm parameters for which network was searched, are provided (Bayesian Search).

Then, analysis of conditional probabilities was carried out in secondary nodes for the obtained network. These analyses may be carried out straight on the Bayesian network diagram basing on the possibility of checking conditional probabilities on condition that a specific event will take place.

For example, if we assume that the value of the discretized variable *Stocking_density_discreet* takes the second value, it means then that stocking density belongs to the second range of values (from 0.25 to 0.50 [SD $\cdot$ ha^{-1} AL]). At such assumption, probability of such occurrence is 100% (for the node *Stocking_density_discreet*), but in the secondary nodes which depend on this node, probabilities of particular events will also change. Distribution of conditional probabilities of particular values occurrence in the network nodes is the same as on Figure 10.

Occurrence of the above described event results in the probability change only in the node networks which depend on the node *Stocking_density_discreet*

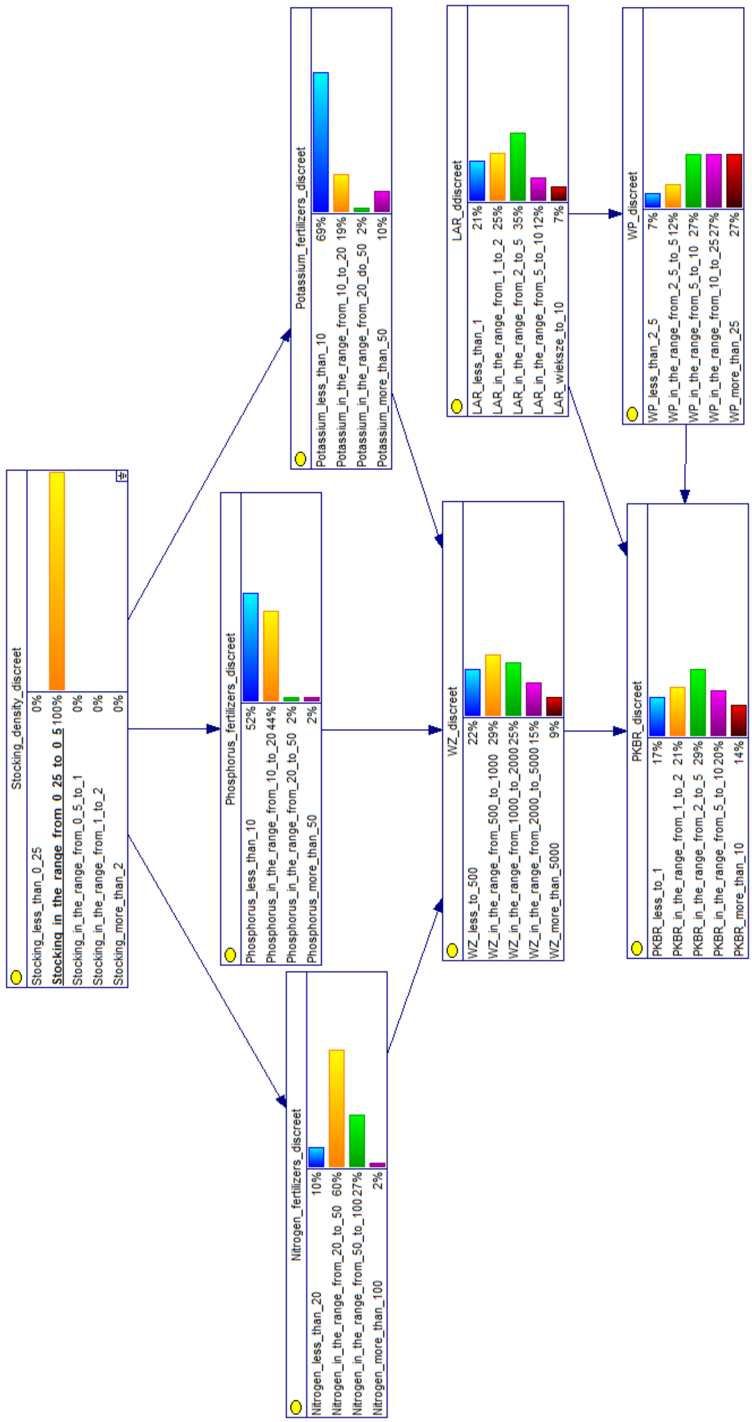

Fig. 10. Distribution of conditional probabilities for variables if the event Stocking_density_discreet takes place, belongs to the second cluster

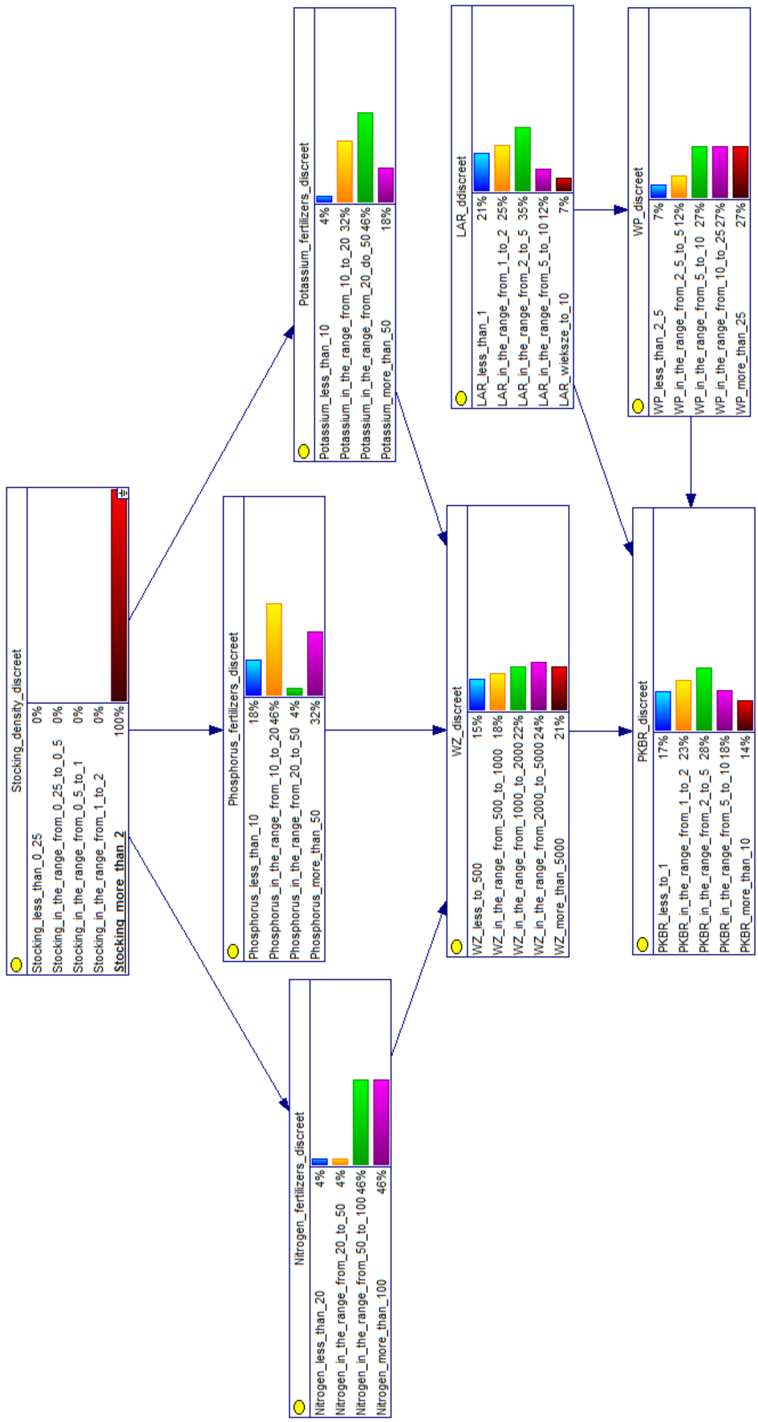

Fig. 11. Distribution of conditional probabilities for variables if the event Stocking_density_discreet takes place, belongs to the fifth cluster

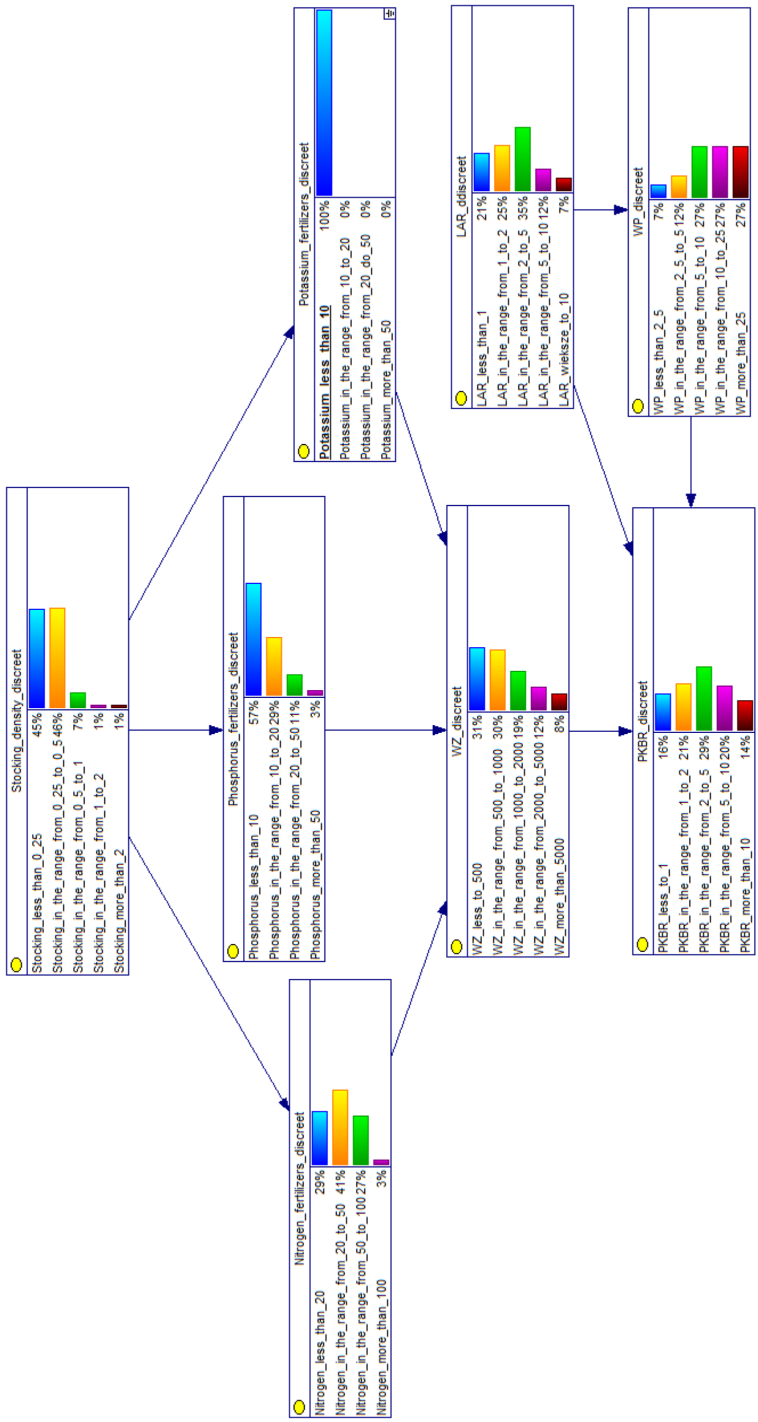

Fig. 12. Distribution of conditional probabilities of variables if the event Potassium_fertilizers_discreet takes place, belongs to the first cluster

in particular, the consumption of mineral nitrogen fertilizers. For example probability values in the nodes *LAR_discreet* and *WP_discreet* do not change. And thus, an increase of probability (from 38% to 69%) of occurrence of an event that the value of the node *Potassium_fertilizers_discreet* takes the first discreet value is reported (i.e. consumption of potassium fertilizers will be lower than 10 [$kg \cdot ha^{-1}$ AL]). In the same node *Potassium_fertilizers_discreet* probability decreases (from 21% to 2%) of the third value occurrence, namely, chances that consumption of potassium fertilizers consumption takes the value from the range from 20 [$kg \cdot ha^{-1}$ AL] to 50 [$kg \cdot ha^{-1}$ AL] fall down. At the same time it is noticed that probability changes for particular values of variables *WZ_discreet* and further *PKBR_discreet* but these changes are not as characteristic as for the node which describes a discreet level of mineral fertilization.

Another example of the change of probability in nodes takes place in case of an event that *Stocking_density_discreet* assumes the last value, which means that stocking density is higher than 2 [$SD \cdot ha^{-1}$ AL]. The following diagram presents distribution of probability in dependent nodes at such event (Fig. 11).

Moving on to this probability level for the node *Stocking_density_discreet* results in a noticeable change in the probability distribution for particular ranges of land efficiency (WZ_discreet) except for changes in the nodes which represent fertilization. This situation also influences, although to a smaller extent, the distribution of the value for the gross national product in agriculture (PKBR_discreet).

The analyses which were carried out with the use of Bayesian networks enable some conclusions. They concern mutual and significant relations of indicators which describe data referring to farms in the analysed countries of the World and Europe. A schematic representation (Fig. 12) which presents the change of probability distribution in the node which refers to the land efficiency indicator (WZ_discreet) in a situation when the level of mineral (potassium) fertilization is lower than 10 [$kg \cdot ha^{-1}$ AL], can serve as an example.

Conclusion

The analyses and economic experiments which were carried out prove that agriculture of EU and the world countries is considerably varied. The land efficiency indicator is mainly the rate which differentiates the analysed countries and at the same time decides on the competitiveness of agriculture. It depends on many factors, among which the most important are: soil quality, climatic conditions, fertilization, plant protection, timeliness of agri-technical treatments, level of inputs, production trend, selection of varieties. Based on the agri-economic analyses on account of the sustainable agriculture, networks were built based on the previous experiments which simultaneously reflect relations between the analysed variables (Fig. 9). Change of probabilities of the analysed variables in comparison to conditional probabilities proves mutual and significant relations of agri-economic indicators which describe the investigated World and European countries and in particular it proves sensitivity of some indicators, when others assume particular values.

On the basis of the completed studies, it could be stated that the appropriate tool which supports decisions under uncertainty, is the properly constructed Bayesian network, which enabling decision-making processes by taking into account information of various nature.

Using the tools of the theory of probability in accordance with the Bayesian law, creates a possibility to build a model of the farm, which is part of the strategies of the EU, whose main objective is to improve the competitiveness of agriculture, sustainable management of natural resources and climate action, and balanced territorial development of rural areas.

Additionally, capabilities of acquiring knowledge from the database of economic by using the new technology will enable the modification of such a model according to preferences and experts' ratings under uncertainty.

In summary, based on the knowledge obtained from the analyses, the analysed algorithm of Bayesian modelling could be used in further research and on other objects in direct practice for developing an optimal model of a farm located in a well-organized technical and economic and informative infrastructure which mainly meets the conditions of sustainable agriculture.

References

Aczel A.D. 2005. *Statystyka w zarządzaniu*. Wydawnictwo Naukowe PWN, Warszawa.

Apollo M., Miszewska-Urbańska E. 2014. *Decision making under uncertainty using Bayesian Networks – case study*. Logistics, 6: 1496–1504.

Bartnik G., Kusz A. 2005. *Sieci probalistyczne jako system reprezentacji wiedzy diagnostycznej*. Inżynieria Systemów Bioagrotechnicznych, Politechnika Warszawska, 5(14): 5–12.

Baum R. 2006. *Zrównoważony rozwój w organizacji i zarządzaniu gospodarstwem rolnym*. Roczn. Nauk. SERiA, Poznań, VIII(1): 14–18.

Bujak K., Frant M. 2009. *Wpływ uproszczeń w uprawie roli i poziomu nawożenia mineralnego na zachwaszczenie potencjalne gleby*. Acta Agrophysica, 13(2): 311–320.

Campos L.M. de, Castellano J.G. 2007. *Bayesian network learning algorithms using structural restrictions*. International Journal of Approximate Reasoning, 45(2): 233–254.

Grotkiewicz K., Kowalczyk Z. 2015. *Methodological notes concerning determination of the scientific and technical progress rate and its efficiency*. Agricultural Engineering, 4(156): 149–156.

Grotkiewicz K., Michałek R. 2009. *Postęp naukowo-techniczny a wydajność ziemi i pracy w rolnictwie*. Inżynieria Rolnicza, 6(115): 109–116.

Grotkiewicz K., Peszek A., Kowalczyk Z. 2016. *Weryfikacja wskaźników ekonomiczno-rolniczych z wykorzystaniem metod statystycznych na przykładzie gospodarstw indywidualnych*. Inżynieria Rolnicza, 3(159).

JONGSAWAT N., TUNGKASTHAN A., PREMCHAISWADI W. 2010. *Dynamic Data Feed to Bayesian Network Model and SMILE Web Application*. In: *Bayesian Network*. Ed. A. Rebai. Sciyo, DOI: 10.5772/56654.

KOPIŃSKI J., TUJAKA A. 2009. *Bilans azotu i fosforu w rolnictwie polskim. Woda – Środowisko – Obszary Wiejskie*. IMUZ Falenty, 9, 4(28): 103–116.

KRASOWICZ S. 2005. *Cechy zrównoważonego rolnictwa*. In: *Koncepcja badań nad rolnictwem społecznie zrównoważonym*. Raporty IERGŻ-PIB, 11: 23–39.

KUSZ A., MARCINIAK A. W. 2006. *Dynamiczne sieci probabilistyczne jako system reprezentacji wiedzy*. Inżynieria Rolnicza, 12(87): 285–294.

KUSZ A., MARCINIAK A., SKWARCZ J. 2015. *Implementation of computation process in a bayesian network on the example of unit operating costs determination*. Eksploatacja i Niezawodność, 17(2): 266–272.

MAKSYM P. 2011. *Podstawowe zasady modelowania procesu produkcji rolniczej*. Inżynieria Rolnicza, 1(126): 161–165.

MICHAŁEK R., GROTKIEWICZ K. 2010. *Miejsce i rola postępu naukowego w warunkach rolnictwa zrównoważonego*. Problemy Inżynierii Rolniczej, 1: 1–8.

MICHAŁEK R., KUBOŃ M., GROTKIEWICZ K., PESZEK A. 2013. *Postęp naukowo-techniczny w procesie modernizacji polskiego rolnictwa i obszarów wiejskich*. Polskie Towarzystwo Inżynierii Rolniczej, Kraków.

MORZY T. 2007. *Eksploracja danych*. Nauka, 3: 83–104.

OIJEN M. VAN, ROUGIER J., SMITH R. 2005. *Bayesian calibration of process-based forest models: bridging the gap between models and data*. Tree Physiology, 25(7): 915–927.

OLBRYŚ J. 2007. *Sieć bayesowska jako narzędzie pozyskiwania wiedzy z ekonomicznej bazy danych*. Zeszyty Naukowe Politechniki Białostockiej, 2.

PARK H.S., BAIK D.K. 2006. *A study for control of client value using cluster analysis*. Journal of Network and Computer Applications, 29(4): 262–276.

RAFTERY A.E. 1999. *Bayes factors and BIC – Comment on "A critique of the Bayesian information criterion for model selection"*. Sociological Methods and Research, 27: 411–427.

Rocznik Statystyczny. 2013. GUS. Warszawa.

Rocznik Statystyki Międzynarodowej. 2015. GUS, Warszawa.

SAGRADOA J. del, SÁNCHEZA J.A., RODRÍGUEZA F., BERENGUELA M. 2016. *Bayesian networks for greenhouse temperature control*. Journal of Applied Logic, 17: 25–35.

SUCHETA N., PRAKASH P. 2004. *A causal mapping approach to constructing Bayesian networks*. Journal Decision Support Systems, 38(2): 259–281.

SVENSSON M., JANSSON P.E., GUSTAFSSON D., KLEJA D.B., LANGVALL O., LINDROTH A. 2008. *Bayesian calibration of a model describing carbon, water and heat fluxes for a Swedish boreal forest stand*. Ecological Model Ling, 213: 331–344.

TILMAN D., CASSMAN K.G., MATSON P.A., NAYLOR R., POLASKY S. 2002. *Agricultural sustainability and intensive production practices*. Nature, 418: 671–677.

WANG Q.J., ROBERTSON D.E., HAINES C.L. 2009. *A Bayesian network approach to knowledge integration and representation of farm irrigation*. 1. *Model development*. Water Resources Research, 45(2), doi:10.1029/2006WR005419.

Technical Sciences, 2017, 20(3), 227–240

Quarterly peer-reviewed scientific journal
ISSN 1505-4675
e-ISSN 2083-4527
TECHNICAL SCIENCES
Homepage: www.uwm.edu.pl/techsci/

ANALYSIS OF SELECTED MATHEMATICAL MODELS OF HIGH-CYCLE S-N CHARACTERISTICS

Przemysław Strzelecki, Janusz Sempruch, Tomasz Tomaszewski

Computer Methods Department
Institute of Mechanics and Machine Design
University of Science and Technology in Bydgoszcz

Received 6 October 2016, accepted 6 April 2017, available online 13 April 2017.

Key words: high-cycle fatigue, S-N curve, fatigue tests, number of specimen, steel strength.

Abstract

The paper presents two approaches of determining S-N fatigue characteristics. The first is a commonly used and well-documented approach based on the least squares method and staircase method for limited fatigue life and fatigue limit, accordingly. The other approach employs the maximum likelihood method. The analysis of the parameters obtained through both approaches exhibited minor differences. The analysis was performed for four steel construction materials, i.e. C45+C, 45, SUS630 and AISI 1045. It should be noted that the quantity of samples required in the second approach is significantly smaller than with the first approach, which translates into lower duration and costs of tests.

Introduction

The designing of new structural elements subjected to stress that is variable in time, i.e. bicycle frames, load-bearing parts of ship hulls, bogies frames or bodies of rail vehicles requires determining their endurance or fatigue strength for the assumed life ERRI B12 RP 17 8 edition (1996), KOZAK and GÓRSKI (2011), PN-EN 14764 (2007). These calculations require obtaining

Correspondence: Przemysław Strzelecki, Zakład Metod Komputerowych, Instytut Mechaniki i Konstrukcji Maszyn, Wydział Inżynierii Mechanicznej, Uniwersytet Technologiczno-Przyrodniczy w Bydgoszczy, al. Prof. S. Kaliskiego 7, 85-796 Bydgoszcz, phone: +48 52 340-82-02, e-mail: p.strzelecki@utp.edu.pl

the S-N fatigue characteristics, which, for most construction materials, is divided into two scopes. The first scope is related to limited fatigue strength, which is usually expressed with the following equation:

$$\log(N) = m \log(S) + b \tag{1}$$

where:
N – number of cycles,
S – stress amplitude [MPa],
m – slope coefficient,
b – intercept term.

The other scope is related to unlimited fatigue life, which, at its upper side, is limited by the fatigue limit. The description of this area will be presented in the further part of this article.

Fatigue calculations often include calculating the safety factor. In the case when fixed amplitude of stress on the structural element is assumed, the safety factor is calculated according to the following KOCAŃDA and SZALA (1997) correlations:

$$\delta = \frac{Z_N}{S} \tag{2}$$

where:
δ – safety factor for constants stress amplitude,
S – stress amplitude,
Z_N – fatigue strength for the required fatigue life according the formula (1).

Normative characteristics as per PN-EN 1993-1-9, (2007) requirements or guidelines of classification associations, e.g. ERRI B12 RP 17 8 edition (1996), HOBBACHER (2009), KOCAK et al. (2006) may be used for the calculations. Examples of diagrams for different categories of welded joints are presented on Figure 1. The individual characteristics refer to various categories of welded joints, referred to as FAT classes. The values assigned in the legend define the value of fatigue strength for strength $2 \cdot 10^6$.

Application of the analytical methods requires credible parameters for equation (1), which are estimated from experimental data. 2 models are used for estimating these values. The first model, marked as I, is the conventional approach defined in normative documents, e.g. ASTM E-739-91 (2006), ISO-12107 (2003), PN-EN-3987 (2010), PN-H-04325:1976 (1976), which the documents were compared in the paper STRZELECKI et al. (2015). The other model,

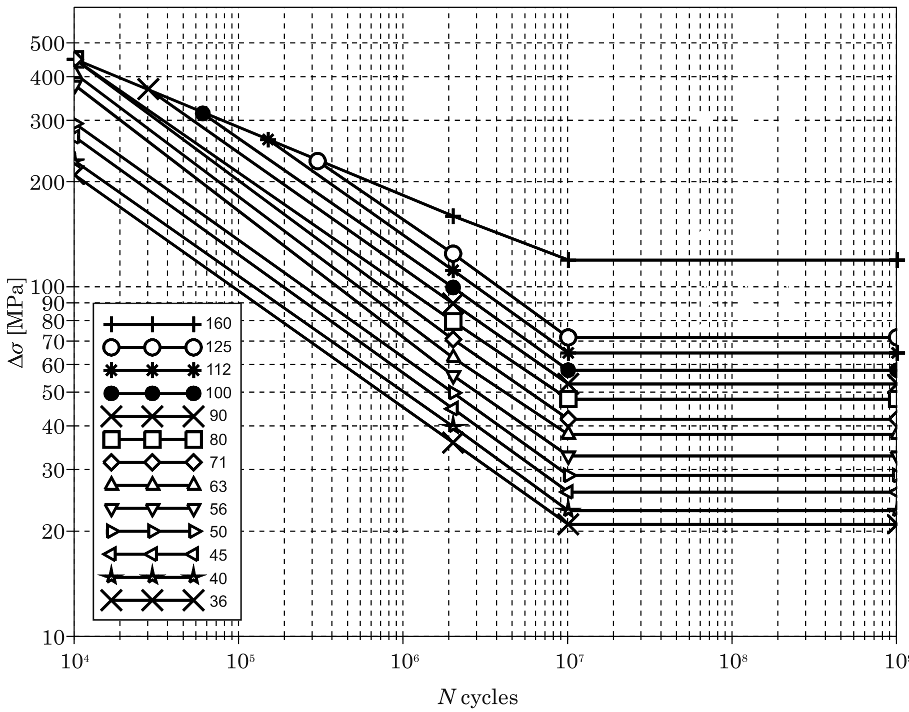

Fig. 1. Examples of graphs for different categories of fatigue of welded joints according Hobbacher
Source: based on HOBBACHER (2009).

marked as II, is an alternative approach, the description of which is contained in the paper PASCUAL and MEEKER (1999). Parameter estimate procedure can be found in the paper COVA and TOVO (2016). Comparisons of the model II, particularly focusing on the accuracy and sensitivity to changes in test parameters, have been a subject of numerous papers. Its further verification is justified, however.

The purpose of this paper is presentation of the method II used for determining the S-N characteristics in a manner more accurate than hitherto made in scientific literature. It was decided that the analysis of this method will be carried out based on own experimental results, as well as existing scientific resources, which should render the conclusions as objective as possible.

Authors didn't compare other models like STROHMEYER (1914), PALMGREN (1924), WEIBULL (1949), STÜSSI (1955), CASTILLO (1985), KOHOUT and VACHET (2001). This can be found in others papers like KUREK et al. (2014), KOHOUT and VECHET (2001), BANDARA et al. (2016) and books CASTILLO and FERNÁNDEZ-CANTELI (2009) or SZALA and LIGAJ (2011). In nonlinear models, coefficient

$S0$ is referred as fatigue limit, but it is only mathematical coefficient. This value must be lower than the lowest stress level of the sample, and it is usually differs from the 50% fatigue limit, see paper GOGLIO and ROSSETTO (2004). For this reason only model PASCUAL and MEEKER (1999) was chosen.

Conventional method of determining the S-N characteristics

It should be noted that the diagrams presented above apply to 75% confidence, with 95% reliability (HOBBACHER 2008, PN-EN 1993-1-9 2007). When using a new material or manufacturing technology, the fatigue characteristics of the given element is often not available; it is also commonly known that fatigue strength of this elements changes. Due to this, fatigue examinations, aiming at determining the S-N relationship are carried out. They are most often performed according to standardized guidelines (e.g. ASTM E-739-91 2006, ISO-12107 2003, PN-EN-3987 2010, PN-H-04325:1976 1976). The documents referred to above apply to determining a fatigue relationship in the scope of limited fatigue life. The number of tests to be performed is different, depending on the documents referred to. According to the Polish standard, the minimum number of samples tested is 15. It is recommended that the tests are performed at 5 stress levels, with 3 samples each. ISO-12107 (2003) standard, on the other hand, requires that at least 7 tests are made as part of preliminary examination, and that at least 28 sample are used for determining reliability. The ASTM E-739-91 (2006) standard was used for deciding on the number of levels; the standard specifies the replication requirements as follows:

$$\mathrm{PR} = 100\left[1 - \left(\frac{Sl}{n}\right)\right] \; [\%] \tag{3}$$

where:
Sl – number of stress level,
n – the total number of specimens.

The recommended replication percentage values are presented in Table 1.

PN-EN-3987, (2010) standard, on the other hand, does not specify the quantity of samples definitely. It merely contains a guideline saying that the tests should be started at a load at which a crack may be expected, with around 105 cycles. The tests should be carried out at least 5 stress levels.

Another approach can be found in the Guidelines of the International Institute of WELDING HOBBACHER (2008), where it is suggested that the tests are carried out at 2 stress levels, for at least 10 samples. The tests should be performed within the range of fatigue strength for $10^5 \div 10^6$ cycles.

Table 1

Guidelines recommend that the percent replication for various tests

Type of Tests	Percent Replication
Preliminary and exploratory (research and development tests)	17 to 33
Research and development testing of components and specimens	33 to 50
Design allowable data	50 to 75
Reliability data	75 to 88

Source: ASTM E-739-91 (2006).

Researchers often limit the number of test samples due to extensive time requirements and high costs generated by the procedures. For instance, in order to perform 10^5 cycles at 30 Hz stress frequency, the total duration of the test must be around 55 min. To perform 10^6 cycles, the test would last 9 hours. Sample preparation time not included. It must be noted that the strength testing machines often allow to obtain a much lower frequency, e.g. 5 Hz, or smaller, which significantly increases the test duration.

The results obtained from the tests allow to determine the S-N characteristics. Linear regression according to correlation (1) is commonly applied. The least squares method, as specified in w ASTM E-739-91 (2006), HOBBACHER (2008) among others, is used to determine parameters of equation (1).

An example of scheme for evaluation of the fatigue diagram is presented on Figure 2. Note that a fatigue limit, marked on the figure as Z_G often applies to construction materials, e.g. steel. The step method, described in the KOCAŃDA and SZALA (1997), LEE et al. (2005) or in the ISO-12107 (2003) standard is usually used to determine this value. The test must be performed on at least 15 samples to determine the fatigue limit using the staircase method. Assuming the value of basic quantity of cycles N_G as $5 \cdot 10^6$, the total duration, at an assumed stress frequency of 30 Hz, is ~470 hours. This is equivalent to 20 days.

The test duration calculations presented above show that the time required to determine the full stress characteristics is at least a month. This generates high time requirements and costs, which in turn causes significant limitations in performing such examinations. Due to this, the stress examinations are reduced to minimum by the broadest possible employment of characteristics already at hand. This can lead to obtaining inaccurate calculation results, however. The procedure described above will be referred to as model I.

Alternative method of determining the S-N characteristics

As exhibited in previous works of other authors, for instance STRZELECKI et al. (2016), STRZELECKI and SEMPRUCH (2016), an alternative method may be used. The advantage of that method is the ability to evaluate a full fatigue

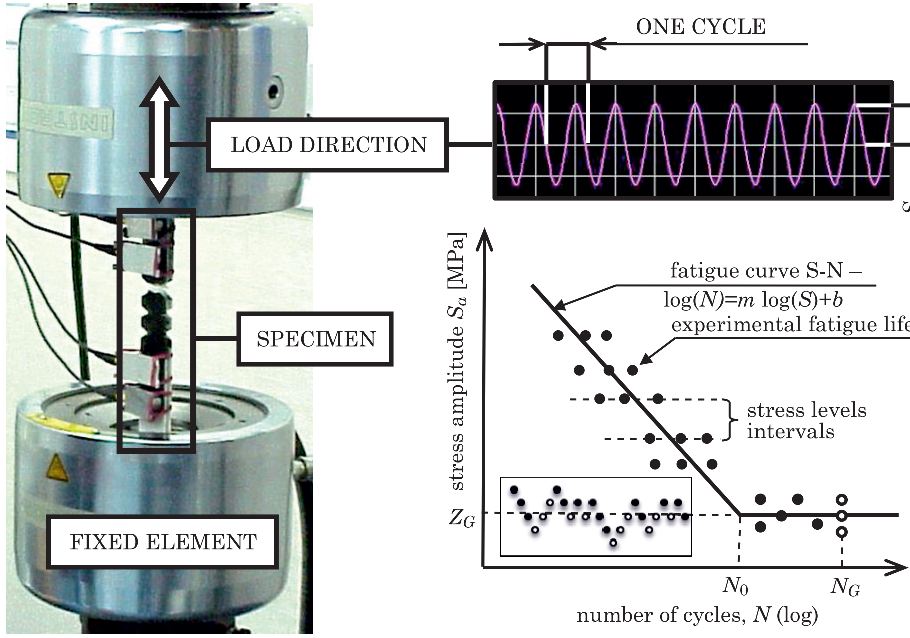

Fig. 2. Scheme of estimate fatigue curve in high cycle range and fatigue limit useing standard test machine

relationship for a smaller experimental data set. This model assumes that the fatigue strength logarithm and the fatigue limit have a normal distribution, which the distributions can be expressed as follows:

$$f(N) = \frac{1}{\sqrt{2\pi\sigma_n^2}} \exp\left(\frac{(\log(N) - (m\log(S) + b))^2}{\sigma_n^2}\right) \tag{4}$$

where:
σ_n – standard deviation,

$$f(S) = \frac{1}{\sqrt{2\pi\sigma_s^2}} \exp\left(\frac{(S - Z_G)^2}{\sigma_s^2}\right) \tag{5}$$

where:
σ_s – standard deviation.

This is considering that cracks may occur in case of applying stress higher than the Z_G threshold, and in case of obtaining strength higher or equal to the strength described in equation (5). Also, considering that these values are

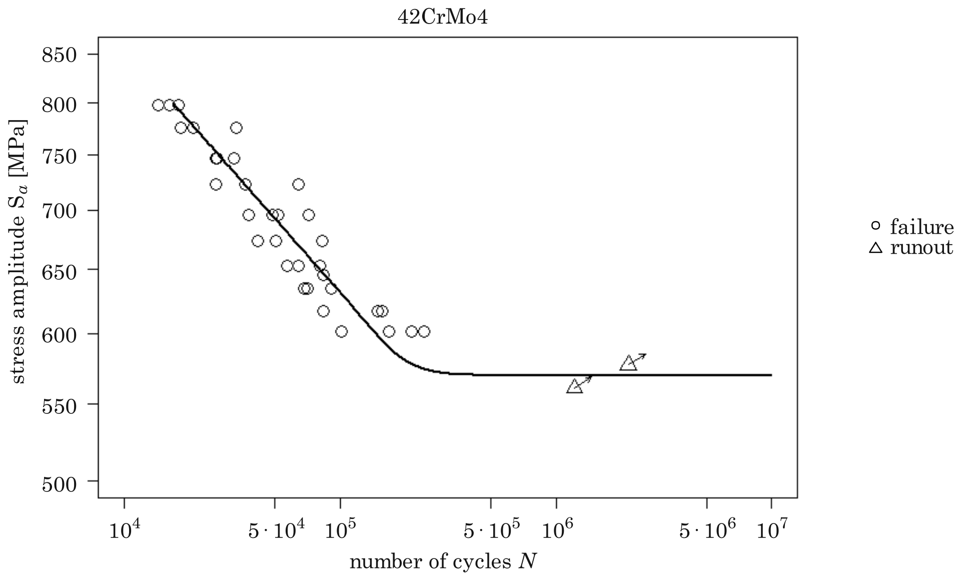

Fig. 3. Example of S-N curve for 42CrMo4 steel (own work) estimated by alternative method

random, it should be assumed that the likelihood of fracture will be equal to the likelihood of fulfilling function (5) and function (6). With this assumption, the probability of fracture for the limited and unlimited fatigue life scope may be expressed as follows (LORÉN, LUNDSTRÖM 2005):

$$P(N < N_i) = \Phi\left(\frac{\log N_i - (a \cdot \log S_i + b)}{\sigma_v}\right) \cdot \Phi\left(\frac{S_i - Z_s}{\sigma_v}\right) = q \tag{6}$$

where:
Φ – the normal distribution function,
q – the probability of specimen failure.

The maximum likelihood method was employed for determining the values of parameters of equation (7). The advantage of this statistical method is the possibility of taking into account the samples that did not fracture during the test. Reliability function for this method is expressed as follows (PASCUAL, MEEKER 1999):

$$L(\theta) = \Phi\left(\frac{\log N_i - (a \cdot \log S_i + b)}{\sigma_v}\right)^{\delta_i} \cdot \Phi\left(\frac{S_i - Z_{xe}}{\sigma_{xe}}\right)^{\delta_i} \cdot \left(1 - \left(\Phi\left(\frac{\log N_i - (a \cdot \log S_i + b)}{\sigma_v}\right) \cdot \right.\right.$$
$$\left.\left. \cdot\ \Phi\left(\frac{S_i - Z_{xe}}{\sigma_{xe}}\right)\right)\right)^{1-\delta_i} \tag{7}$$

where:
φ – the normal distribution density function.

$$\delta_j = \begin{cases} 1 & \text{if } N_i \quad \text{if specimen failure} \\ 0 & \text{if } N_i \quad \text{if specimen runout} \end{cases} \tag{8}$$

The example of a diagram obtained using the method presented above is shown in Figure 3. The presented diagram applies to a likelihood of 50%.

Experimental method and results

Data derived from fatigue tests examinations for C45+C steel were used to compare the two models. The fatigue test was performed on a test stand described in the paper STRZELECKI and SEMPRUCH (2012). Test has been carrying out using the rotary-bending fatigue machine. The test stand had been verified earlier. The machine verification involved determining the maximum error of the bending moment applied. The calculations of that value were made compliant with the norm ISO-1143 (2010) and it was 1.15%. The admissible value here was 1.3%. The admissible value here was 1.3%. Specimen was made from bar with diameter 10 mm. In measurement places there was ø5 mm and radius 25 mm. It should be noted that the samples were made of a drawn rod in as-delivered condition. Static properties of the tested material are presented in Table 2.

Results of the experimental tests of material C45+C, along with characteristics determined according to model I and II are presented on Figure 4*a*. The tests were performed on 31 samples for limited fatigue life, and 19 for fatigue limit (7 cracked, and 12 reached the limit number of cycles N_G). It must be noted that the characteristics presented are estimated for a 50% likelihood of failure. All the calculations were made in R Core Team (2015) software. Additionally, Figure 4*b* presents the results obtained using the staircase method.

Table 2

Properties of materials C45+C from Strzelecki and Sempruch

Property of material	Value
Ultimate strength S_u [MPa]	826
Yield stress S_y [MPa]	647
Hardness HB	232

Source: STRZELECKI, SEMPRUCH (2012).

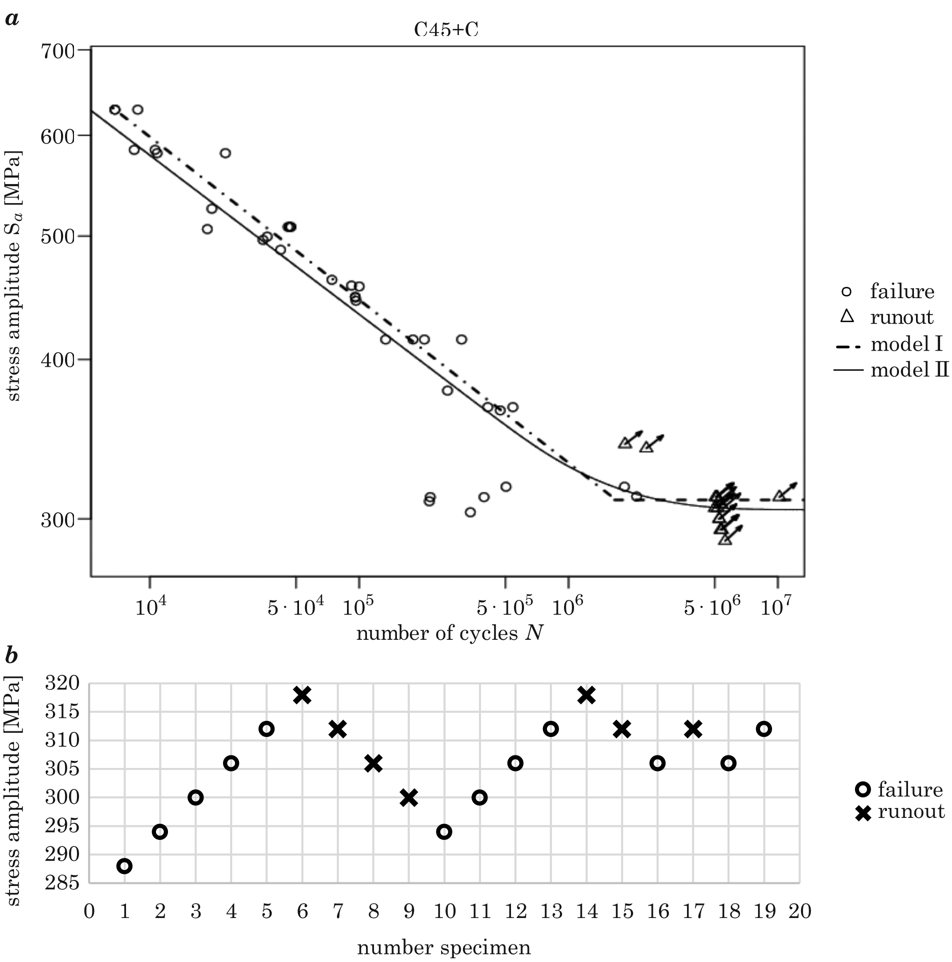

Fig. 4. S-N curve and fatigue data for steel C45+C: *a* – S-N curves, *b* – staircase method

Comparison of methods I and II

Comparison of the methods discussed was also carried out for steel 45, the test results for which are presented in the LING and PAN (1997). The experiment was performed on samples with a notch of stress concentration factor equal 2. The samples were loaded to axial load with asymmetry factor equal -1. The characteristics obtained are presented on Figure 5*a*.

Also compared were the results obtained for steel SUS630 (EN equivalent: X5CrNiCuNb16-4). The description of tests performed on this material can be found in the paper MOHD et al. (2015). The tests were performed on smooth samples, at stress frequency of 100 Hz. Load asymmetry factor was -1. The experiment was performed with axial load. The characteristics obtained are presented on Figure 5*b*.

The last material for comparison was AISI 1045 steel. The test results were derived from paper AVILES et al. (2013). The tests were performed on smooth samples, stressed from rotational bending at 33.3 Hz frequency. The characteristics obtained are presented on Figure 5*c*.

Results of estimated parameters for all the materials are shown in Table 3. No fatigue limit was determined for material 45, since the required number of experimental data was not available. Full characteristics was determined in this case.

Table 3

Estimated parameters for method I i II

Material	Method	a	b	σ_v	Z_s	σ_s
C45+C	I	-7.8	25.7	0.28	310.3	11.4
	II	-8.0	26.0	0.29	304.9	20.0
45	I	-8.5	26.5	0.12	–	–
	II	-8.6	26.9	0.12	301.8	30.0
SUS630	I	-9.2	31.9	0.17	651.5	6.7
	II	-9.9	34.1	0.27	649.6	7.0
AISI 1045	I	-8.1	26.5	0.13	352.0	7.7
	II	-8.6	28.0	0.20	351.0	7.2

Calculations for evaluating the value of fatigue strengths according to correlation (1) were performed in order to compare the estimated parameters according to method I and II. Then, the difference between the values obtained was calculated. It must be mentioned that the calculations were performed for different stress amplitude levels, which the amplitude corresponded to the scope of the high-cycle tests. The results obtained are presented in Table 4.

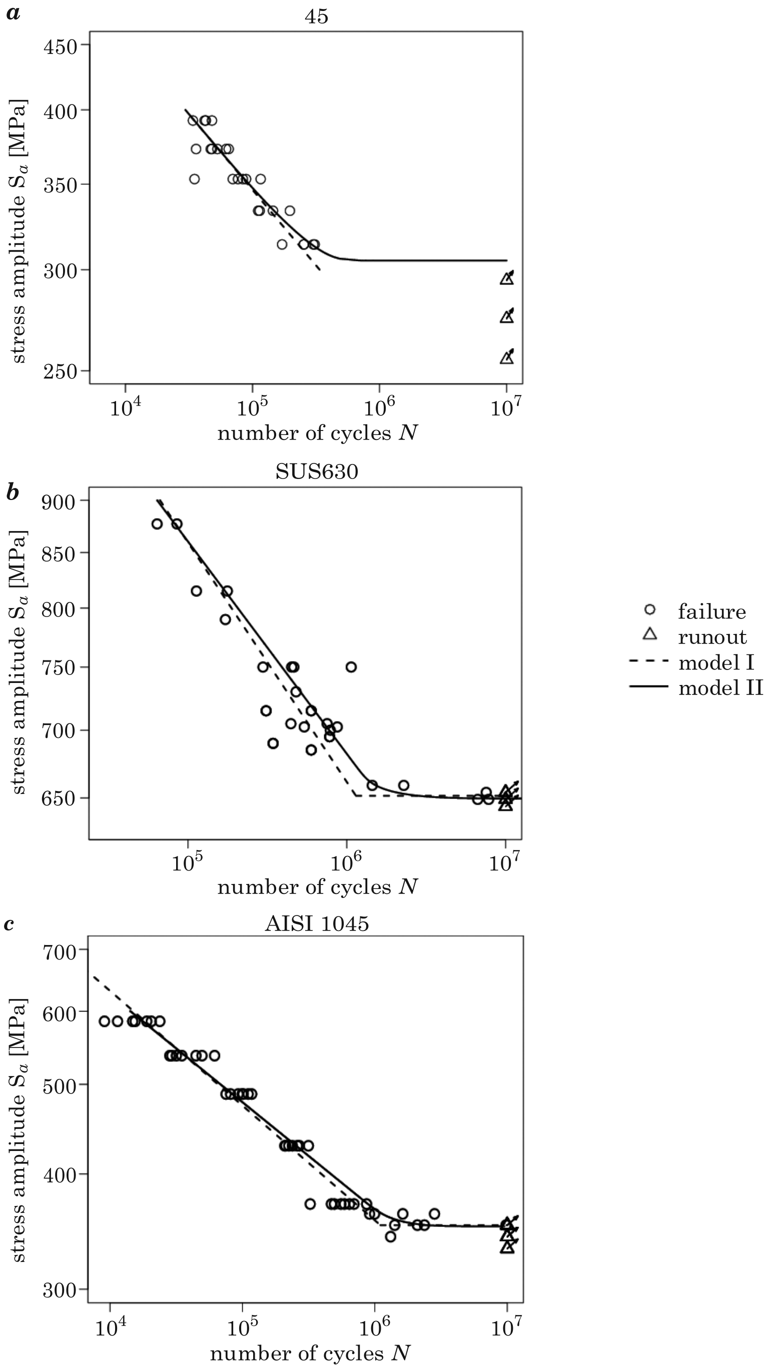

Fig. 5. S-N curve for: a – steel 45 (from paper LING and PAN 1997, b – steel SUS630 (from paper MOHD et al. 2015), c – steel AISI (from paper AVILES 2013)

Table 4

The values obtained by the sustainability model I i II

Material	log(S)	log(N_1) – method I	log(N_2) – method II	log(N_1) – log(N_2)	σ_v – method I
C45+C	2.80	3.84	3.81	0.02	0.28
	2.65	4.97	4.88	0.09	
	2.54	5.82	5.68	0.14	
45	2.60	4.47	4.46	0.01	0.12
	2.56	4.86	4.86	0.0	
	2.51	5.29	5.30	0.01	
SUS630	2.91	5.18	5.21	0.03	0.17
	2.88	5.49	5.56	0.07	
	2.84	5.84	5.95	0.11	
AISI 1045	2.77	4.25	4.27	0.02	0.13
	2.69	4.92	4.90	0.02	
	2.57	5.95	5.86	0.09	

Summary and conclusions

The characteristics obtained for material C45+C according to model I and II are different. They are shown on the graphical presentation in Figure 4*a*. Considering that the model II characteristics is shifted to the left, which results in underestimation of strength, the situation may be deemed safe (conservative). Moreover, standard deviations of the number of cycles for the limited and unlimited strength scope are higher in case of model II. This is related to a proportionally higher dispersion of the strength of samples around the fatigue limit.

For material 45, the differences between the estimated parameters according to the described methods in terms of limited fatigue life are significantly smaller than for the previous material. Standard deviations were equal. Determination of the fatigue limit for steel 45 was possible only by application of model II. This fact suggests superiority of the alternative method.

When analysing the characteristics of SUS630 steel, a clear difference in limited fatigue life was noted. According to the authors, this is related to the higher number of samples for stress level nearing the fatigue level, compared to high stress levels. This should be taken into consideration for any subsequent fatigue tests. When evaluating the fatigue limit, the differences should be assumed as marginal (difference in value smaller than standard deviation).

For material AISI 1045, the differences between the estimation of fatigue strength for limited fatigue life around the fatigue limit were the highest and noticeable (see Fig. 5*c*). The differences in the estimated fatigue limit were below 50% of standard deviation. They may be deemed as insignificant, therefore.

To conclude, the following conclusions has been formulated:

a) The method II described herein reduces the required number of samples for evaluating SN characteristics.

b) The time savings from the performance of the test is significant, considering that the method does not require a large amount of samples for unlimited fatigue life tests, where the test duration is the highest.

c) In contrast to the conventional method marked as I, it should be noted that the difference in values of estimated parameters is small.

d) By analysing the results presented in Table 3 and Table 4 it may be concluded that the differences in the fatigue limit and the estimated fatigue life are below standard deviations.

e) In the case of estimating the fatigue life, the largest differences may be noted around the stress nearing the fatigue limit.

References

AVILES R., ALBIZURI J., RODRIGUE A., LOPEZ DE LACALLE L.N. 2013. *Influence of low-plasticity ball burnishing on the high-cycle fatigue strength of medium carbon AISI 1045 steel*. International Journal of Fatigue, 55: 230–244. http://doi.org/10.1016/j.ijfatigue.2013.06.024 (access: 5.09.2016).

BANDARA C.S., SIRIWARDANE S.C., DISSANAYAKE U.I., DISSANAYAKE R. 2016. *Full range S-N curves for fatigue life evaluation of steels using hardness measurements*. International Journal of Fatigue, 82: 325–331. http://doi.org/10.1016/j.ijfatigue.2015.03.021 (access: 29.09.2016).

CASTILLO E., FERNÁNDEZ-CANTELI A. 2009. *A Unified Statistical Methodology for Modeling Fatigue Damage*. Springer, Dordrecht. http://doi.org/10.1007/978-1-4020-9182-7 (access: 23.01.2016).

COVA M., TOVO R. 2016. *Fitting fatigue data with a bi-conditional model*. Fatigue & Fracture of Engineering Materials & Structures, p. 1–17. http://doi.org/10.1111/ffe.12541 (access: 10.09.2016).

GOGLIO L., ROSSETTO M. 2004. *Comparison of fatigue data using the maximum likelihood method*. Engineering Fracture Mechanics, 71(4–6): 725-736. http://doi.org/10.1016/S0013-7944(03)00009-2 (access: 30.01.2015).

HOBBACHER A.F. 2008. *Recommendations for fatigue design of welded joints and components*. IIW document IIW-1823-07. International Institute of Welding, Paris.

HOBBACHER A.F. 2009. *The new IIW recommendations for fatigue assessment of welded joints and components – A comprehensive code recently updated*. International Journal of Fatigue, 31(1): 50–58. http://doi.org/10.1016/j.ijfatigue.2008.04.002 (access: 20.08.2015).

ISO-1143. 2010. *Metallic materials – Rotating bar bending fatigue testing*. Geneva.

ISO-12107. *2003. Metallic materials – fatigue testing – statistical planning and analysis of data.* Geneva.

KOCAK M., WEBSTER S., JANOSCH J.J., AINSWORTH R.A., KOERS R. 2006. *FITNET Fitness-for-Service PROCEDURE – FINAL DRAFT MK7*. Vol. I. FITNET FFS Procedure, European Fitness-for-Service Thematic Network – FITNET.

KOCAŃDA S., SZALA J. 1997. *Basis of calculation of fatigue*. Wydawnictwo Naukowe PWN, Warszawa.

KOHOUT J., VECHET S. 2001. *A new function for fatigue curves characterization and its multiple merits*. International Journal of Fatigue, 23(2): 175–183. http://doi.org/10.1016/S0142-1123(00)00082-7 (access: 04.10.2016).

KOZAK J., GÓRSKI Z. 2011. *Fatigue strength determination of ship structural joints*. Polish Maritime Research, 18(2): 28-36. http://doi.org/10.2478/v10012-011-0009-8 (access: 20.08.2015).

KUREK M., LAGODA T., KATZY D. 2014. *Comparison of Fatigue Characteristics of some Selected Materials*. Materials Testing, 56(2): 92–95. http://doi.org/10.3139/120.110529 (access: 30.06.2016).

LEE Y.L., PAW J., HATHAWAY R.B., BARKEY M.E. 2005. *Fatigue Testing and Analysis – Theory and Practice*. Elsevier Butterworth-Heinemann, Burlington, Oxford.

LING J., PAN J. 1997. *An engineering method for reliability analyses of mechanical structures for long fatigue lives*. Reliability Engineering & System Safety, 56:: 135–142. http://doi.org/10.1016/S0951-8320(97)00012-4 (access: 22.01.2015)

LORÉN S., LUNDSTRÖM M. 2005. *Modelling curved S-N curves*. Fatigue and Fracture of Engineering Materials and Structures, 28: 437–443. http://doi.org/10.1111/j.1460-2695.2005.00876.x (access: 27.01.2015).

MOHD S., BHUIYAN M.S., NIE D., OTSUKA Y., MUTOH Y. 2015. *Fatigue strength scatter characteristics of JIS SUS630 stainless steel with duplex S-N curve*. International Journal of Fatigue, 82: 371–378. http://doi.org/10.1016/j.ijfatigue.2015.08.006 (access: 28.06.2016).

PASCUAL F.G., MEEKER W.Q. 1999. *Estimating Fatigue Curves with the Random Fatigue-Limit Model*. Technometrics, 41(4): 277–290. http://doi.org/10.2307/1271342 (access: 19.03.2015).

PN-EN 14764. 2007. *Rowery miejskie i wycieczkowe. Wymagania bezpieczeństwa i metody badań*.

PN-EN 1993-1-9. 2007. *Eurokod 3: Designing steel structures. Part 1-9: Fatigue*.

PN-EN-3987. 2010. *Aerospace series – Test methods for metallic materials – Constant amplitude force-controlled high cycle fatigue testing*.

PN-H-04325:1976. 1976. *Badanie metali na zmęczenie – Pojęcia podstawowe i ogólne wytyczne przygotowania próbek oraz przeprowadzenia prób*.

R: A language and environment for statistical computing. 2015. Vienna, Austria: R Foundation for Statistical Computing. http://www.r-project.org/ (access:05.05.2015).

Standard Practice for Statistical Analysis of Linear or Linearized Stress-Life (S-N) and Strain-Life (ε-N) Fatigue Data. 2006. ASTM E-739-91. DOI: 10.1520/E0739-10R15.

STRZELECKI P., SEMPRUCH J. 2012. *Experimental Verification of the Analytical Method for Estimated S-N Curve in Limited Fatigue Life*. Materials Science Forum, 726: 11–16. http://doi.org/10.4028/www.scientific.net/MSF.726.11 (access:09.04.2015).

STRZELECKI P., SEMPRUCH J. 2016. *Experimental method to plot S-N curve with a small number of specimens*. Polish Maritime Research (accepted for publication).

STRZELECKI P., SEMPRUCH J., NOWICKI K. 2015. *Comparing guidelines concerning construction of the S-N curve within limited fatigue life range*. Polish Maritime Research, 22(3): 67–74.

STRZELECKI P., SEMPRUCH J., TOMASZEWSKI T. 2016. *Alternative Method for the Determination of a Full S-N Fatigue Profile*. Solid State Phenomena, 250: 209–216. http://doi.org/10.4028/www.scientific.net/SSP.250.209 (access:30.06.2016).

SZALA G., LIGAJ B. 2011. *Dwuparametryczne charakterystyki zmęczeniowe stali konstrukcyjnych i ich eksperymentalna weryfikacja*. Uniwersytet Technologiczno-Przyrodniczy im. J.J. Śniadeckich – Instytut Technologii Eksploatacji – PIB, Bydgoszcz.

Wagons – Programme of tests to be carried out on wagons with steel underframe and body structure (suitable for being fitted with the automatic buffing and draw coupler) and on their cast steel frame bogies. 1996. 8 edition. ERRI B12 RP 17.

Technical Sciences, 2017, 20(3), 241–257

Quarterly peer-reviewed scientific journal
ISSN 1505-4675
e-ISSN 2083-4527
TECHNICAL SCIENCES
Homepage: www.uwm.edu.pl/techsci/

EVALUATION OF MODELS FOR THE DEW POINT TEMPERATURE DETERMINATION

Krzysztof Górnicki, Radosław Winiczenko, Agnieszka Kaleta, Aneta Choińska

Faculty of Production Engineering
Warsaw University of Life Sciences

Received 7 October 2016, accepted 14 April 2017, available online 4 May 2017.

Key words: dew point temperature, relative humidity, model, artificial neural networks.

Abstract

The accuracy of the available from the literature models for the dew point temperature determination was compared. The proposal of the modelling using artificial neural networks was also given. The experimental data were taken from the psychrometric tables. The accuracies of the models were measured using the mean bias error MBE, root mean square error RMSE, correlation coefficient R, and reduced chi-square χ^2. Model M3, especially with constants A=237, B=7.5, gave the best results in determining the dew point temperature (MBE: -0.0229 – 0.0038 K, RMSE: 0.1259 – 0.1286 K, R=0.9999, χ^2: 0.0159 – 0.0166 K^2). Model M1 with constants A=243.5, B=17.67 and A=243.3, B=17.269 can be also considered as appropriate (MBE=-0.0062 and -0.0078 K, RMSE=0.1277 and 0.1261 K, R=0.9999, χ^2=0.0163 and 0.0159 K^2). Proposed ANN model gave the good results in determining the dew point temperature (MBE=-0.0038 K, RMSE=0.1373 K, R=0.9999, χ^2=0.0189 K^2).

Symbols

A, B, C, D – odel coefficients,
c – number of constants,
e – partial pressure of water vapour [Pa],
e_s – partial saturation pressure of water vapour [Pa],
n – number of observations,
L – enthalpy of vaporization [J · kg^{-1}],
R_w – gas constant for water vapour [J · kg^{-1} · K^{-1}],
RH – relative humidity, decimal,
RH$_{\%}$ – relative humidity [%],
t – temperature [°C],
T – temperature [K],
$_FT$ – temperature [F],

Correspondence: Krzysztof Górnicki, Katedra Podstaw Inżynierii, Wydział Inżynierii Produkcji, Szkoła Główna Gospodarstwa Wiejskiego, ul. Nowoursynowska 164, 02-787 Warszawa, phone: +48 22 59 346 24, e-mail: krzysztof_gornicki@sggw.pl

Subscript
DP – dew point,
m – measured value,
p – predicted value.

Introduction

The relative humidity and dew point temperature are widely used indicators of the amount of moisture in air (LAWRENCE 2005).

The dew point temperature can be defined as the temperature at which the partial vapour pressure of water in moist air would be sufficient to saturate the air. It can be therefore stated that the partial vapour pressure is equal to the partial saturation vapour pressure at the dew point temperature (WOOD 1970). In other words, the dew point temperature is that at which water vapour starts to condense out of the air or the temperature at which air becomes completely saturated. The following conclusion can be drawn from this definition: if the air relative humidity is low, the dew point temperature is below the air temperature but if, however, the air relative humidity is high, the dew point temperature is close to the air temperature (BROOKER et al. 1992).

Relative humidity RH is the ratio of the mole fraction of water vapour in a given volume of moist air to the mole fraction of water vapour in the same volume of saturated moist air at the same temperature and pressure. For the ideal gas mixtures assumed in this paper the equivalent definition of relative humidity can be formulated in the following way: RH is the ratio of the partial pressure e of water vapour in moist air to the partial saturation pressure of water vapour e_s at the temperature of the air (WOOD 1970, WILHELM 1976).

Knowledge of the psychrometric properties of an air-water vapour mixture, among them dew point temperature and relative humidity, is fundamental to the design environmental control system for plants, crops, animals, and human beings. Psychrometric properties of the moist air are useful in plant materials drying and storage, and in heating, ventilating, air-conditioning, meteorology (SINGH et al. 2002, LOPES et al. 2009).

Dew point temperature is preferred by meteorologists over relative humidity as an indicator of human comfort (BOHREN, ALBRECHT 1998). Dew point temperature is useful in the designing of traditional evaporative coolers, and it is the theoretical minimum temperature achieved by modern indirect evaporative coolers (LAWRENCE 2005, ZHAO et al. 2008, RIANGVILAIKUL KUMAR 2010a, 2010b). Dew point temperature coupled with wet-bulb temperature can be applied to determine air temperature, allowing producers to respond to potential frosts that may damage crops (SNYDER, DE

MELO-ABREU 2005). The knowledge of dew point temperature is indispensable for estimating the height convection cloud base. This height has a very important meaning for glider pilots (SALWIŃSKI 2002). If a glass barriers in building are cooled below the dew point, the air in contact with these surfaces will become saturated and dew will form on the surfaces what causes problems for the building users (GERYŁO 2008).

Nowadays, the modelling of different processes is a very important task. The principle of modelling is based on having a set of mathematical equations that can adequately describe the operation (EFREMOV 2013, GOLISZ et al. 2013, KALETA et al. 2013). Many agronomical, ecological, hydrological, and climatological models require dew point temperature as an input to estimate evapotranspiration (HUBBARD et al. 2003). In literature there are equations which represent the dew point temperature as a function of the temperature and relative humidity or as a function of partial saturation pressure of water vapour. However, different values of models coefficients were given and no the comparison of these models accuracy.

An artificial neural network (ANN) is an information processing system, which learns from input/output data to determine the relationships between input/output data, and is used in pattern recognition, classification, etc. Unlike other modelling techniques such as differential equations and regression equations, an ANN can handle more than two variables to predict two or more outputs. The regression equations or statistical models are subject to assumptions and cautions inherent in the analyses. ANNs have attracted researchers in many disciplines of science and engineering, since they are capable of correlating large and complex data sets. ANNs are used for their learning or adapting ability, and they do not need much knowledge of underlying relationships between their input and output variables. The network learns from the input and data itself, repeatedly. It also can approximate any continuous or discontinuous linear or nonlinear function. Therefore such networks are very useful for modelling some not-well-understood processes as reported by MITTAL (1996).

The psychrometric chart reflects the relationships between thermodynamic properties of moist air. If the relationships can be learned by an ANN with valid thermodynamic properties of air, then the trained ANN can be used as a database of air properties for real-time calculations, simply by multiplying input and weight matrices. An ANN offers an efficient means of analysing process data to obtain relationships descriptive of various process trends (MITTAL, ZHANG 2003).

SREEKANTH et al. (1998) made a first attempt to predict psychrometric parameters using NN. Neural network models were developed for the each of the three main variables: dry bulb temperature, wet-bulb temperature and relative humidity, as a function of the other two variables. Models were also developed for the prediction of the dew point temperature using the dry bulb and wet bulb temperatures, and for the saturation vapor pressure as a function of the dry bulb temperature. The prediction accuracy of the neural network models were found to be very good, with errors less than 4%. Relative errors were as high as 0.18% ± 0.17% for predicting dew point temperature. MITTAL and ZHANG (2003) used ANN to predict dew point temperature, wet bulb temperature, enthalpy, humidity ratio, specific volume as a function of dry wet bulb temperature and relative humidity with relative error <5%. For ANN training, validation and testing SREEKANTH et al. (1998) and MITTAL and ZHANG (2003) used data taken from models of dew point temperature. SHROFF and DABHI (2013a,b) used Gene Expression Programming for modelling of dew point.

Many authors used intelligent models to predict daily dew point temperature. Dew point temperature has been estimated and analysed for trends dew point temperature prediction. The overall goal of the research was to develop ANN models for predicting hourly dew point temperatures. Specific objectives were to identify the important weather-related inputs that affect dew point temperature prediction, to determine the preferred values of the ANN parameters, and to determine the preferred duration of prior data for each lead time.

SHIRI et. al (2014) assessed the capability of two different artificial neural network (ANN) models and gene expression programming (GEP) technique for estimate daily dew point temperature in two weather stations in Korea (8 years of daily records of air temperature, wind speed, relative humidity, atmospheric pressure, incoming solar radiation and dew point temperature). Authors noted that the GEP model surpasses ANN in estimating daily dew point temperature values. AMIRMOJAHEDI et al. (2016) used method by hybridizing the extreme learning machine (ELM) with wavelet transform (WT) algorithm to predict daily dew point temperature. Daily climate data of an Iranian station placed in the south costal of the country were utilized as a case study. Average air temperature, relative humidity and atmospheric pressure, were considered as input elements. Based upon the achieved results it was conclusively proved that the hybrid ELM-WT approach favourably outperforms other examined techniques. SHANK et al. (2008) utilized ANN technique for prediction of dew point temperature from 1 to 12 h ahead based upon the previous weather data sets. They used measured data of 20 stations in Georgia State in USA for developing general models to predict dew point temperature in the whole Georgia State. HUBBARD et al. (2003) developed a regression model for estimating the daily average dew point temperature, using the daily mean, minimum, and maximum air temperature as inputs.

Their research used 14 year of data for six cities in the USA. Their regression equation based on multiple cities was more accurate than the regression equations for each of the individual cities, with a mean absolute error (MAE) of 2.2°C for the most accurate regression equation. This study's estimations were useful for determining the values for missing historical weather data, but did not allow the prediction of future values. ZOUNEMAT-KERMANI (2012) evaluated the capability of multi linear regression (MLR) and Levenberg–Marquardt (LM) feed-forward neural network for estimation of hourly dew point temperature in Ontario (Canada). It was found that LM–NN model provide further accuracy compared to the MLR model. NADIG et al. (2013) developed combined air and dew point temperatures models using ANN technique to provide an enhancement in the predictions of both temperatures. Their results demonstrated that the combined method decline the predictions error. KIM et al. (2015) utilized two soft computing techniques for estimation of daily dew point temperature in California, USA. By providing comparisons with a conventional regression model, they found that developed soft computing models are more precise in estimating daily dew point temperature. MOHAMMADI et al. (2016) applied adaptive neuro fuzzy inference system (ANFIS) to select the most influential parameters for prediction of daily dew point temperature. They analysed the influence of eight different parameters on dew point temperature prediction in two cities of Iran. Their results showed that, despite climate difference between the selected studied areas, for both cities water vapour pressure was the most relevant parameter while relative humidity was the least relevant parameter. They concluded that using more than two input parameters couldn't be proper and advisable. JALAL et al. (2014) estimated of daily dew point temperature using genetic programming and neural networks approaches.

The objective of this study was the comparison of the accuracy of the available from the literature models for the dew point temperature determination and the proposal of the modelling using artificial neural networks.

Materials and Methods

The models used to determine the dew point temperature are shown in Table 1. The accuracy of the models under consideration was checked using data (about 8000) taken from psychrometric tables (ROJECKI 1959). Statistical parameters of the used data are shown in Table 2.

Table 1

Models for the determination of dew point temperature

Model no.	Model equation	Model coefficients	References
M1	$t_{DP}(t,\mathrm{RH}) = \dfrac{A\left(\ln(\mathrm{RH}) + \dfrac{Bt}{A+t}\right)}{B - \ln(\mathrm{RH}) - \dfrac{Bt}{A+t}}$	A=241.2; B=17.5043	Own working out after: https://pl.wikipedia.org/wiki/Temperatura_punktu_rosy
		A=243.5; B=17.67	Own working out after: http://www.srh.noaa.gov/images/epz/wxcalc/rhTdFromWetBulb.pdf http://www.emc.ncep.noaa.gov/gmb/yzhu/imp/i201204/NAEFS_Science_Documentation.pdf
		A=237.7; B=17.27	Own working out after: SIMONS 2008
		A=237.3; B=17.269	Own working out after: GERYŁO (2008), WEISS (1977)
		A=243.04; B=17.625	LAWRENCE (2005)
M2	$t_{DP}(t,\mathrm{RH}) = \dfrac{A\left(\ln(\mathrm{RH}) + \dfrac{Bt}{C+t}\right)}{B - \ln(\mathrm{RH}) - \dfrac{Bt}{C+t}}$	A=237; B=17.27; C=237.3	Own working out after: holmes.iigw.pl/??mbodzion/dydaktyka/hydro/pliki/wilgotnosc.pdf
		A=237.7; B=17.67; C=243.5	Own working out after: http://www.srh.noaa.gov/images/epz/wxcalc/rhTdFromWetBulb.pdf
M3	$t_{DP}(t,\mathrm{RH}) = \dfrac{A\left(\log(\mathrm{RH}) + \dfrac{Bt}{A+t}\right)}{B - \log(\mathrm{RH}) - \dfrac{Bt}{A+t}}$	A=237; B=7.5	Own working out after: SALWIŃSKI (2002)
		A=237.3; B=7.5	Own working out after: http://web.mit.edu/weather/info/Frequently_Asked_Questions-temp-dewpoint; http://www.srh.noaa.gov/images/epz/wxcalc/wetBulbTdFromRh.pdf
		A=237.7; B=7.5	Own working out after: http://www.crh.noaa.gov/Image/epz/wxcalc/wetBulbTdFromRh.pdf
M4	$t_{DP}(t,\mathrm{RH}) = (\mathrm{RH})^{1/8}(112+0.9t) + 0.1t - 112$		http://www.ajdesigner.com/phphumidity/dewpoint_equation_dewpoint_temperature.php
M5	$t_{DP} = t - \left(\dfrac{100 - \mathrm{RH}_{\%}}{5}\right)$, for $\mathrm{RH}_{\%} > 50\%$		LAWRENCE (2005)
M6	$T_{DP} = T\left(1 - \dfrac{T\ln(\mathrm{RH})}{\dfrac{L}{R_w}}\right)^{-1}$	R_w=461.5 $\mathrm{J \cdot kg^{-1} \cdot K}$	LAWRENCE (2005)

cont. table 1

Model no.	Model equation	Model coefficients	References
M7	$t_{DP} = (0.198 + 0.0017t)\ RH_{\%} +$ $- 0.84t - 19.2$ for $40 \leq RH_{\%} \leq 100\%$; $0 < t < 30°C$		Sargent (1980), Lawrence (2005)
M8	$t_{DP} = t - A + B \cdot RH_{\%}$	$A=17.9$; $B=0.18$ for $65 \leq RH_{\%} \leq 100\%$ $A=22.5$; $B=0.25$ for $45 \leq RH_{\%} \leq 65\%$	Sargent (1980), Lawrence (2005)
M9	$t_{DP} = t - \left(\frac{100 - RH_{\%}}{5}\right)\left(\frac{T}{300}\right) -$ $- 0.00135(RH_{\%} - 84)^2 + 0.35$ for $40 \leq RH_{\%} \leq 100\%$; $0 < t < 30°C$		Lawrence (2005)
M10	$RH = \left(\frac{173 - 0.1_F T + {}_F T_{DP}}{173 + 0.9_F T}\right)^8$		Bosen (1958)
M11	$t_{DP} = A\ B\ \ln(e) + C(\ln(e))^2$ where: a) $\ln(e_s) = -\frac{7511.52}{T} + 89.63121 +$ $+ 0.23998970\ T - 1.1654551 \cdot$ $\cdot 10^{-5}T^2 \cdot 1.2810336 \cdot 10^{-8}T^3 +$ $+ 2.0998405 \cdot 10^{-11}T^4 - 12.15079\ln(T)$ b) $e_s = 0.61078\exp\left(\frac{17.269382t}{237.30 + t}\right)$	$A=6.983$; $B=14.38$; $C=1.079$ for $0 \leq t \leq 50°C$	Wilhelm (1976), Weiss (1977)
M12	$t_{DP} = A + B\ln(e) + C(\ln(e))^2 +$ $+ D(\ln(e))^3 + De^{0.1984}$ $\ln(e) = -5.8002 \cdot 10^3/T - 55163 -$ $- 4.864 \cdot {}^{-2}T + 4.1765 \cdot 10^{-5}$ $T - 1.4452 \cdot 10^{-8}\ T + 6.546{*}\ln(T)$	$A=6.09$; $B=12.608$; $C=0.4959$ for $t_{DP} \leq 0°C$ $A=6.54$; $B=14.526$; $C=0.7389$; $D=0.09486$; $E=0.4569$ for $0 < t_{DP} \leq 93°C$	Ashrae (1993), Mittal, Zhang (2003)

Table 2

Statistical parameters of the used data

Parameter	Unit	Statistical parameters					
		mean	maximum	minimum	standard deviation	coefficient of variation	skewness coefficient
t	°C	22.5	37	0	10.1	0.45	-0.44
$RH_{\%}$	%	55.4	100	14	24.4	0.44	0.13
t_{DP}	°C	11.6	37	-20	11.7	1.02	-0.15

ANN modelling was carried out with Matlab 7.0. The dew point temperature was predicted with feedforward multilayer perceptron artificial neural networks. In this study 8000 cases were chosen for our experiments. Chosen cases were randomly divided into the following sets: for training 5,600 samples (consisted of ≈70% cases), for validation 1,200 samples (≈15% cases) and for testing 1,200 samples (≈15% cases). Inputs (t_{DP} and $RH_{\%}$) were normalized to obtain values in range 0–1. The values of dry bulb temperatures and relative humidity were normalized by dividing them by 37 and 100 respectively. The values of dew point temperatures (output) were divided by 37.

The goodness of fit of the tested models and ANN to the data taken from psychrometric tables was evaluated with the mean bias error MBE:

$$\mathrm{MBE} = \frac{1}{n}\sum_{i=1}^{n}(x_{i,p} - x_{i,m}) \tag{1}$$

the root mean square error RMSE:

$$\mathrm{RMSE} = \sqrt{\frac{1}{n}\sum_{i=1}^{n}(x_{i,p} - x_{i,m})^2} \tag{2}$$

the correlation coefficient R:

$$R = \sqrt{\frac{\sum_{i=1}^{n}(x_i - x_{i,p}) \cdot \sum_{i=1}^{n}(x_i - x_{i,m})}{\sqrt{\sum_{i=1}^{n}(x_i - x_{i,p})^2 \cdot \sum_{i=1}^{n}(x_i - x_{i,m})^2}}} \tag{3}$$

and reduced chi-square χ^2:

$$\chi^2 = \frac{\sum_{i=1}^{n} (x_{i,m} - x_{i,p})^2}{n - c} \tag{4}$$

The higher the R value, and lower the MBE, RMSE, and χ^2 values confirm the better the goodness of fit (KALETA, GÓRNICKI 2010).

Results and Discussion

Models of dew point temperature

The results of statistical analysis undertaken on the considered models are given in Table 3. The statistical analysis results shown that model M3 best determining the dew point temperature. The values of statistical parameters from this model (for different model coefficients) were following: MBE=-0.0229 – 0.0038 K, RMSE=0.1259 – 0.1286 K, R=0.9999, χ^2=0.0159 – 0.0166 K^2. The values of all statistical parameters from this model with constants A=237, B=7.5 were the smallest (MBE=0.0038 K, RMSE=0.1259 K, R=0.9999, χ^2=0.0159 K^2).

Model M1 can be also considered as appropriate (MBE=-0.0225 – -0.0062 K, RMSE=0.1261 – 0.1286 K, R=0.9999, χ^2=0.0159 – 0.0165 K^2). For model M1 with constants

A=243.3, B=17.269 the root mean square error and chi-square were the smallest (0.1261 K and 0.0159 K^2 respectively) and with constants A=243.5, B=17.67 mean bias error was the smallest (MBE=-0.0062 K). The values of all statistical parameters from model M1 with constants A=237.7, B=17.27 were the worst.

Model M2 only with constants A=237, B=17.27, C=237.3 gave good results (MBE=-0.0218 K, RMSE=0.1218 K, R=0.9999, χ^2=0.0166 K^2) and was not much better than Models M4 and M10. The values of statistical parameters for Models M4 and M10 were following: MBE: -0.0239 and -0.0331 K, RMSE: 0.1466 and 0.1488 K, R=0.9999, χ^2: 0.0215 and 0.0222 K^2, respectively.

Some models to determine dew point temperature gave good results, but can be only used in a narrow range of t and $RH_{\%}$. The values of statistical parameters from model M9 were the small: MBE=0.0098 K, RMSE=0.1502 K, R=0.9999, χ^2=0.0226 K^2. This model can be used to determine dew point

Table 3

Comparison of results of statistical analyses on the modelling of dew point temperature

Model no.	Model coefficients	MBE, K	RMSE, K	R, –	χ^2, K^2
M1	A=241.2; B=17.5043	-0.0167	0.1280	0.9999	0.0164
	A=243.5; B=17.67	-0.0062	0.1277	0.9999	0.0163
	A=237.7; B=17.27	-0.0225	0.1286	0.9999	0.0165
	A=237.3; B=17.269	-0.0078	0.1261	0.9999	0.0159
	A=243.04; B=17.625	-0.0152	0.1286	0.9999	0.0165
M2	A=237; B=17.27; C=237.3	-0.0218	0.1288	0.9999	0.0166
	A=237.7; B=17.67; C=243.5	-0.2827	0.4085	0.9999	0.1669
M3	A=237; B=7.5	0.0038	0.1259	0.9999	0.0159
	A=237.3; B=7.5	-0.0076	0.1261	0.9999	0.0159
	A=237.7; B=7.5	-0.0229	0.1286	0.9999	0.0166
M4		-0.0239	0.1466	0.9999	0.0215
M5*		0.0606	0.5944	0.9988	0.3534
M6		-0.0809	0.2016	0.9999	0.0406
M7*		0.0779	0.4400	09987	0.1937
M8*	A=17.9; B=0.18	0.1825	0.4065	0.9996	0.1654
	A=22.5; B=0.25	0.8329	1.1375	0.9994	1.2954
M9*		0.0098	0.1502	0.9999	0.0226
M10		-0.0331	0.1488	0.9999	0.0222
M11a	A=6.983; B=14.38; C=1.079	0.0760	0.2664	0.9998	0.0710
M11b		0.0774	0.2677	0.9998	0.0717
M12*	A=6.09; B=12.608; C=0.4959	-0.6578	0.8255	0.9995	0.6830
	A=6.54; B=14.526; C=0.7389; D=0.09486; E=0.4569	-0.0271	0.5255	0.9999	0.2764
M13 (ANN)		-0.0038	0.1373	0.9999	0.0189

* Limited range of data

temperature only for $40 \leq RH_{\%} \leq 100\%$ and $0<t<30$. Model M5 (for $RH_{\%}>50\%$) was easy to use and fairly accurate, values of statistical parameters were following: MBE=0.0606 K, RMSE=0.5944 K, R=0.9988, χ^2=0.3534 K^2.

Models M8 (for $45 \leq RH_{\%} \leq 65\%$; with constants A=22.5, B=0.25) and M12 (for $t_{DP} \leq 0^{o}C$) can not be recommended for the determination of dew point temperature, because their MBE, RMSE, and χ^2 values were found too high (MBE: 0.8329 and -0.6578 K, RMSE: 1.1375 and 0.8255 K, χ^2: 1.2954 and 0.6830 K^2, respectively).

Artificial neural network

Determination of the best ANN topology for predicting a desire response is a very critical stage. Generally, the trial–and–error approach is used. A large number of different topologies have been constructed, trained and tested. NAZGHELICHI et al. (2011) and AGHBASHLO et al. (2011) reported that one hidden layer ANN with sigmoid transfer function is normally appropriate to provide an accurate prediction and can be the first choice for any practical feed-forward network design. A sigmoid function is a widely used non-linear activation function whose output is between 0 and 1 and is defined as:

$$f(x) = \frac{1}{1 + \exp(-x)} \tag{5}$$

In addition, more hidden layers may cause overfitting and the model cannot adapt to new inputs as reported by OMID et al. (2009).

The number of hidden nodes in a network is critical to network performance. Too many nodes can lead the system toward memorizing the patterns in the data. Too few nodes can lead to underfitting as informed by ERB (1993). Recently, many researchers successfully used response surface methodology and genetic algorithm to solve this problem (NAZGHELICHI et al. 2011, NOURBAKHSHA et al. 2014, WINICZENKO et al. 2016).

In this study, different activation functions (tansig, logsig and linear) and number of neurons varied from 2–6 were used to obtain the optimal architecture of the network. Finally, the simulation results shows that a MLP ANN with one hidden layer, 3 nodes in the hidden layer and sigmoid activation function is found to have the best performance.

The optimal architecture of the ANN was constructed as 2–3–1 NN and activation functions in hidden layer and output layer were respectively "logsig" and "purelin". Schematic of three layer neural network is shown in Figure 1.

The network was trained with Levenberg-Marquardt backpropagation algorithm (trainlm) (see Fig. 2). The algorithm stopped, when the validation error increased for six iterations, which occurred at iteration 482. LM is often the fastest available back-propagation algorithm and highly recommended as the first choice supervised algorithm, although it requires more memory than other algorithms as informed by KHALAJ et al. (2013). In our study LMBP method was used because of mean-squared error (MSE) values for LM method were lower compared with those Bayesian regulation in the training stages, the LM method was preferred in the modelling of the experimental data.

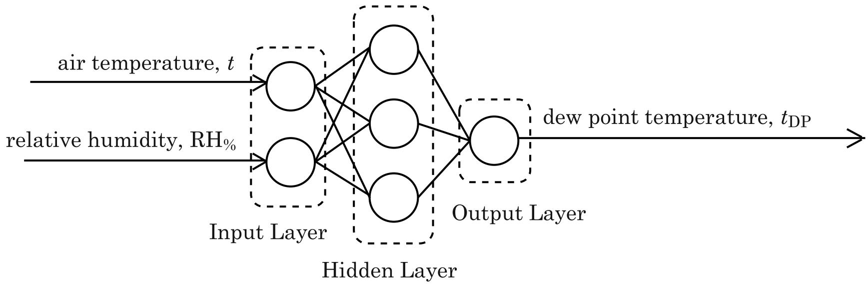

Fig. 1. Neural network architecture

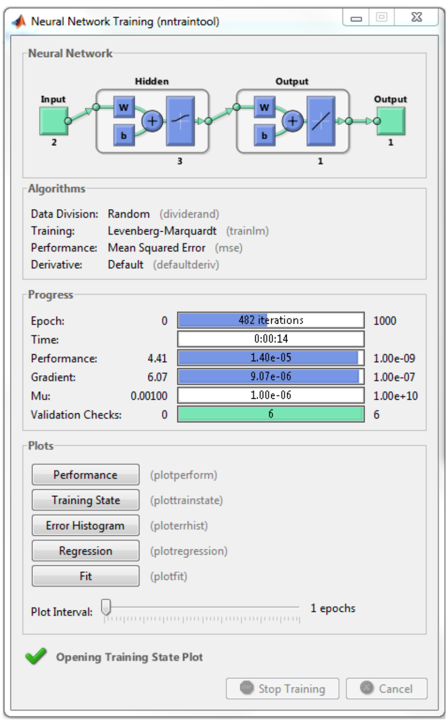

Fig. 2. Neural network training window

The mean square error changes at the epochs shown in Figure 3. As can be seen from the graph, the best validation performance $1.3429 \cdot 10^{-5}$ has occurred at epoch 476. Therefore, the final mean square error is small. Moreover, the test set error and the validation set error have similar characteristics. Additionally, no significant overfitting has occurred, where the best validation performance occurs.

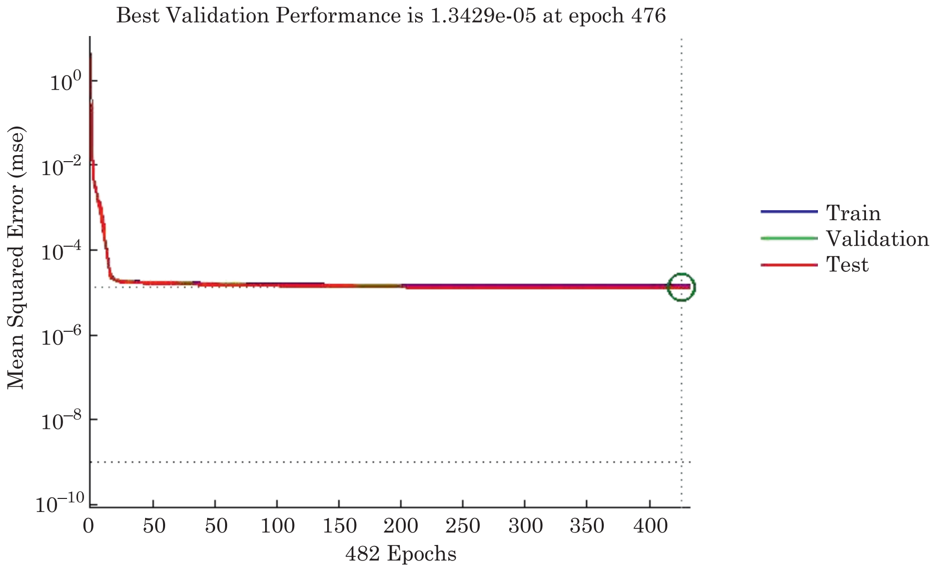

Fig. 3. Performance goal of neural network

Linear regression analyses were performed to compute the correlation coefficient R between the experimental and predicted values (see Fig. 4). As can be seen from the graphs, the output tracks the targets very well both for training (Fig. 4*a*),validation (Fig. 4*b*), and testing (Fig. 4*c*), respectively. In addition, the R-value is over 0.99 for the total response (Fig. 4*d*).

To determine the dew point temperature t_{DP} was derived from the ANN (model M13):

$$t_{\mathrm{DP}} = -5.2686 \cdot F_1 + 11.5088 \cdot F_2 - 5.2164 \cdot F_3 - 6.3302 \tag{6}$$

where $F_{(i=1,2,3)}$ can be calculated using:

$$F_i = \frac{1}{1 + \exp^{-W_i}} \tag{7}$$

and W_1–W_3 can be determined as follows:

$$W_i = D_{1i} \cdot t + D_{2i} \cdot \mathrm{RH} + D_{3i} \tag{8}$$

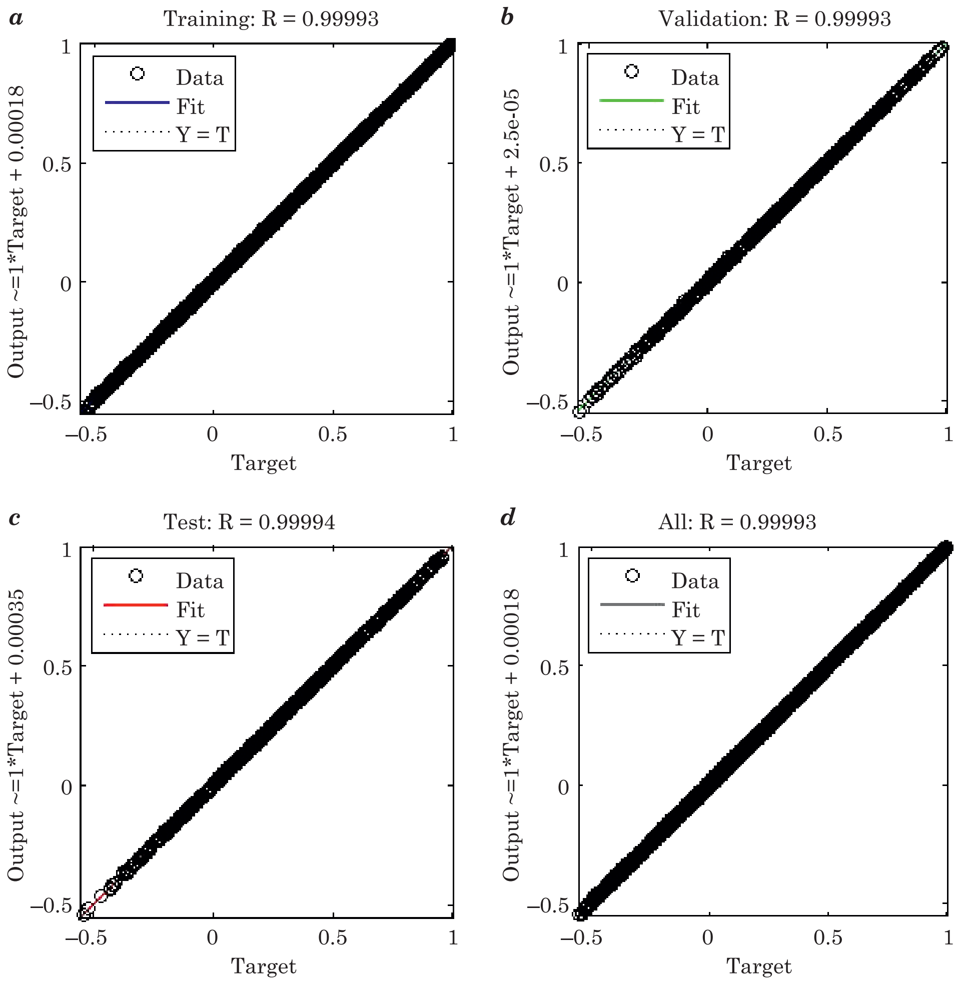

Fig. 4. A linear regression graph for observed and predicted values of dew point temperature: *a* – training, *b* – validation, *c* – testing, *d* - all samples

Weights: D_{1i}, D_{2i} and bias D_{3i} in Eq. (8) are given in Table 4 for algorithm with three neurons.

Presented ANN (consists of Eqs. (6) – (8) and Table 3) can be easy to use model. The model M13 (ANN) gave good results in determining the dew point temperature. The values of statistical parameters from ANN model (Tab. 2) were following: MBE=0.0038 K, RMSE=0.1373 K, R=0.9999, χ^2=0.0189 K^2. Those parameters were little worse than for model M3 with constants A=237, B=7.5.

Table 4

Weights and biases between input layer and hidden layer

No.	Weight		Bias
i	D_{1i}	D_{2i}	D_{3i}
1	0.4894	0.4559	-1.3690
2	0.2403	-4.1578	-2.8064
3	0.4680	-0.1209	1.1178

Conclusions

It turned out from the investigations that model M3, especially with constants A=237, B=7.5, gave the best results in determining the dew point temperature. Model M1, especially with constants A=243.3, B=17.269 and A=243.5, B=17.67 can be also considered as appropriate. Model M9 can be used to determine dew point temperature, but only for $40 \leq RH_{\%} \leq 100\%$ and $0<t<30$.

Proposed model M13 (ANN) gave good results in determining the dew point temperature. The ANN have 2 input (t and RH%) hidden layer (3 neurons) and 1 output – t_{DP}, activation functions in hidden layer and output layer were "logsig" and "purelin" respectively.

References

AGHBASHLO M, KIANMEHR M.H, NAZGHELICHI T, RAFIEE S. 2011. *Optimization of an artificial neural network topology for predicting drying kinetics of carrot cubes using combined response surface and genetic algorithm*. Drying Technology, 29: 770–779.

AJ Design Software. Science Math Physics Engineering And Finance Calculators. Dew Point Equations Formulas Calculator. Meteorology Weather Water Vapor. http://www.ajdesigner.com/phphumidity/dewpoint_equation_dewpoint_temperature.php (access: 5.05.2016).

AMIRMOJAHEDI M., MOHAMMADI K., SHAMSHIRBAND S., DANESH A.S., MOSTAFAEIPOUR A., KAMSIN A. 2016. *A hybrid computational intelligence method for predicting dew point temperature*. Environmental Earth Sciences, 75: 415.

ASHRAE Handbook-Fundamentals. 1993. ASHRAE, Atlanta, GA.

BOHREN C., ALBRECHT B. 1998. *Atmospheric Thermodynamics*. Oxford University Press, p. 402.

BOSEN J.F. 1958. *An approximation formula to compute relative humidity from dry bulb and dew point temperatures*. Monthly Weather Review, 86(12): 486.

BROOKER D.B., BARKER-ARKEMA F.W., HALL C.W. 1992. *Drying and storage of grains and oilseeds*. AVIBook, New York.

CUI B., ZHU Y. *Section 6: Bias correction and statistical down-scaling for 2-meter dew-point temperature and relative humidity*. National Weather Service. Environmental Modeling Center. http://www.emc.ncep.noaa.gov/gmb/yzhu/imp/i201204/NAEFS_Science_Documentation.pdf (access: 5.05.2016).

EZFREMOV G. 2013. *Describing of generalized drying kinetics with application of experiment design method.* Technical Sciences, (16)4: 309–322.

ERB R.J. 1993. *Introduction to backpropagation neural network computation*. Pharmaceutical Research, 10(2): 165–170.

GERYŁO R. 2008. *Powierzchniowa kondensacja pary wodnej*. Świat Szkła, 9.

GOLISZ E., JAROS M., KALICKA M. 2013. *Analysis of convectional drying pracess of peach*. Technical Sciences, 16(4): 333–343.

HUBBART K.G., MAHMOOD R., CARLSON C. 2003. *Estimating daily dew point temperature for the northern Great Plains using maximum and minimum temperature*. Agronomy Journal, 95(2): 323–328.

Instytut Inżynierii i Gospodarki Wodnej. Politechnika Krakowska. M. Bodziony. Wilgotność powietrza. http://holmes.iigw.pl/~mbodzion/dydaktyka/hydro/pliki/wilgotnosc.pdf (access: 5.05.2016).

JALAL S., SUNGWON K., OZGUR K. 2014. *Estimation of daily dew point temperature using genetic programming and neural networks approaches*. Hydrology Research. An International Journal, 45.2: 165–181.

KALETA A., GÓRNICKI K., WINICZENKO R., CHOJNACKA A. 2013. *Evaluation of drying models of apple (var. Ligol) dried in a fluidized bed dryer.* Energy Conversion and Management, 67: 179–185.

KALETA A., GÓRNICKI K., 2010. *Some remarks on evaluation of drying models of red beet particles*. Energy Conversion and Management, 51(12): 2967–2978.

KHALAJ G., AZIMZADEGAN T., KHOEINI M., ETAAT M. 2013. *Artificial neural networks application to predict the ultimate tensile strength of X70 pipeline steels. w*Neural Computing and Applications, 23(7–8): 2301–2308.

KIM S., SINGH V.P., LEE C.J., SEO Y. 2015. *Modeling the physical dynamics of daily dew point temperature using soft computing techniques*. KSCE Journal of Civil Engineering, 19(6): 1930–1940.

LAWRENCE M.G. 2005. *The relationship between relative humidity and the dewpoint temperature in moist air. A simple conversion and applications.* American Meteorological Society, 2: 225–233.

LOPES D.C., MELO E.C., MARTINS J.H., GRACIA L.M.N, GUIMARÁES A.C. 2009. *Grapsi Draw Digital Psychrometric Chart*. In: *Computer and Computing Technologies in Agriculture II*. Vol. 1. Ed. D. Li, Ch. Zhao. IFIP Advances in Information and Communication Technology, Springer, Boston, p. 519–528.

Massachusetts Institute of Technology. http://web.mit.edu/weather/info/Frequently_Asked_Questions-temp-dewpoint (access: 5.05.2016).

MITTAL G.S. 1996. *Computerized Control Systems in the Food Industry*. CRC Press.

MITTAL G.S., ZHANG J. 2003. *Artificial neural network-based psychrometric predictor.* Biosystems Engineering, 85(3): 283–289.

MOHAMMADI K., SHAMSHIRBAND S., PETKOVIĆ D., YEE P.L., MANSOR Z. 2016. *Using ANFIS for selection of more relevant parameters to predict dew point temperature.* Applied Thermal Engineering, 96: 311–319.

NADIG K., POTTER W., HOOGENBOOM G., MCCLENDON R. 2013. *Comparison of individual and combined ANN models for prediction of air and dew point temperature*. Applied Intelligence, 39(2): 354–366.

National Weather Service. Environmental Modeling Center. http://www.srh.noaa.gov/images/epz/wxcalc/rhTdFromWetBulb.pdf (access: 5.05.2016).

National Weather Service. Environmental Modeling Center. http://www.srh.noaa.gov/images/epz/wxcalc/wetBulbTdFromRh.pdf (access: 5.05.2016)

National Oceanic and Atmospheric Administration. National Weather Service. Wet-bulb Temperature and Dewpoint Temperature from Air Temperature and Relative Humidity. http://www.crh.noaa.gov/Image/epz/wxcalc/wetBulbTdFromRh.pdf (access: 5.05.2016).

NAZGHELICHI T., AGHBASHLO M., KIANMEHR M.H 2011. *Optimization of an artificial neural network topology using coupled response surface methodology and genetic algorithm for fluidized bed drying.* Computer and Electronics in Agriculture, 75: 84–91.

NOURBAKHSHA H., EMAM-DJOMEH Z., OMID M., MIRSAEEDGHAZI H., MOINI S. 2014. *Prediction of red plum juice permeate flux during membrane processing with ANN optimized using RSM*. Computers and Electronics in Agriculture, 102: 1–9.

OMID M. BAHARLOOEI A., AHMADI H. 2009. *Modeling drying kinetics of pistachio nuts with multi-layer feed-forward neural network.* Drying Technology, 27: 1069–1077.

RIANGVILAIKUL B., KUMAR S. 2010a. *An experimental study of a novel dew point evaporative cooling system.* Energy and Buildings, 42: 637–644.

RIANGVILAIKUL B., KUMAR S. 2010b. *Numerical study of a novel dew point evaporative cooling system.* Energy and Buildings, 42: 2241–2250.

ROJECKI A. 1959. *Tablice psychrometryczne*. Wyd. 2 poprawione i uzupełnione. Wydawnictwa Komunikacyjne, Warszawa.

SALWIŃSKI J. 2002. *Jak za pomocą higrometru określić termiczność?* http://old.szybowce.com/termicznosc.php (access: 5.05.2016).

SARGENT G.P. 1980. *Computation of vapour pressure, dew-point and relative humidity from dry- and wet-bulb temperatures.* Meteorological Magazine, 109: 238–246.

SHANK D.B., HOOGENBOOM G., MCCLENDON R.W. 2008. *Dew point temperature prediction using artificial neural networks*. Journal of Applied Meteorology and Climatology, 47(6): 1757–1769.

SHIRI J., KIM S., KISI O. 2014. *Estimation of daily dew point temperature using genetic programming and neural networks approaches*. Hydrology Research, 45(2): 165–181.

SHROFF S., DABHI V. 2013a. *Dew Point modelling using GEP based multi objective optimization.* arXiv preprint arXiv:1304.5594.

SHROFF S., DABHI V. 2013b. *Multiobjective optimization in Gene Expression Programming for Dew Point.* arXiv preprint arXiv:1304.5594.

SIMONS R.E. 2008. *Estimating dew point temperature for water cooling applications*. Electronics cooling 1. http://www.electronics-cooling.com/2008/05/estimating-dew-point-temperature-for-water-cooling-applications (access: 5.05.2016).

SINGH A.K., SINGH H., SINGH S.P., SAWHNEY R.L. 2002. *Numerical calculation of psychrometric properties on a calculator.* Building and Environment, 37: 415–419.

SNYDER R.L., DE MELO-ABREU J.P. 2005. *Frost protection: fundamentals, practice and economics.* Vol. 1. Food and Agricultural Organization of the United Nations, Rome.

SREEKANTH S., RAMASWAMY H.S., SABLANI S. 1998. *Prediction of psychrometric parameters using neural networks*. Drying Technology, 16(3–5): 825–837.

WEISS A. 1977. *Algorithms for the calculation of moist air properties on hands calculator.* Transaction of ASAE, 20: 1133-1136.

Wikipedia. Wolna Encyklopedia. Temperatura punktu rosy. http://pl.wikipedia.org/wiki/Temperatura_punktu_rosy (access: 5.05.2016).

WILHELM L.R. 1976. *Numerical calculation of psychrometric properties*. Transactions of ASAE, 19(2): 318-325.

WINICZENKO R., GÓRNICKI K., KALETA A., JANASZEK-MAŃKOWSKA M. 2016. *Optimisation of ANN topology for predicting the rehydrated apple cubes colour change using RMS and GA*. Neural Computing and Applications, 1-15. DOI: 10.1007/s00521-016-2801-y.

WOOD L.A. 1970. *The use of dew-point temperature in humidity calculations*. Journal of Research of the National Bureau of Standards – C. Engineering and Instrumentation, 74C(3,4): 117–122.

ZHAO X., LI J.M., RIFFAT S.B. 2008. *Numerical study of a novel counter-flow heat and mass exchanger for dew point evaporative cooling*. Applied Thermal Engineering, 28: 1942–1951.

ZOUNEMAT-KERMANI M. 2012. *Hourly predictive Levenberg–Marquardt ANN and multi linear regression models for predicting of dew point temperature*. Meteorology and Atmospheric Physics, 117(3–4): 181–192.

Technical Sciences, 2017, 20(3), 259–273

Quarterly peer-reviewed scientific journal
ISSN 1505-4675
e-ISSN 2083-4527
TECHNICAL SCIENCES
Homepage: www.uwm.edu.pl/techsci/

APPROXIMATED MATHEMATICAL MODEL OF HYDRAULIC DRIVE OF CONTAINER UPTURNING DURING LOADING OF SOLID DOMESTIC WASTES INTO A DUSTCART

Oleg Berezyuk, Valeriy Savulyak

Faculty of Machine Building and Transport
Vinnytsia National Technical University
Vinnytsia, Ukraine

Received 2 November 2016, accepted 21 June 2017, available online 22 June 2017.

Key words: container upturning, Laplace transform, dustcart, hydraulic drive, mathematical model, solid domestic wastes.

Abstract

A simplified mathematical model of hydraulic drive of container upturning during loading of solid domestic wastes into a dustcart is proposed. Approximated analytical time dependencies of pressure in a delivery pipe of a hydrocylinder, angular velocity and the angle of container upturning are obtained. Approximated duration dependence of container upturning from main parameters of hydraulic drive is detected. Optimal values of main parameters of working organs, which ensure minimum time of container upturning during loading of solid domestic wastes into a dustcart are defined.

Introduction

In obedience to statistical data, the yearly volume of solid domestic wastes (SDW), produced in the populated areas of Ukraine, exceeds 46 million m^3. Their overwhelming majority is buried on polygons and dumps. SDW collecting is a main task of sanitary cleaning of the populated areas and is carried out by more than 4.1 thousand special cars (dustcarts), and that is why it is

Correspondence: Oleg Berezyuk, Faculty of Machine Building and Transport, Vinnytsia National Technical University, 95 Khmelnytske shose, Vinnytsia, Ukraine, 21021, e-mail: berezyukoleg@yandex.ru

associated with considerable financial expenses (BEREZYUK 2009). Before SDW transportation by dustcarts to the place of their utilization, the waste loading is performed. According to approximate calculations, almost 2.7 thousand tone of fuel is yearly spent on the SDW loading by communal enterprises of Ukraine. “The Stockholm Convention on persistent organic pollutants” requires the SDW processing, collecting, transportation and storage in environmentally friendly manner. In particular, actual there is a problem of providing reducing the fuel consumption during SDW loading into a dustcart.

The analysis (SAVULYAK, BEREZYUK 2006) of developments in the field of SDW loading has shown that waste loading into the overwhelming majority of dustcarts is performed by means of a hydraulic drive of working organs. It has been found that the operation of SDW loading into a dustcart consists from turn of a lever and upturning of a container capture. The article (BEREZYUK 2013) provides a mathematical model of hydraulic drive of container upturning during SDW loading into dustcart as a substantially non-linear system of differential equations, that cannot be solved by known analytical methods in the permissible limits of error. Compared to the publications of previous authors, the scientific novelty of this article is as follows:

– a simplified mathematical model of hydraulic drive of container upturning during loading of solid domestic wastes into dustcart is proposed;

– approximated analytical time dependencies of pressure in a delivery pipe of hydrocylinder, angular velocity and the angle of container upturning are obtained;

– approximated duration dependence of container upturning from main parameters of hydraulic drive is detected;

– optimal values of the main parameters of working organs which ensure a minimum time of container upturning during loading of solid domestic wastes into a dustcart are defined.

The purpose of the study is to define optimal values of main parameters of working organs, which ensure the reduction of fuel consumption by means of time minimization of container upturning during SDW loading into a dustcart.

Methods

During the study such methods were used: imitative computer modeling, Laplace transform (SVESHNIKOV, TIHONOV 2005), decomposition into simple fractions. Table 1 shows the comparison of assumptions, taken into account during the development of full and simplified mathematical models.

Table 1
Comparison of assumptions, taken into account during the development of full and simplified mathematical models

Full mathematical model	Simplified mathematical model
Pressures at the pump output and at the hydrocylinder input are different	pressures at the pump output and at the hydrocylinder input are same
Pressures in drain pipes are more than zero	pressures in drain pipes are around zero
Influence of the force of viscous friction on functioning of a hydraulic drive is essential	influence of the force of viscous friction on functioning of a hydraulic drive is unessential
Shoulders of appendix of efforts to executive organs take into account the change of angular velocity of the container	shoulders of appendix of efforts to executive organs do not take into account the change of angular velocity of the container

Results and Discussion

Figure 1 presents a calculated scheme for a simplified mathematical model of hydraulic drive of container upturning during SDW loading into dustcart when using the back scheme of SDW loading by which such known brands of dustcarts are functioning: Norba N-Series (*Norba. Refuse Collection...* 1977), Schörling Olympus (*Schörling: Vehicle Technology...* 1990), Zoeller Magnum (*Zoeller* 1990, p. 8), Faun Europress (*Pressmullfahrzeuge Faun Europress* 1995) and others.

The following structural elements are marked on the scheme: *Cn* – container, *Cp* – capture, *L* – lever, *HC* – hydrocylinder, *HD* – hydrodistributor, *HP* – hydropump, *SV* – safety valve, *F* – filter, *T* – tank with working fluid, and also the main geometrical, kinematics and power parameters:

p_1, p_2, p_3, p_4 – pressures at the output of a hydropump, at the input of a hydrocylinder, at the output of a hydrocylinder and at the input of a filter, accordingly; W_1, W_2, W_3, W_4 – volumes of pipelines between the hydropump and the hydrodistributor, the hydrodistributor and the input of the hydrocylinder, the output of the hydrocylinder and the hydrodistributor, the hydrodistributor and the filter, Q_P – actual hydropump feeding, S_D – area of a passable hole of a hydrodistributor, S_F – surface area of a filter element, D, d – diameters of a piston and a rod, J – inertia moment of moving elements, G_C – weight of the container, R – rotation radius of moving elements, l_P – distance between rotation centers of the capture and the rod, h_C – altitude of the container, α – angle between the axes of a lever and the shoulder of a hydrocylinder, γ – angle which takes into account the position deflection of masses center, δ – angle between the shoulder of a capture and a horizontal, λ – inclination

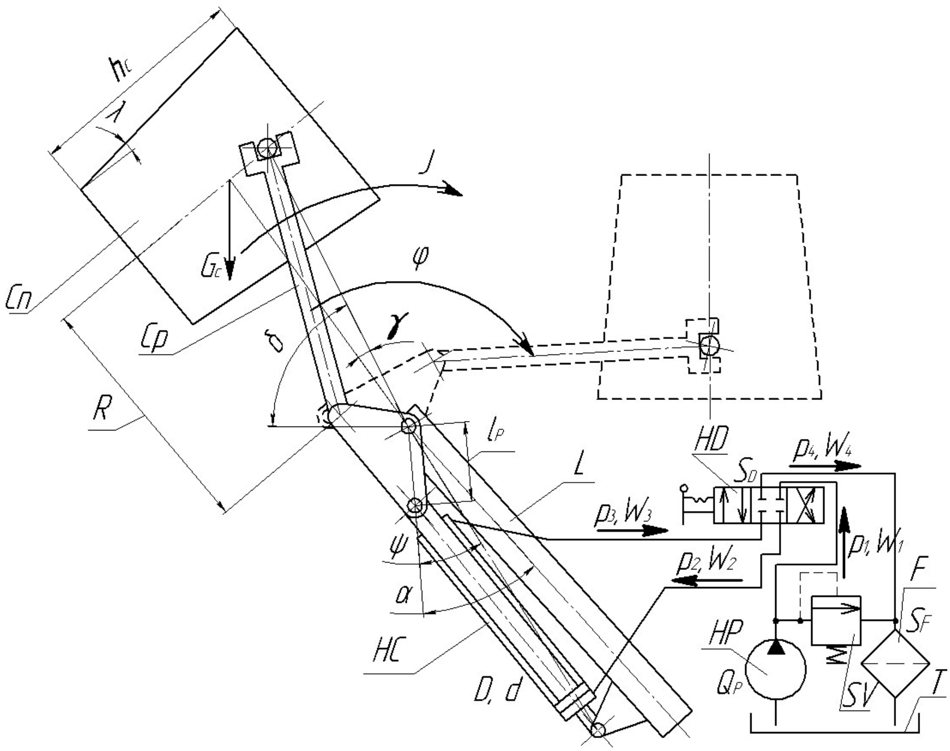

Fig. 1. Calculated scheme for a simplified mathematical model of hydraulic drive of container upturning during SDW loading into a dustcart (description in the text)

angle of a container wall, ψ – angle between the axis of a hydrocylinder shoulder and the axis which passes between the rotation centers of a capture and a hydrocylinder, φ – angle of capture rotation.

The analysis of the conducted studies of a full mathematical model (BEREZYUK 2013) has shown, that $p_1 \approx p_2 \approx p_{12}$, and the influence of pressure in drain pipes, forces influence of viscous friction on functioning of hydraulic drive is unessential.

Process of container upturning can be divided into two phases:

– phase of container turning to equilibrium position ($\delta + \varphi - \lambda \leq \pi/2$);

– phase of SDW emptying from the container into a basket of a dustcart ($\delta + \varphi - \lambda > \pi/2$).

Thus, the system of differential equations of full mathematical model turns into such systems of differential equations, which correspond to the phases, accepted above.

Phase of container turning to equilibrium position can be described by the system of differential equations:

$$\begin{cases} Q_P = \dot{\varphi} S_{C1} l_P \sin(\varphi + \psi) + \sigma p_{12} + K W_{12} \dot{p}_{12} & (1) \\ p_{12} S_{C1} l_P \sin(\varphi + \alpha) = J\ddot{\varphi} + GR\cos(\varphi + \delta - \gamma) & (2) \end{cases}$$

where:
$W_{12} = W_1 + W_2$.

For linearization of trigonometric functions of the system of differential equations we will introduce replacements:

$$\cos(\varphi + \delta - \gamma) \approx \cos(\omega_0 t + \delta - \gamma) \tag{3}$$

$$\sin(\varphi + \alpha) \approx \sin(\bar{\varphi}_1 + \alpha) \tag{4}$$

$$\sin(\varphi + \psi) \approx \sin(\bar{\varphi}_1 + \psi) \tag{5}$$

where:
$\omega_0 \approx \dfrac{Q_P}{2S_{C1}R}$ – average value of angular velocity of a container upturning at a first approximation;

(6)

$S_{C1} = \pi(D^2 - d^2)/4$ – area of a rod cavity of a hydrocylinder;
$\bar{\varphi}_1 = (\pi/2 + \lambda - \delta)/2$ – average value of the angle upturning of a container at a first approximation for the first phase.

Therefore, a simplified mathematical model of hydraulic drive of the first phase of container upturning during SDW loading into a dustcart looks like this:

$$\begin{cases} Q_P = 2\omega S_{C1} l_P \sin(\bar{\varphi}_1 + \psi) + \sigma p_{12} + K W_{12} \dot{p}_{12} & (7) \\ p_{12} S_{C1} l_P \sin(\bar{\varphi}_1 + \alpha) = J\dot{\omega} + GR\cos(\omega_0 t)\cos(\delta - \gamma) - GR\sin(\omega_0 t)\sin(\delta - \gamma) & (8) \end{cases}$$

where:
$\omega = \dot{\varphi} \neq \text{const.}$ – instantaneous value of angular velocity of container upturning.

For further study of a simplified mathematical model we use Laplace transform (SVESHNIKOV, TIHONOV 2005), according to which we get:

$$\begin{cases} Q_P/S = \Omega(s)2S_{C1}l_P\sin(\bar{\varphi}_1 + \psi) + P(s)\sigma + P(s)sKW_{12} & (9) \\ P(s)S_{C1}l_P\sin(\bar{\varphi}_1 + \alpha) = \Omega(s)sJ + \dfrac{sGR\cos(\delta - \gamma)}{s^2 + \omega_0^2} - \dfrac{\omega_0 GR\sin(\delta - \gamma)}{s^2 + \omega_0^2} & (10) \end{cases}$$

Substituting equation (10) into equation (9), we get

$$\Omega_1(s) = \frac{-b_3s^3 + b_2s^2 - b_1s + b_0}{s(s^2 + \omega_0^2)(a_2s^2 + a_1s + a_0)} \tag{11}$$

where:
$a_2 = KW_{12}J$; $a_1 = \sigma J$; $a_0 = 2S_{C1}^2l_P^2\sin(\bar{\varphi}_1 + \alpha)\sin(\bar{\varphi}_1 + \psi)$; $b_3 = KW_{12}GR\cos(\delta - \gamma)$; $b_2 = Q_PS_{C1}l_P\sin(\bar{\varphi}_1 + \alpha) - \sigma GR\cos(\delta - \gamma) + KW_{12}\omega_0GR\sin(\delta - \gamma)$; $b_1 = \sigma\omega_0GR$x $\sin(\delta - \gamma)$; $b_0 = Q_P\omega_0^2S_{C1}l_P\sin(\bar{\varphi}_1 + \alpha)$

(12)

By the method of the expression (11) decomposition into simpler fractions after transformation to canonical form we get

$$\Omega_1(s) = A_1\frac{1}{s} + B_1\frac{s}{s^2 + \omega_0^2} + \frac{D_1}{a_2}\frac{s + a_1/(2a_2)}{[s + a_1/(2a_2)]^2 + (4a_0a_2 - a_1^2)/(4a_2^2} +$$

$$+ \frac{C_1}{\omega_0}\frac{\omega_0}{s^2 + \omega_0^2} + \frac{4E_1 - D_1a_1}{2\sqrt{4a_0a_2 - a_1^2}}\frac{\sqrt{4a_0a_2 - a_1^2}/(2a_2)}{[s + a_1/(2a_2)]^2 + (4a_0a_2 - a_1^2)/(4a_2^2)}, \tag{13}$$

where:
$A_1 = b_0/(a_0\omega_0^2)$; $B_1 = [(b_2\omega_0^2 - b_0)(a_0 - a_2\omega_0^2) - a_1\omega_0^2(b_3\omega_0^2 - b_1)]/\{\omega_0^2[(a_0 - a_2\omega_0^2)^2 + + a_1^2\omega_0^2]\}$; $C_1 = (b_3\omega_0^2 - b_1 + B_1a_1\omega_0^2)/(a_0 - a_2\omega_0^2)$; $D_1 = -a_2(A_1 + B_1)$; $E_1 = -b_3 + + D_1a_1/a_2 - C_1a_2$

(14)

We find the original of an image (13)

$$\omega_1(t) = A_1 + B_1\cos(\omega_0t) + \frac{C_1}{\omega_0}\sin(\omega_0t) + \frac{D_1}{a_2}e^{-\frac{a_1}{2a_2}t}\cos\left(\frac{\sqrt{4a_0a_2 - a_1^2}}{2a_2}t\right) +$$

$$+ \frac{4E_1 - D_1a_1}{2\sqrt{4a_0a_2 - a_1^2}}e^{-\frac{a_1}{2a_2}t}\sin\left(\frac{\sqrt{4a_0a_2 - a_1^2}}{2a_2}t\right) \tag{15}$$

After excluding minor coefficients of the expression (15) which have a higher order of smallness, and after taking into account the agreed designations according to (6), (12), (14), the angular velocity of container upturning during the first phase is presented by such equation:

$$\omega_1(t) \approx \frac{Q_P S_{C1} l_P \sin(\bar{\varphi}_1 + \alpha) - \sigma G R \cos(\delta - \gamma)}{2S_{C1}^2 l_P^2 \sin(\bar{\varphi}_1 + \alpha) \sin(\bar{\varphi}_1 + \psi)} \left[1 - e^{-\frac{\sigma}{2KW_{12}} t} \times \right.$$
$$\left. \times \cos\left(S_{C1} l_P \sqrt{\frac{2 \sin(\bar{\varphi}_1 + \alpha) \sin(\bar{\varphi}_1 + \psi)}{KW_{12} J}}\, t\right)\right] \tag{16}$$

For angle definition of container upturning during the first phase we integrate the equation (16) and, taking into account the initial conditions $\varphi(0) = 0$, we get:

$$\varphi_1(t) = \frac{Q_P S_{C1} l_P \sin(\bar{\varphi}_1 + \alpha) - \sigma G R \cos(\delta - \gamma)}{2S_{C1}^2 l_P^2 \sin(\bar{\varphi}_1 + \alpha) \sin(\bar{\varphi}_1 + \psi)} \left\{ \frac{e^{-\frac{\sigma}{2KW_{12}} t}}{8KW_{12} S_{C1}^2 l_P^2 \sin(\bar{\varphi}_1 + \alpha) \sin(\bar{\varphi}_1 + \psi) + J\sigma^2} \times \right.$$
$$\times \left[2KW_{12} J \sigma \cos\left(S_{C1} l_P \sqrt{2\sin(\bar{\varphi}_1 + \alpha)\sin(\bar{\varphi}_1 + \psi)/(KW_{12} J)}\, t\right) - 4K^{1.5} W_{12}^{1.5} S_{C1} l_P \times \right. \tag{17}$$
$$\left.\left. \times \sqrt{2J \sin(\bar{\varphi}_1 + \alpha) \sin(\bar{\varphi} + \psi)} \sin\left(S_{C1} l_P \sqrt{2\sin(\bar{\varphi}_1 + \alpha) \sin(\bar{\varphi}_1 + \psi)/(KW_{12} J)}\, t\right)\right] + t \right\}$$

After excluding minor coefficients of expression (17), which have a higher order of smallness, we receive a simplified equation of angle change of upturning container during the first phase:

$$\varphi_1(t) \approx \frac{Q_P S_{C1} l_P \sin(\bar{\varphi}_1 + \alpha) - \sigma G R \cos(\delta - \gamma)}{2S^2_{C1} l^2_P \sin(\bar{\varphi}_1 + \alpha) \sin(\bar{\varphi}_1 + \psi)}\, t \tag{18}$$

We define the duration of container upturning during the first phase by the equation (18):

$$t_1 \approx \frac{2S^2_{C1} l^2_P \sin(\bar{\varphi}_1 + \alpha) \sin(\bar{\varphi}_1 + \psi)}{Q_P S_{C1} l_P \sin(\bar{\varphi}_1 + \alpha) - \sigma G R \cos(\delta - \gamma)}\, \varphi \tag{19}$$

After placing the changes $\sin(\bar{\varphi}_1 + \alpha)\sin(\bar{\varphi}_1 + \psi) \approx \sin^2(\bar{\varphi}_1 + (\alpha + \psi)/2)$ and $\bar{\varphi}_1 \to \varphi_1(t)$ in the equation (16) we get:

$$\omega_1(t) \approx \frac{Q_P S_{C1} l_P \sin\left(\dfrac{Q_P}{2S_{C1} l_P \sin(\bar{\varphi}_1 + \psi)} t + \alpha\right) - \sigma G R \cos(\delta - \gamma)}{2S^2_{C1} l^2_P \sin^2\left(\dfrac{Q_P}{2S_{C1} l_P \sin(\bar{\varphi}_1 + \psi)} t + \dfrac{\alpha + \psi}{2}\right)} \times \tag{20}$$

$$\times \left[1 - e^{-\frac{\sigma}{2KW_{12}} t} \cos\left(S_{C1} l_P \sin\left(\frac{Q_P}{2S_{C1} l_P \sin(\bar{\varphi}_1 + \psi)} t + \frac{\alpha + \psi}{2}\right) \sqrt{\frac{2}{KW_{12} J}}\, t\right)\right]$$

After solving a system of equations (9, 10) relative to $P(s)$ after transformation to canonical form we get:

$$P_1(s) = A_{1p} \frac{1}{s} + \frac{B_{1p} - C_{1p} - F_{1p}}{KW_{12}} \frac{1}{s^2 + \sigma/(KW_{12})} - D_{1p} \frac{s}{s^2 + \omega^2_0} - \frac{E_{1p}}{\omega_0} \frac{\omega}{s^2 + \omega^2_0} - \frac{G_{1p}}{a_2} \times$$

$$\times \frac{s + a_1/(2a_2)}{[s + a_1/(2a_2)]^2 + (4a_0 a_2 - a^2_1)/(4a^2_2)} - \frac{4H_{1p} - G_{1p} a_1}{2\sqrt{4a_0 a_2 - a^2_1}} \times \tag{21}$$

$$\times \frac{\sqrt{4a_0 a_2 - a^2_1}/(2a_2)}{[s + a_1/(2a_2)]^2 + (4a_0 a_2 - a^2_1)/(4a^2_2)}$$

where:

$A_{1p} = (Q_P - 2A_1 S_{C1} l_P \sin(\bar{\varphi}_1 + \psi))/\sigma$; $B_{1p} = -KW_{12}(Q_P - 2A_1 S_{C1} l_P \sin(\bar{\varphi}_1 + \psi))/\sigma$,
$C_{1p} = -2S_{C1} l_P KW_{12}(B_1 \sigma - C_1 KW_{12}) \sin(\bar{\varphi}_1 + \psi)/(\sigma^2 + K^2 W^2_{12} \omega^2_0)$,
$D_{1p} = 2S_{C1} l_P (B_1 \sigma - C_1 KW_{12}) \sin(\bar{\varphi}_1 + \psi)/(\sigma^2 + K^2 W^2_{12} \omega^2_0)$,
$E_{1p} = 2S_{C1} l_P (B_1 KW_{12} \omega^2_0 + C_1 \sigma) \sin(\bar{\varphi}_1 + \psi)/(\sigma^2 + K^2 W^2_{12} \omega^2_0)$,
$H_{1p} = 2S_{C1} l_P (E_1(a_1 KW_{12} - a_2) - D_1 a_0 KW_{12}) \sin(\bar{\varphi}_1 + \psi)]/(a_1 KW_{12} \sigma - a_2 \sigma^2 - a_0 K^2 W^2_{12})$,
$F_{1p} = 2S_{C1} l_P KW_{12}(D_1 \sigma - E_1 KW_{12}) \sin(\bar{\varphi}_1 + \psi)/(a_1 KW_{12} \sigma - a_2 \sigma^2 - a_0 K^2 W^2_{12})$,
$G_{1p} = 2S_{C1} l_P a_2 (D_1 \sigma - E_1 KW_{12}) \sin(\bar{\varphi}_1 + \psi)/(a_1 KW_{12} \sigma - a_2 \sigma^2 - a_0 K^2 W^2_{12})$
(22)

We find the original of an image (21):

$$p_1(t) = A_{1p} + \frac{B_{1p} - C_{1p} - F_{1p}}{KW_{12}} e^{-\frac{\sigma}{2KW_{12}} t} - D_{1p} \cos(\omega_0 t) - \frac{E_{1p}}{\omega_0} \sin(\omega_0 t) -$$

$$- \frac{G_{1p}}{a_2} e^{-\frac{\sigma}{2a_2} t} \cos\left(\frac{\sqrt{4a_0 a_2 - a_1^2}}{2a_2} t\right) - \frac{4H_{1p} - G_{1p} a_1}{2\sqrt{4a_0 a_2 - a_1^2}} e^{-\frac{\sigma}{2a_2} t} \sin\left(\frac{\sqrt{4a_0 a_2 - a_1^2}}{2a_2} t\right) \tag{23}$$

After excluding minor coefficients of expression (23) which have a higher order of smallness, and after considering the agreed designations according to (6), (12), (14), (22) and the initial condition $p(0) = 0$, the pressure in a delivery pipe of a hydrocylinder can be described by the equation:

$$p_1(t) \approx \frac{GR}{S_{C1}l_P \sin\left(\frac{Q_P}{2S_{C1}l_P \sin(\bar{\varphi}_1 + \psi)} t + \alpha\right)} + \frac{Q_P}{S_{C1}l_P \sin\left(\bar{\varphi}_1 + \frac{\alpha + \psi}{2}\right)} \times$$

$$\times \sqrt{\frac{J}{2KW_{12}}}\, e^{-\frac{\sigma}{2KW_{12}} t} \sin[S_{C1}l_P \sin(\bar{\varphi}_1 + (\alpha + \psi)/2)\sqrt{2/(KW_{12}J)}t + \tag{24}$$

$$- \arcsin(\sqrt{2KW_{12}J}\sigma GR \cos(\delta - \gamma) \sin(\bar{\varphi}_1 + (\alpha + \psi)/2)/(Q_P \sin \alpha))]$$

Phase of SDW emptying from the container into a basket of the dustcart can be described by a system of differential equations:

$$\begin{cases} Q_P = 2\dot{\varphi}S_{C1}l_P \sin(\varphi + \psi) + \sigma p_{12} + KW_{12}\dot{p}_{12} & (25) \\ p_{12}S_{C1}l_P \sin(\varphi + \alpha) = J\ddot{\varphi} + (GR - V_C\rho_w x(1 + 2\mathrm{tg}\lambda)Rg/h_C)\cos(\varphi + \delta - \gamma) & (26) \\ g \sin(\varphi + \delta - \lambda) = \ddot{x} + f_w g \cos(\varphi + \delta - \lambda) & (27) \end{cases}$$

For linearization of trigonometric functions in the system of differential equations we will introduce the replacements:

$$\cos(\varphi + \delta - \gamma) \approx \cos(\omega_0 t + \delta - \gamma) \approx \cos(\bar{\varphi}_2 + \delta - \gamma) \tag{28}$$

$$\sin(\varphi + \delta - \gamma) \approx \sin(\omega_0 t + \delta - \gamma) \tag{29}$$

$$\sin(\varphi + \alpha) \approx \sin(\bar{\varphi}_2 + \alpha) \tag{30}$$

$$\sin(\varphi + \psi) \approx \sin(\bar{\varphi}_2 + \psi) \tag{31}$$

where:
$\bar{\varphi}_2 = 0.75\pi + 1.5\lambda - \delta$ – average value of the angle of container upturning at a first approximation for the second phase.

Therefore a simplified mathematical model of a hydraulic drive of the second phase of container upturning during SDW loading into a dustcart looks like this:

$$\begin{cases} Q_P = 2\omega S_{C1} l_P \sin(\bar{\varphi}_2 + \psi) + \sigma p_{12} + KW_{12}\dot{p}_{12} & (32) \\ p_{12} S_{C1} l_P \sin(\bar{\varphi}_2 + \alpha) = J\dot{\omega} + GR\cos(\omega_0 t)\cos(\delta - \gamma) - \\ - GR\sin(\omega_0 t)\sin(\delta - \gamma) - V_C\rho_w x(1 + 2\mathrm{tg}\lambda)\, Rg\cos(\bar{\varphi}_2 + \delta - \gamma)/h_C & (33) \\ g\sin(\omega_0 t + \delta - \lambda) = \ddot{x} + f_w g\cos(\omega_0 t + \delta - \lambda) & (34) \end{cases}$$

Solving a simplified mathematical model of the second phase in a similar way to solution the of a simplified mathematical model of the first phase, we get:

$$\omega_2(t) \approx \frac{Q_P S_{C1} l_P \sin(\bar{\varphi}_2 + \alpha) - \sigma GR\cos(\delta - \gamma)}{2S_{C1}^2 l_P^2 \sin(\bar{\varphi}_2 + \alpha)\sin(\bar{\varphi}_2 + \psi)} + \left[\frac{2S_{C1}R}{Q_P}\sin\left(\frac{Q_P}{2S_{C1}R}t\right) - t\right] \times$$
$$\times \frac{\sigma V_C\rho_w(1 + 2\mathrm{tg}\lambda)\, R^2 g^2\, [\cos(\delta - \lambda) + f_w\sin(\delta - \lambda)]\cos(\bar{\varphi}_2 + \delta - \gamma)}{Q_P S_{C1} l_P^2 \sin(\bar{\varphi}_2 + \alpha)\sin(\bar{\varphi}_2 + \psi) h_C} \quad (35)$$

$$\varphi_2(t) = \frac{Q_P S_{C1} l_P \sin(\bar{\varphi}_2 + \alpha) - \sigma GR\cos(\delta - \gamma)}{2S_{C1}^2 l_P^2 \sin(\bar{\varphi}_2 + \alpha)\sin(\bar{\varphi}_2 + \psi)} t - \left[\frac{t^2}{2} + \frac{4S_{C1}^2 R^2}{Q_P^2}\left(\cos\left(\frac{Q_P}{2S_{C1}R}t\right) - 1\right)\right] \times$$
$$\times \frac{\sigma V_C\rho_w(1 + 2\mathrm{tg}\lambda)\, R^2 g^2\, [\cos(\delta - \lambda) + f_w\sin(\delta - \lambda)]\cos(\bar{\varphi}_2 + \delta - \gamma)}{Q_P S_{C1} l_P^2 \sin(\bar{\varphi}_2 + \alpha)\sin(\bar{\varphi}_2 + \psi) h_C} \quad (36)$$

$$t_2 \approx \frac{2S_{C1}^2 l_P^2 \sin(\bar{\varphi}_2 + \alpha)\sin(\bar{\varphi}_2 + \psi)}{Q_P S_{C1} l_P \sin(\bar{\varphi}_2 + \alpha) - \sigma GR\cos(\delta - \gamma)}\varphi - \frac{2l_P}{Rg} \times$$
$$\times \sqrt{\frac{-Q_P S_{C1} l_P^2 \sin(\bar{\varphi}_2 + \alpha)\sin(\bar{\varphi}_2 + \psi) h_C \varphi}{\sigma V_C\rho_w(1 + 2\mathrm{tg}\lambda)\, R^2 g^2\, [\cos(\delta - \lambda) + f_w\sin(\delta - \lambda)]\cos(\bar{\varphi}_2 + \delta - \gamma)}} \quad (37)$$

$$p_2(t) \approx \frac{V_C\rho_w(1 + 2\mathrm{tg}\lambda)\, R^2 g^2 \cos(\bar{\varphi}_2 + \delta - \gamma)}{16Q_P^2 l_P h_C \sigma\sin(\bar{\varphi}_2 + \alpha)} \{S_{C1}R\sigma[\sin(\delta - \lambda) - f_w\cos(\delta - \lambda)] \times$$
$$\times [\cos(Q_P/(2S_{C1}R)t) - 1] - 8KW_{12}Q_P[\cos(\delta - \lambda) + f_w\sin(\delta - \lambda)]\} \quad (38)$$

The dynamics of container upturning can be approximately described on the basis of the obtained functional dependencies for separate phases as follows:

$$\omega(t) = \begin{cases} \omega_1(t), \text{ for } \varphi \le \pi / 2 - \delta + \lambda \\ \omega_2(t), \text{ for } \varphi > \pi / 2 - \delta + \lambda \end{cases} \tag{39}$$

$$\varphi(t) = \frac{Q_P S_{C1} l_P \sin(\bar{\varphi} + \alpha) - \sigma G R \cos(\delta - \gamma)}{2S_{C1}^2 l_P^2 \sin(\bar{\varphi} + \alpha) \sin(\bar{\varphi} + \psi)} t - \left[\frac{t^2}{2} + \frac{4S_{C1}^2 R^2}{Q_P^2}\left(\cos\left(\frac{Q_P}{2S_{C1}R} t\right) - 1\right)\right] \times$$
$$\times \mathbf{1}\left(\varphi - \frac{\pi}{2} + \delta - \lambda\right) \frac{\sigma V_C \rho_w (1 + 2\mathrm{tg}\lambda) R^2 g^2 \left[\cos(\delta - \lambda) + f_w \sin(\delta - \lambda)\right] \cos(\bar{\varphi}_2 + \delta - \gamma)}{Q_P S_{C1} l_P^2 \sin(\bar{\varphi}_2 + \alpha) \sin(\bar{\varphi}_2 + \psi) h_C} \tag{40}$$

$$p(t) = \begin{cases} p_1(t), \text{ for } \varphi \le \pi / 2 - \delta + \lambda \\ p_2(t), \text{ for } \varphi > \pi / 2 - \delta + \lambda \end{cases} \tag{41}$$

where:
$\bar{\varphi} = (\bar{\varphi}_1 + \bar{\varphi}_2)/2$ – average value of the angle of container upturning at a first approximation.

Comparison of the results, obtained with the use of full and simplified mathematical models of a hydraulic drive of container upturning during SDW loading into a dustcart, as well as by means of the equations, obtained in the result of the analytical solution of a simplified model is presented in Figure 2.

When using the equations (19), (37), such duration dependence of container upturning during SDW loading into a dustcart from the main parameters of its hydrodrive is obtained.

$$t = \begin{cases} t_1(\varphi), \text{ for } \varphi \le \pi / 2 - \delta + \lambda \\ t_2(\varphi), \text{ for } \varphi > \pi / 2 - \delta + \lambda \end{cases} \tag{42}$$

When comparing the duration of container upturning, obtained with the use of a full mathematical model and equations (39, 40, 41), obtained in the result of analytical solution of a simplified mathematical model of hydraulic drive of container upturning during SDW loading into a dustcart, an error makes up about 10% at the beginning of motion and reduces to about 2–5% at the end of motion in comparison with the full mathematical model, that is acceptable for the execution of previous project calculations. If necessary, the values of the main parameters can be specified at the final stage of projecting by means of a full mathematical model.

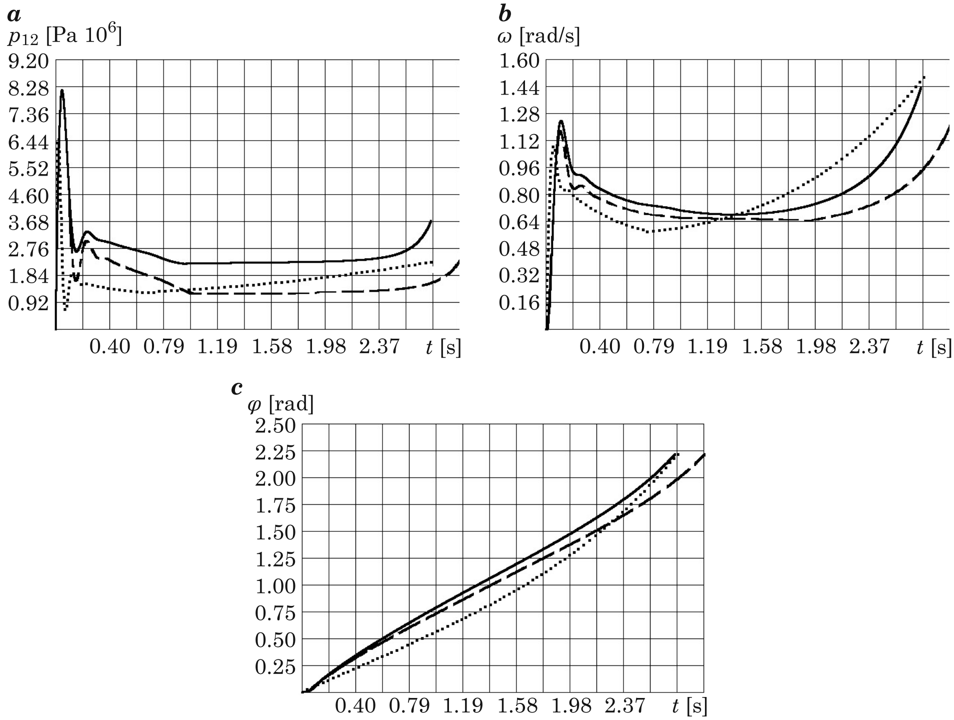

Fig. 2. Comparison of results, obtained with the use of full (——) and simplified (- - -) mathematical models of hydraulic drive of container upturning during SDW loading into a dustcart, as well as by means of equations obtained as result of its analytical solution (·····): *a* – change of pressure in the hydrocylinder, *b* – change of angular velocity, *c* – change of rotation angle

The obtained regression equation (42) allows to approximately define the duration of container upturning during SDW loading into a dustcart that can be used during performing of project calculations of new dustcarts constructions without the necessity of studying a full mathematical model of hydrodrive of its working organs, and also during the optimization of main parameters of a hydraulic drive.

Figure 3 shows the duration dependence of container upturning t from the distance between rotation centers of a capture and a rod l_p and the angle between axes of a lever and a shoulder of a hydrocylinder α, built according to the regression equation (42).

Comparison of power and speed characteristics for basic and optimal values of the main parameters of working organs of container upturning during SDW loading into a dustcart is presented in Figure 4. Reducing of the process duration of container upturning is accompanied by increased pressure in a delivery pipe of a hydrocylinder (Fig. 4a) and by increased angular velocity of container upturning (Fig. 4b).

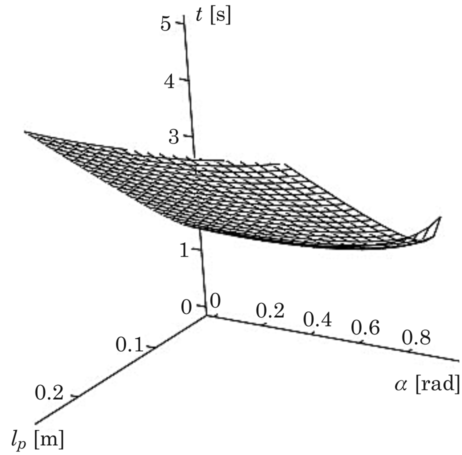

Fig. 3. The duration dependence of container upturning t from distance between rotation centers of a capture and a rod l_p and from the angle between axes of a lever and a shoulder of a hydrocylinder α

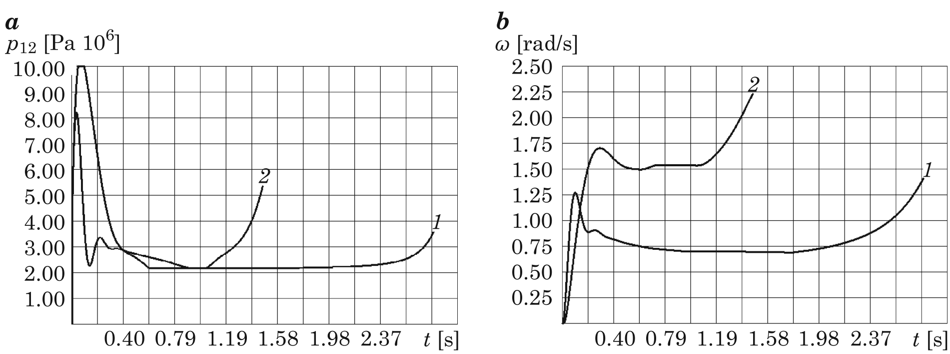

Fig. 4. Comparison of power (*a*) and speed (*b*) characteristics for basic (*1*) and optimal (*2*) values of main parameters of working organs of container upturning during SDW loading into a dustcart

By means of dependence (42) in MathCAD environment, the optimal values of the distance between the rotation centers of the capture and the rod $l_{p.\text{opt}}$ = 38 mm and the angle between the axes of a lever and a shoulder of a hydrocylinder α_{opt} = 11° for which duration of container upturning will be minimal $t_{\min}$ = 1.468 s are defined, that can be used for process intensification of SDW loading into a dustcart with the reduction purpose of fuel consumption.

We define the yearly fuel savings for public utilities of Ukraine by the formula:

$$Q_S = q_{ro}K_cN_d\left(\frac{t_c}{t_c - n_c(t_{uc.b} - t_{uc.\min})/3{,}600} - 1\right) = 10 \cdot 1276 \cdot 4{,}100 \times$$
$$\times\left(\frac{1.89}{1.89 - 21(2{,}755 - 1.468)/3{,}600} - 1\right) = 208{,}690(l) \approx 209 \text{ [tons]} \tag{43}$$

where:

q_{ro} – rate of fuel consumption during one working cycle of SDW collecting into a basket of a dustcart [l],

K_c – yearly quantity of working cycles of a dustcart [units],

N_d – dustcarts quantity of public utilities of Ukraine [units],

t_c – duration of a working cycle of SDW collecting into a basket of a dustcart [h],

n_c – quantity of containers with SDW, that can be loaded into a basket of a dustcart per one cycle [units],

$t_{uc.b}$, $t_{uc.\min}$ – duration of container upturning for basic and optimal values of the main parameters of working organs, respectively [s].

Conclusions

1. For performing of project calculations of new constructions of dustcarts the approximate analytical time dependencies of pressure in a delivery pipe of a hydrocylinder, angular velocity and angle container upturning on the basis of a proposed simplified mathematical model of a hydraulic drive of container upturning during loading of solid domestic wastes into a dustcart are obtained.

2. Approximate duration dependence of container upturning from the main parameters of hydraulic drive is detected, on the basis of which the optimal values of distance between the rotation centers of a capture and a rod $l_{P.\mathrm{opt}}$ = 38 mm and the angle between the axes of a lever and a shoulder of a hydrocylinder α_{opt} = 11° are defined, for which the duration of container upturning will be minimal $t_{\min}$ = 1.468 s, that can be used for intensification of the loading process of solid domestic wastes with the reduction purpose of fuel consumption at 209 tons/year.

References

BEREZYUK O.V. 2009. *Mathematical modelling of forecasting of the volumes forming of solid domestic waste and the areas of polygons and dumps in Ukraine.* Modern Technologies, Materials and Constructions in Civil Engineering, 2: 88–91.

BEREZYUK O.V. 2013. *Mathematical modeling of the dynamic of hydraulic drive of working organs of container upturning during solid domestic waste loading into the dustcart.* Herald of Khmelnytskyi national university. Technical Sciences, 5: 60–64.

Norba. Refuse Collection Vehicle Kl-10. 1977. Blomstermala, 3–4.
Pressmullfahrzeuge Faun Europress. 1995. Osterholz-Scharmbeck, 2–3.
SAVULYAK V.I., BEREZYUK O.V. 2006. *Technical support of collecting, transportation and preparations of solid domestic wastes to processing*. Monograph. Universum-Vinnytsia, Vinnytsia.
Schörling: Vehicle Technology for the Environment. 1990. Hannover.
SVESHNIKOV A.G., TIHONOV A.N. 2005. *Functions theory of a complex variable*. Fizmatlit, Moscow.
Zoeller. 1990. Stockerau.

Technical Sciences, 2017, 20(3), 275–288

Quarterly peer-reviewed scientific journal
ISSN 1505-4675
e-ISSN 2083-4527
TECHNICAL SCIENCES
Homepage: www.uwm.edu.pl/techsci/

DESIGN CONCEPT AND PARAMETERS OF A CONICAL BAR SEPARATOR

Beata Jadwisieńczak, Zdzisław Kaliniewicz

Department of Heavy Duty Machines and Research Methodology
University of Warmia and Mazury in Olsztyn

Received 13 December 2016, accepted 5 June 2017, available online 22 June 2017.

Key words: seeds, cleaning and separation, separator, geometrical relationships.

Abstract

The process of adapting a screen separator to seeds of a given species and variety requires a corresponding set of replaceable screens. Screen replacement is a time-consuming process. Screens are often selected from the available size range, therefore, cleaning and separation processes are not always optimized. This study proposes a design concept of a new device for cleaning and separating seeds, which features a conical bar screen that rotates around its own axis. The screen has grooves whose width is smallest at the beginning of the screen and increases along the screen surface. Seeds can be sorted into various size fractions by changing the position of collecting buckets under the screen. The functional parameters of the separating device were designed based on a review of publications describing the size of the most popular agricultural seeds. The basic geometrical relationships in the proposed conical bar screen were described. The geometrical parameters of the screen were selected on the assumption that the radius at which bars are fixed to the screen can range from 200 mm to 400 mm and that bar diameter can range from 5 mm to 10 mm. Two variants of the device were proposed as a replacement for one universal separating screen. The first variant will be used to sort small seeds, including seeds of small-seeded legumes, seeds of major cereal species and medium-sized seeds with dimensions similar to cereal seeds, whereas the second variant will be applied to separate large seeds, including seeds of large-seeded legumes and plumper seeds from the medium-size fraction. The width of grooves at the beginning and end of the screen should equal 1 mm and 5 mm in the first variant and 2.5 mm and 13 mm in the second variant, respectively.

Symbols:
CV – coefficient of variation of a trait [%],
d – bar diameter [mm],
L – length of bar screen [mm],
n – number of grooves in the screen,

Correspondence: Zdzisław Kaliniewicz, Katedra Maszyn Roboczych i Metodologii Badań, Uniwersytet Warmińsko-Mazurski w Olsztynie, ul. Oczapowskiego 11/B112, 10-719 Olsztyn, phone: 48 89 523 39 34, e-mail: zdzislaw.kaliniewicz@uwm.edu.pl

r_1 – bar spacing at the beginning of the screen [mm],
r_2 – bar spacing at the end of the screen [mm],
R_1 – radius at which bars are fixed to clamp rings at the beginning of the screen [mm],
R_2 – radius at which bars are fixed to clamp rings at the end of the screen [mm],
s – groove width at distance x from the beginning of the screen [mm],
s_1 – groove width at the beginning of the screen [mm],
s_2 – groove width at the end of the screen [mm],
SD – standard deviation of seed thickness [mm],
x – distance from the beginning of the screen [mm],
β – base angle of a conical screen [degrees],
γ – opening angle of a conical screen [degrees].

Introduction

Seed mixtures are most often cleaned and sorted with the use of pneumatic and screen separators on account of their high efficiency (GROCHOWICZ 1994). Every screen separator is equipped with a collecting bucket and a set of mostly flat screens. Screens have openings that are formed through the appropriate arrangement of wires or perforations in sheet metal. The shape and size of openings is designed based on the separator's efficiency and the species of separated seeds. The openings in every screen have identical geometry and dimensions. The seeds are separated into two fractions: the fraction that is retained by the screen (retained fraction) and the fraction that passes through the screen (sifted fraction). The screens installed in collecting buckets are set at an angle to ensure that the retained fraction is set into motion by a moving bucket and to guarantee the continuity of the sorting process.

Most separators are equipped with a set of screens. Screens are replaced to account for the parameters of different seed species or same-species batches with various seed plumpness. This laborious process has prompted researchers to design new devices where the seed separation process, regardless of crop species, would not require time-consuming modifications. One of such solutions involves a string sieve where strings are stretched between horizontal bars (KALINIEWICZ 2013b, 2015). At the beginning of the screen, strings are attached to a bar in a single row at equal distances, and at the end of the screen, strings are attached to at least one bar, where one string is placed under another to create grooves whose width increases with the distance from the beginning of the screen. Seeds are sorted into various size fractions by changing the position of collecting buckets under the string sieve. A theoretical analysis of the sorting process (KALINIEWICZ 2013a) revealed that seeds are propelled into motion when the string sieve is positioned at an estimated angle of 45°, and to ensure the continuity of the sorting process, the string sieve should be set at an angle of around 50°. The choice of such a large inclination angle leads to an excessive increase in the dimensions of the screen separator, in particular height, and lowers separation efficiency. To avoid the above scenario, the inclination angle of a string sieve should not exceed 10°, and seeds should be propelled into motion by a moving collecting bucket (KALINIEWICZ, DOMAŃSKI 2013). In the analyzed case, the angular velocity of the transmission shaft has to be higher than the speed of conventional collecting buckets because at lower angular velocity, seeds will be wedged in grooves, thus clogging the screen. Due to the numerous disadvantages of such separators, the solution proposed in this study was based on a conical bar separator (JADWISIEŃCZAK et al. 2016).

The aim of this study was to analyze the structure and geometrical parameters of a conical bar separator, and to determine whether it can be adjusted to clean and separate seeds of basic crop species.

Materials and Methods

In the present experiment, the parameters of a conical bar separator were selected based on geometrical relationships between the separator's working elements and the physical properties of seeds. This study is constitutes the first stage of comprehensive research investigating the conical separator. The next stages of research will include the development of a mathematical model of the seed separation process carried out with the use of the proposed separator, and experimental verification and validation of the model. Our findings will be discussed in separate articles.

The following assumptions were made in the initial stages of designing a conical separator:

– the separator is to replace a conventional screen separator for cleaning and sorting agricultural seeds, equipped with replaceable screens with longitudinal openings,

– the working element of the proposed separator is the inner surface of a truncated cone with grooves along the perimeter. Groove width increases towards the end of the screen,

– the screen is positioned at a small angle to move seeds towards the end of the screen when it is set in rotary motion,

– the screen is composed of bars with identical diameter, permanently attached to two clamp rings (Fig. 1) with a smaller diameter at the inlet and a larger diameter at the outlet,

– groove width at the beginning of the screen is smaller than the thickness of the smallest seeds of the principal species, and groove width at the end of the screen is larger than the thickness of the largest seeds of the principal species,

– the screen can be formed by bars which have different sections (circular, square, triangular, hexagonal, etc.) and are made of various materials,

– collecting buckets for different seed fractions are positioned under the screen.

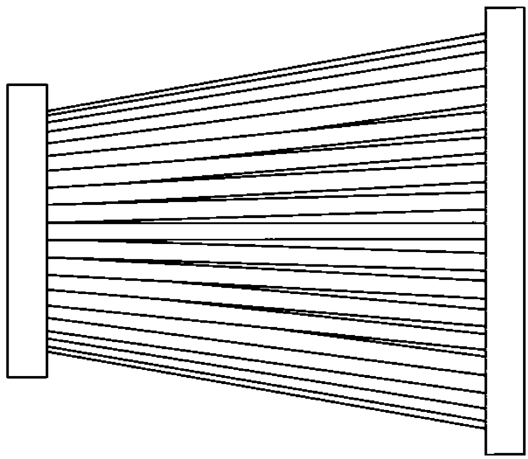

Fig. 1. View of a conical bar screen

Results and Discussion

Geometrical relationships in a bar screen

The screen will be composed of cylindrical bars with diameter d (Fig. 2). Bars will be fixed to clamp rings at equal distances, and the size of the resulting grooves will change from s_1 to s_2 between the beginning and end of the screen. Bar spacing at the beginning and end of the screen can be calculated with the use of the below formulas:

$$r_1 = s_1 + d \tag{1}$$

$$r_2 = s_2 + d \tag{2}$$

The following relationships can be derived based on the n number of grooves along the screen perimeter:

$$2 \cdot \pi \cdot R_1 = n \cdot r_1 \tag{3}$$

$$2 \cdot \pi \cdot R_2 = n \cdot r_2 \tag{4}$$

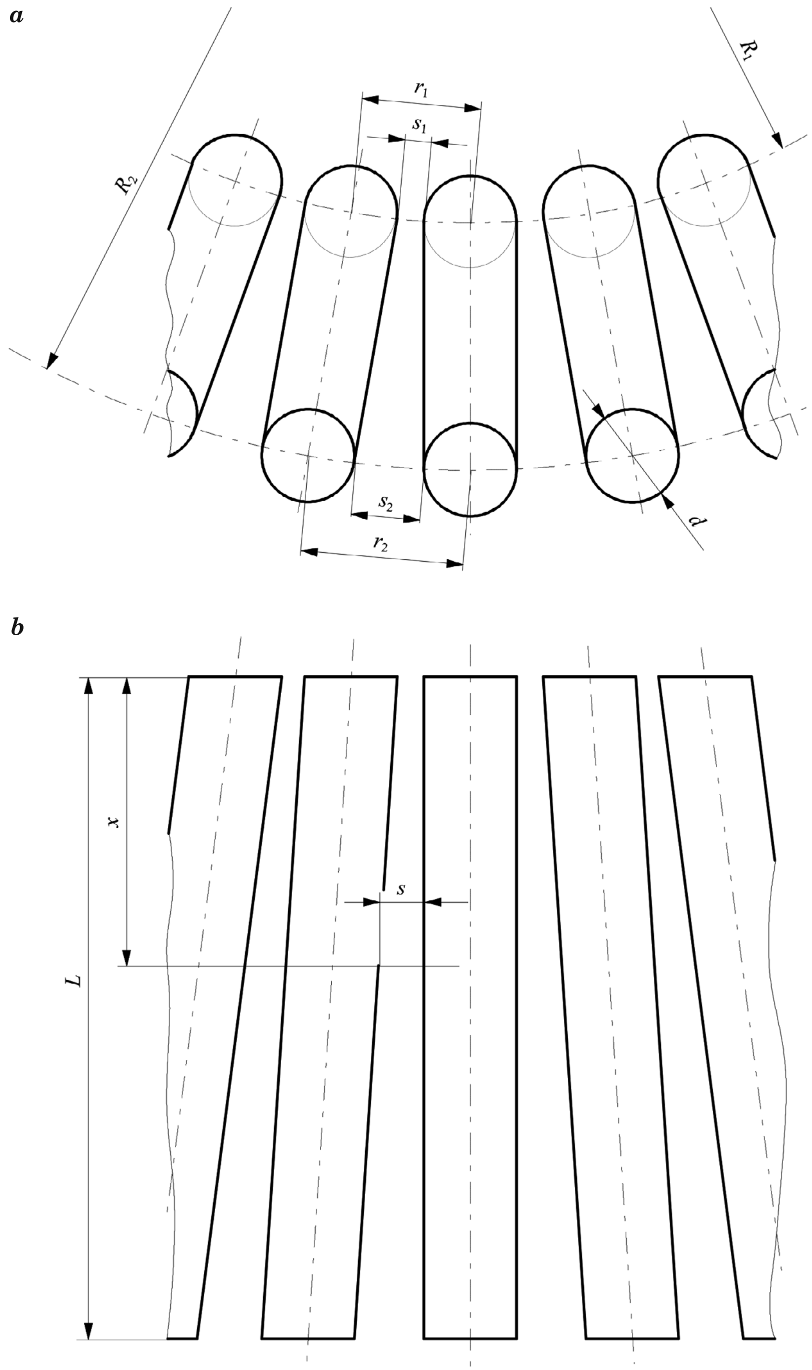

Fig. 2. Arrangement of bars in a conical screen: a – rear view, b – top view

Formulas (1) and (2) are substituted and equation (3) is divided by equation (4) to produce the following dependence:

$$\frac{2 \cdot \pi \cdot R_2}{2 \cdot \pi \cdot R_1} = \frac{n \cdot (s_2 + d)}{n \cdot (s_1 + d)} \tag{5}$$

which can be transformed to:

$$R_2 = R_1 \cdot \frac{s_2 + d}{s_1 + d} \tag{6}$$

The above formula suggests that radius R_2 at which bars are fixed to the ring at the end of the screen is determined by four parameters: radius R_1 at which bars are fixed to the ring at the beginning of the screen, groove width s_1 and s_2 at the beginning and at the end the screen, respectively, and bar diameter d.

Groove width at a given point on the screen is determined by the distance from the beginning of the screen. In line with the similar triangles theorem, the result is:

$$\frac{(s - s_1)}{x} = \frac{(s_2 - s_1)}{L} \tag{7}$$

Formula (7) is transformed, and groove width s is calculated with the use of the below equation:

$$s = \frac{(s_2 - s_1) \cdot x}{L} + s_1 \tag{8}$$

Seeds whose thickness is identical to the calculated groove width should pass through the screen at that point into the corresponding collecting bucket, whereas thicker seeds should be set into motion by the rotating screen and should move along the rotation axis until they reach a groove opening with the corresponding size.

Based on general trigonometric identities, the opening angle γ of bars can be calculated with the use of the below formula:

$$\gamma = \text{arc tg} \frac{s_2 - s_1}{L} \tag{9}$$

The slant height of a truncated cone meets the cone axis at angle β which can be determined from the below trigonometric equation:

$$\sin \beta = \frac{R_2 - R_1}{L} \tag{10}$$

Equations (1) to (4) are substituted into formula (10) to produce:

$$\beta = \text{arc sin} \frac{n \cdot (s_2 - s_1)}{2 \cdot \pi \cdot L} \tag{11}$$

Geometrical parameters of seeds

The process of designing new devices for seed cleaning and sorting requires knowledge about the physical properties of the separated material (GROCHOWICZ 1994). The relevant data are used select the appropriate screen and the sequence of separation processes to produce material of desired quality (GROCHOWICZ 1994, MAJEWSKA et al. 2000). Information about the physical parameters of seeds is also needed when modeling and designing other processes, including seed production, harvesting, transport, cleaning, sorting, drying, storage and processing (GROCHOWICZ 1994, ÇALIŞIR et al. 2005, ALTUNTAS, DEMIRTOLA 2007, BOAC et al. 2010, KALKAN, KARA 2011).

Seeds of the same crop species and variety can also differ in plumpness. Their parameters are influenced by many factors, in particular soil and climatic conditions, cultivation practices, genetic factors, moisture content and even position on the maternal plant (GEODECKI, GRUNDAS 2003, ÇALIŞIR et al. 2005, ALTUNTAS, DEMIRTOLA 2007, YALÇIN et al. 2007, KALKAN, KARA 2011, GRZESIK et al. 2012, MIRZABE et al. 2012, KIM et al. 2014). The designed device poses an alternative to screen separators with longitudinal openings, therefore, the basic geometrical parameters of the separated seeds, in particular distribution of seed thickness, have to be determined.

Table 1 presents the parameters of seeds of principal crop species with moisture content adequate for storage, without classification into groups based on varieties and cultivation practices (the relevant references are cited under the table). The thickness of small seeds (group I – rapeseed, mustard) ranges from 1.1 to 2.5 mm. The thickness of medium-sized seeds (group II) ranges from 1.2 mm (oats and rye) to 6.1 mm (vetch). In the group of principal cereal species (group IIa), seed thickness varies from 1.2 mm to 4.7 mm. The greatest variation in thickness is observed in the group of large seeds (group III).

Table 1

Range of variation in the geometrical properties of selected seeds

Size fraction	Species	Seed group	Seed dimensions thickness [mm]	width [mm]	length [mm]	References
Small	mustard	I	1.1–2.4	1.1–2.7	1.4–3.0	3, 36
	rapeseed		1.2–2.5	1.6–2.8	1.7–2.8	1, 3, 9, 23
Medium	barley	IIa	1.4–4.7	2.0–5.0	7.0–14.6	4, 14, 15, 21, 23
	oats		1.2–3.6	1.4–4.0	8.0–18.6	4, 15, 23
	rye		1.2–4.4	1.5–4.9	5.0–10.5	10, 22, 27
	triticale		1.7–4.2	1.9–4.3	5.3–10.4	10, 29, 37
	wheat		1.4–3.9	1.6–4.5	4.3–10.2	4, 7, 10, 23, 24, 33
	buckwheat	IIb	2.0–4.2	3.0–5.2	4.4–8.0	4, 6, 16, 35
	rice		1.6–2.5	2.0–3.6	5.3–9.8	19, 23
	sunflower		1.7–6.0	3.5–9.9	7.5–24.3	4, 23, 28
	vetch		2.0–6.1	3.2–6.3	3.2–7.5	4, 12, 35
Large	corn	III	2.6–12.8	4.8–16.4	7.7–20.3	13, 23, 25, 30, 32
	faba bean		3.1–9.9	4.8–12.9	7.1–21.8	2, 31, 34, 35
	lupine		2.9–8.5	3.1–8.5	3.9–13.6	5, 8, 11, 20, 35
	pea		3.5–10.1	3.7–10.2	4.0–10.5	4, 17, 20, 35
	soybean		3.3–8.1	5.0–9.5	5.2–11.2	18, 23, 26

1 – Rawa et al. (1990), 2 – Mieszkalski (1991), 3 – Choszcz, Wierzbicki (1994), 4 – Grochowicz (1994), 5 – Zduńczyk et al. (1996), 6 – Kim et al. (2002), 7 – Mabille, Abecasis (2003), 8 – Mańkowski (2004), 9 – Çalişir et al. (2005), 10 – Hebda, Micek (2005), 11 – Lema et al. (2005), 12 – Taser et al. (2005), 13 – Coşkun et al. (2006), 14 – Rybiński, Szot (2006), 15 – Hebda, Micek (2007), 16 – Kram et al. (2007), 17 – Yalçin et al. (2007), 18 – Cho et al. (2008), 19 – Varnamkhasti et al. (2008), 20 – Rybiński et al. (2009), 21 – Sýkorová et al. (2009), 22 – Zdybel et al. (2009), 23 – Boac et al. (2010), 24 – Kalkan, Kara (2011), 25 – Tarighi et al. (2011), 26 – Xu et al. (2011), 27 – Jouki et al. (2012), 28 – Mirzabe et al. (2012), 29 – Tomporowski (2012), 30 – Babić et al. (2013), 31 – Kara et al. (2013), 32 – Akinyosoye et al. (2014), 33 – Kim et al. (2014), 34 – Sundaram et al. (2014), 35 – Kaliniewicz et al. (2015), 36 – Mieszkalski et al. (2015), 37 – Suleiman et al. (2015).

In corn, this parameter ranges from 2.6 mm to even 12.8 mm. The data presented in Table 1 indicate that the parameters of the evaluated seeds fall into the below range of values:
– seed thickness – 1.1÷12.8 mm,
– seed width – 1.1÷16.4 mm,
– seed length – 1.4÷21.8 mm.

Parameters of a conical bar screen

Groove width in a conical bar screen for cleaning and sorting seeds of three size fractions is presented in Table 2. As previously indicated, groove width at the beginning of the screen should be somewhat smaller than the thickness of the smallest seeds of the principal species, whereas groove width at the end of the screen should be somewhat larger than the thickness of the largest seeds of the principal species. Therefore, groove width for small seeds (group I) should be set at 1 mm at the beginning of the screen and 3 mm at the end of the screen. For the seeds of major cereal species (group IIa), groove width should be set at 1 mm and 5 mm, respectively. The resulting screen can also be used for sorting seeds of small-seeded legumes. Medium-sized seeds should be separated with the use of screens with groove width of 1 mm and 6.5 mm, and large seeds – with the use of screens with groove width of 2.5 mm and 13 mm, respectively. A universal device for sorting seeds from all size fractions should be fitted with a screen with groove width of 1 mm and 13 mm, respectively. Similar conclusions relating to groove width were formulated by KALINIEWICZ (2013b) in a study of a string sieve.

Table 2

Parameters of a conical bar screen

Screen parameter	Seed group						
	I	IIa	I+IIa	IIb	I+II	III	I+II+III
s_1 [mm]	1.0	1.0	1.0	1.5	1.0	2.5	1.0
s_2 [mm]	3.0	5.0	5.0	6.5	6.5	13.0	13.0
L [mm]	534	1067	1067	889	1467	1120	3200
γ [°]	0.215	0.215	0.215	0.322	0.215	0.537	0.215

I – small seeds (mustard, rapeseed),
IIa – principal cereal species (barley, oats, rye, triticale and wheat),
IIb – other medium-sized seeds (buckwheat, rice, sunflower, vetch),
II – medium-sized seeds (IIa + IIb),
III – large seeds (corn, faba bean, lupine, pea, soybean).

For the sorting process to effectively separate seeds into at least 3 size fractions, the seeds of a given species and variety should be sorted along a screen segment of minimum 30 cm. The coefficients of variation in seed dimensions are generally determined in the range of 6% to 20%. For the needs of this study, the coefficient of variation in seed thickness was set at CV = 12%. If groove width at the beginning of the screen is equal to the minimum value of a given dimension of the separated seeds, and the range (i.e. the difference between the maximum and minimum values) corresponds to six values of standard deviation SD in seed thickness, then formula (7) takes the following form:

$$\frac{s_1 + 6 \cdot \mathrm{SD} - s_1}{x} = \frac{s_2 - s_1}{L} \tag{12}$$

The equation can be transformed as follows:

$$L = \frac{x \cdot (s_2 - s_1)}{6 \cdot \mathrm{SD}} \tag{13}$$

Standard deviation of a parameter can be determined from the formula for calculating its coefficient of variation CV. In the analyzed case, the formula takes the following form:

$$\mathrm{CV} = 100 \cdot \frac{\mathrm{SD}}{s_1 + 3 \cdot \mathrm{SD}} \tag{14}$$

The equation can be transformed to produce:

$$\mathrm{SD} = \frac{\mathrm{CV} \cdot \mathrm{s}_1}{100 - 3 \cdot \mathrm{CV}} \tag{15}$$

The resulting dependence is substituted into formula (13) to produce the following equation:

$$L = \frac{x \cdot (s_2 - s_1) \cdot (100 - 3 \cdot \mathrm{CV})}{6 \cdot \mathrm{CV} \cdot \mathrm{s}_1} \tag{16}$$

The experimental values of the analyzed parameters, $x = 300$ mm and CV = 12%, are introduced into the above equation:

$$L = \frac{800}{3} \cdot \frac{s_2 - s_1}{s_1} \tag{17}$$

The length of a conical bar screen, determined with the above formula, is given in Table 2. The universal sorting device should have a bar screen with an estimated length of 3.2 m. However, only a small portion of such a screen (30 cm segment) would be used to sort seeds of a given crop species. For this reason, two variants of the proposed device have been designed: one for sorting small seeds, including seeds of small-seeded legumes and seeds of major cereal species (variant 1 for group I+IIa seeds), and the other for sorting large seeds (variant 2 for group III seeds). Each variant will be equipped with a conical bar screen with an estimated length of 1.1 m. Variant 1 will be used to separate seeds of buckwheat, rice and small-seeded varieties of sunflower and vetch, whereas variant 2 will be used to separate seeds of large-seeded varieties of the above species. The opening angle of screen bars will be $\gamma = 0.215^{\circ}$ in variant 1 and $\gamma = 0{,}537^{\circ}$ in variant 2.

According to GROCHOWICZ (1994), the diameter of rotating cylindrical screens and industrial cylindrical graders ranges from 400 mm to 800 mm. Therefore, the radius at which bars are fixed to the clamp ring at the beginning of the screen should be minimum 200 mm, and the radius at which bars are fixed at the end of the screen should not exceed 400 mm. In a given screen variant, the number of grooves is determined by the diameter of screen bars. Based on formulas (3) and (4), the number of grooves should meet the following condition:

$$\frac{2 \cdot \pi \cdot R_1}{s_1 + d} \leq n \leq \frac{2 \cdot \pi \cdot R_2}{s_2 + d} \tag{18}$$

The limiting values of radii at which bars are fixed to clamp rings are substituted into the above formula to produce:

$$\frac{1256.6}{s_1 + d} \leq n \leq \frac{2513.5}{s_2 + d} \tag{19}$$

The left side of the equation representing $n_{\min}$ is rounded up to the nearest integer, and the right side representing $n_{\max}$ is rounded down to the nearest integer. Bars with a diameter of 5 mm to 10 mm will be used to produce a rigid structure, minimize screen weight and produce screens with the highest number of grooves. The parameters of both variants are presented in Table 3. The screen for sorting small seeds and seeds of principal cereal species (variant 1) can be made of bars whose diameters cover the entire range of proposed values. The number of grooves may range from 115 (bar diameter $d = 10$ mm) to even 251 (bar diameter $d = 5$ mm), depending on bar diameter. The base angle of a conical bar screen decreases with an increase in bar diameter from around 3.8° to around 8.4° in variant 1.

The diameter of bars in a conical screen designed for large seeds is more limited and should not exceed 8.12 mm. A screen comprising bars with a diameter of 8.12 mm will have 119 grooves. When bars with a diameter of 9–10 mm are used, the screen will have 101 to 114 grooves and an estimated base angle of 8.8–10°.

Table 3

Parameters of two variants of the proposed conical bar screen

Variant	Parameter	Bar diameter d [mm]					
		5	6	7	8	9	10
V-1 (s_1 = 1 mm, s_2 = 5 mm, L = 1.1 m)	n_{min} [–]	210	180	157	140	126	115
	n_{max} [–]	251	228	209	193	179	167
	R_2/R_1 [–]	1.67	1.57	1.50	1.44	1.40	1.36
	β_{min} [°]	6.981	5.980	5.213	4.647	4.182	3.816
	β_{max} [°]	8.353	7.583	6.947	6.413	5.946	5.546
V-2 (s_1 = 2.5 mm, s_2 =13 mm, L = 1.1 m)	n_{min} [–]	–	–	–	–	110	101
	n_{max} [–]	–	–	–	–	114	109
	R_2/R_1 [–]	–	–	–	–	1.91	1.84
	β_{min} [°]	–	–	–	–	9.620	8.826
	β_{max} [°]	–	–	–	–	9.973	9.532

Conclusions

The proposed variants of a conical bar separator pose an alternative to a conventional separator with a set of screens with longitudinal openings. The first variant has been designed for separating buckwheat seeds, rapeseeds and seeds of principal cereal species, whereas the second variant can be used to separate large seeds. The width of screen grooves changes continuously along the screen and corresponds to the size of the separated seeds. Seeds of a given species and variety could be separated by adjusting the position of collecting buckets under the screen. Screens for separating seeds of major agricultural crops should have an estimated length of 1.1 mm, and groove width at the beginning and end of the screen should equal 1 mm and 5 mm, respectively, in variant 1, and 2.5 mm and 13 mm, respectively, in variant 2. Bar diameter can range from 5 mm to 10 mm in variant 1, and from 8.12 mm to 10 mm in variant 2.

References

Akinyosoye S.T., Adetumbi J.A., Amusa O.D., Olowolafe M.O., Olasoji J.O. 2014. *Effect of seed size on in vitro seed germination, seedling growth, embryogenic callus induction and plantlet regeneration from embryo of maize (Zea mays L.) seed*. Nigerian Journal of Genetics, 28: 1–7. http://dx.doi.org/10.1016/j.nigjg.2015.06.001.

Altuntas E., Demirtola H. 2007. *Effect of moisture content on physical properties of some grain legume seeds*. New Zealand Journal of Crop and Horticultural Science, 35(4): 423–433. http://dx.doi.org/10.1080/01140670709510210.

Babić L.J., Radojçin M., Pavkov I., Babić M., Turan J., Zoranović M., Stanişić S. 2013. *Physical properties and compression loading behaviour of corn seed*. International Agrophysics, 27: 119–126. http://dx.doi.org/10.2478/v10247-012-0076-9.

Boac J.M., Casada M.E., Maghirang R.G., Harner III J.P. 2010. *Material and interaction properties of selected grains and oilseeds for modeling discrete particles*. Transaction of ASABE, 53(4): 1201–1216. http://dx.doi.org/10.13031/2013.32577.

ÇALIŞIR S., MARAKOĞLU T., ÖĞÜT H., ÖZTÜRK Ö. 2005. *Physical properties of rapeseed (Brassica napus oleifera L.)*. Journal of Food Engineering, 69: 61–66. http://dx.doi.org/10.1016/j.jfoodeng.2004.07.010.

CHO G.T., LEE J., MOON J.K., YOON M.S., BAEK H.J., KANG J.H., KIM T.S., PAEK N.CH. 2008. *Genetic diversity and population structure of Korean soybean landrace [Glycine max (L.) Merr.]*. Journal of Crop Science and Biotechnology, 11(2): 83–90. http://dx.doi.org/10.3390/ijms17030370.

CHOSZCZ D., WIERZBICKI K. 1994. *A study the separation of field bedstraw (Galium aparine) seeds from rape and mustard seeds with the use of their geometrical and aerodynamic properties*. Acta Acad. Agricult. Tech. Olst. Aedif. Mech., 25: 61–69 (article in Polish with an abstract in English).

COŞKUN M.B., YALÇIN Í., ÖZARSLAN C. 2006. *Physical properties of sweet corn seed (Zea mays saccharata Sturt.)*. Journal of Food Engineering, 74: 523–528. http://dx.doi.org/10.1016/j.jfoodeng.2005.03.039.

GEODECKI M., GRUNDAS S. 2003. *Characterization of geometrical features of single winter and spring wheat kernels*. Acta Agrophysica, 2(3): 531–538 (article in Polish with an abstract in English).

GROCHOWICZ J. 1994. *Maszyny do czyszczenia i sortowania*. Wydawnictwo Akademii Rolniczej, Lublin.

GRZESIK M., JANAS R., GÓRNIK K., ROMANOWSKA-DUDA Z. 2012. *Biological and physical methods of seed production and processing*. Journal of Research and Applications in Agricultural Engineering, 57(3): 147–152 (article in Polish with an abstract in English).

HEBDA T., MICEK P. 2005. *Dependences between geometrical features of cereal grain*. Inżynieria Rolnicza, 6: 233–241 (article in Polish with an abstract in English).

HEBDA T., MICEK P. 2007. *Geometric features of grain for selected corn varieties*. Inżynieria Rolnicza, 5(93): 187–193 (article in Polish with an abstract in English).

JADWISIEŃCZAK B., JADWISIEŃCZAK K., KALINIEWICZ Z., PAWŁOWSKI K. 2016. *Przesiewacz szczelinowy*. Patent application No. P.418250 of 8.08.2016.

JOUKI M., EMAM-DJOMEH Z., KHAZAEI N. 2012. *Physical properties of whole rye seed (secale cereal)*. International Journal of Food Engineering, 8(4): article 7. http://dx.doi.org/10.1515/1556-3758.2054.

KALINIEWICZ Z. 2013a. *A theoretical analysis of cereal seed screening in a string sieve*. Technical Sciences, 16(3): 234–247.

KALINIEWICZ Z. 2013b. *String sieve: design concept and parameters*. Technical Sciences, 16(2): 119–129.

KALINIEWICZ Z. 2015. *Sito strunowe*. Patent No. 218968, patent application of 24.10.2011, published in the WUP of 27.02.2015.

KALINIEWICZ Z., DOMAŃSKI J. 2013. *A movable string sieve – analysis of seed screening*. Technical Sciences, 16(4): 253–264.

KALINIEWICZ Z., MARKOWSKI P., ANDERS A., JADWISIEŃCZAK K. 2015. *Frictional properties of selected seeds*. Technical Sciences, 18(2): 85–101.

KALKAN F., KARA M. 2011. *Handling, frictional and technological properties of wheat as affected by moisture content and cultivar*. Powder Technology, 213: 116–122. http://dx.doi.org/10.1016/j.powtec.2011.07.015.

KARA M., SAYINCI B., ELKOCA E., ÖZTÜRK I., ÖZMEN T.B. 2013. *Seed size and shape analysis of registered common bean (Phaseolus vulgaris L.) cultivars in Turkey using digital photography*. Tarym Bilimleri Dergisi – Journal of Agricultural Sciences, 19: 219–234.

KIM Y.B., KIM S.L., LEE K.CH., CHANG K.J., KIM N.S., SHIN Y.B., PARK CH.H. 2002. *Interspecific hybridization between Korean buckwheat landraces (Fagopyrum esculentum Moench) and self-fertilizing buckwheat species (F. homotropicum Ohnishi)*. Fagopyrum, 19: 37–42.

KIM K.H., SHIN S.H., PARK S., PARK J.C., KANG C.S., PARK C.S. 2014. *Relationship between pre-harvest sprouting and functional markers associated with grain weight, TaSUS2-2B, TaGW2-6A, and TaCWI-A1, in Korean wheat cultivars*. SABRO Journal of Breeding and Genetics, 46(2): 319–328.

KRAM B.B., WOLIŃSKI J., WOLIŃSKA A. 2007. *Comparative studies on geometric traits of nutlets with and without seed cover in Red corolla buckwheat*. Acta Agrophysica, 9(3): 657–664 (article in Polish with an abstract in English).

LEMA M., SANTALLA M., RODIÑO A.P., DE RON A.M. 2005. *Field performance of natural narrow-leafed lupin from the northwestern Spain*. Euphytica, 144: 341–351. http://dx.doi.org/10.1007/s10681-005-8187-z.

MABILLE F., ABECASSIS J. 2003. *Parametric modelling of wheat grain morphology: a new perspective*. Journal of Cereal Science, 37: 43–53. http://dx.doi.org/10.1006/jcrs.2002.0474.

MAJEWSKA K., GUDACZEWSKI W., FORNAL Ł. 2000. *Size of wheat grains and rheological properties of dough*. Inżynieria Rolnicza, 5(16): 153–162 (article in Polish with an abstract in English).

MAŃKOWSKI S. 2004. *Metoda rozdrabniania nasion łubinu i wydzielania cząstek okrywy nasiennej*. Doctoral dissertation, Faculty of Technical Sciences, UWM in Olsztyn.

MIESZKALSKI L. 1991. *Influence of moisture on the geometrical features of faba bean seeds and also variation of these features with given variety*. Acta Acad. Agricult. Tech. Olst. Aedif. Mech., 22: 43–55 (article in Polish with an abstract in English).

MIESZKALSKI L., ŻUK Z., SZCZYGLAK P. 2015. *Mathematical modeling of the shape of the seed of white mustard (Sinapis alba L.)*. Postępy Techniki Przetwórstwa Spożywczego, 1: 62–66 (article in Polish with an abstract in English).

MIRZABE A.H., KHAZAEI J., CHEGINI G.R. 2012. *Physical properties and modeling for sunflower seeds*. Agricultural Engineering International: The CIGR e-journal, 14(3): 190–202.

RAWA T., WIERZBICKI K., PIETKIEWICZ T. 1990. *Potential effectiveness of rape seeds cleaning according to geometrical characteristics*. Acta Acad. Agricult. Tech. Olst. Aedif. Mech., 20: 117–129 (article in Polish with an abstract in English).

RYBIŃSKI W., SZOT B. 2006. *Estimation of genetic variability of yielding traits and physical properties of seeds of spring barley (Hordeum vulgare L.) mutants*. International Agrophysics, 20(3): 219–227.

RYBIŃSKI W., SZOT B., RUSINEK R., BOCIANOWSKI J. 2009. *Estimation of geometric and mechanical properties of seeds of Polish cultivars and lines representing selected species of pulse crops*. International Agrophysics, 23: 257–267.

SULEIMAN R., XIE K., ROSENTRATER K. 2015. *Physical and thermal properties of chia, kañiwa, triticale and farro as a function of moisture content*. Agricultural and Biosystems Engineering Conference Proceedings and Presentations, Paper Number: 152189412. doi: 10.13031/aim.20152189412.

SUNDARAM P.K., SINGH A.K., KUMAR S. 2014. *Studies on some engineering properties of faba bean seeds*. Journal of AgriSearch, 1(1): 4–8.

SYKOROVÁ A., ŞÁRKA E., BUBNÍK Z., SCHEJBAL M., DOSTÁLEK P. 2009. *Size distribution of barley kernels*. Czech Journal of Food Science, 27: 249-258.

TARIGHI J., MAHMOUDI A., ALAVI N. 2011. *Some mechanical and physical properties of corn seed (Var. DCC 370)*. African Journal of Agricultural Research, 6(16): 3691–3699. doi: 10.5897/AJAR10.521.

TASER O.F., ALTUNTAS T., OZGOZ E. 2005. *Physical properties of Hungarian and common vetch seeds*. Journal of Applied Sciences, 5(2): 323–326. http://dx.doi.org/10.3923/jas.2005.323.326.

TOMPOROWSKI A. 2012. *Filling model for the working multi-disc biomass grain grinding unit*. The Archive of Mechanical Engineering, LIX(2): 2155–174. http://dx.doi.org/10.2478/v10180-012-0008-z.

VARNAMKHASTI M.G., MOBLI H., JARAFI A., KEYHANI A.R., SOLTANABADI M.H., RAFIEE S., KHEIRALIPOUR K. 2008. *Some physical properties of rough rice (Oryza sativa L.) grain*. Journal of Cereal Science, 47: 496–501. http://dx.doi.org/10.1016/j.jcs.2007.05.014.

XU Y., LI H.N., LI G.J., WANG X., CHENG L.G., ZHANG Y.M. 2011. *Mapping quantitative trait loci for seed size traits in soybean (Glycine max L. Merr.)*. Theoretical and Applied Genetics, 122(3): 581–594. http://dx.doi.org/10.1007/s00122-010-1471-x.

YALÇIN Y., ÖZARSLAN C., AKBAŞ T. 2007. *Physical properties of pea (Pisum sativum) seed*. Journal of Food Engineering, 79: 731–735. http://dx.doi.org/10.1016/j.jfoodeng.2006.02.039.

ZDUŃCZYK Z., JUŚKIEWICZ J., FLIS M., AMAROWICZ R., KREFFT B. 1996. *The chemical composition and nutritive value of low-alkaloid varieties of white lupin. 1. Seed, cotyledon and seed coat characteristics*. Journal of Animal and Feed Sciences, 5: 63–72.

ZDYBEL A., GAWŁOWSKI S., LASKOWSKI J. 2009. *Influence of moisture content on some physical properties of rye grains*. Acta Agrophysica, 14(1): 243–255 (article in Polish with an abstract in English).

Technical Sciences, 2017, 20(3), 289–296

Quarterly peer-reviewed scientific journal
ISSN 1505-4675
e-ISSN 2083-4527
TECHNICAL SCIENCES
Homepage: www.uwm.edu.pl/techsci/

UNIWERSYTET WARMIŃSKO-MAZURSKI W OLSZTYNIE

CHANGES OF CRYSTALLITE SIZES IN THE OXIDE LAYER FORMING DURING LONG-TERM OPERATION OF 10CrMo9-10 STEEL

Monika Gwoździk

Institute of Materials Engineering
Faculty of Production Engineering and Materials Technology
Czestochowa University of Technology

Received 26 January 2016, accepted 14 April 2017, available online 4 May 2017.

Key words: 10CrMo9-10 steel, oxide layer, X-ray diffraction, crystallite sizes.

Abstract

The paper contains results of the studies on X-ray diffraction analysis XRD (studying the phase composition, crystallite sizes) of oxide layers on 10CrMo9-10 steel, operated for a long time at an elevated temperature (T = 525°C, t = 200,000 h). The oxide layer was studied on a surface and a cross-section at the outer on the inlet both on the fire and counter-fire side of the tube wall surface. X-ray studies were carried out on the outer surface of a tube, and then the layer surface was polished down and the diffraction measurements were performed again to determine crystallite size in oxide layers. Based on the width and the position of the main coat and substrate reflections, the size of the crystallites was determined using the Scherrer formula.

Introduction

Currently, many scientific centres are conducting diversified materials research related to surface engineering (Frangini et al. 2014, Labisz 2014, 2015, Ţălu et al. 2015, Kulesza, Bramowicz 2014, Szafarska, Iwaszko 2012), particularly with the oxidation of steel used in the power industry (Bischoff et al. 2013, Priss et al. 2014, Antonov et al. 2013).

Correspondence: Monika Gwoździk, Instytut Inżynierii Materiałowej, Politechnika Częstochowska, ul. Armii Krajowej 19, 42-200 Częstochowa, e-mail: gwozdzik.monika@wip.pcz.pl

In the power industry, apart from low-alloy steels like 10CrMo9-10 (10H2M) or 13CrMo4-5 (15HM), also high-alloy steels are used, such as e.g. X10CrMoVNb9-1 (P91), which is characterised primarily by an increased chromium content. A higher chromium content makes that this steel has better anti-corrosion properties as compared with low-alloy steels. However, despite that there is a need to diagnose both this steel and low-alloys steels resistance to the operation of a steam and flue gases environment existing in components operated long time at high temperatures and during a few hundred thousand hours (GWOŹDZIK 2014, 2016, KLEPACKI, WYWROT 2010, KLEPACKI 2006).

Studies carried out have shown that the kinetics of corrosion on steels operating long-term at elevated temperatures is complex and depends inter alia on (GWOŹDZIK 2014): chemical composition of steel, operating temperature of the element, operating time, flowing medium (flue gas side, steam side), flue gas type, morphology of individual oxide layers.

In paper (GWOŹDZIK 2013) it has been found that $NaFePO_4$, $Zn_2P_2O_7$, Na_2SO_4, $Fe_3(PO_4)_2$, Al_2SiO_5, $ZnSO_4$ are formed as a result of long-term operation (t = 100,000 h) of 10CrMo9-10 steel at the temperature of 575°C (directly from the exhaust gas). Hematite (Fe_2O_3) occurs on the outer surface of the tube. Then magnetite (Fe_3O_4) appears below hematite.

Material and Experimental Methods

The material studied comprised specimens of 10CrMo9-10 steel taken from a pipeline operated at the temperature of 525°C during 200,000 hours. The oxide layer was studied on a surface and a cross-section at the outer on the inlet both on the fire and opposite fire (counter-fire) side of the tube wall surface Figure 1.

Thorough examinations of the oxide layer carried out on the outer surface of tube wall comprised:

– microscopic examinations of the oxide layer were performed using an Olympus SZ61 and GX41 optical microscope (LM), Jeol JSM-6610LV scanning electron microscope (SEM),

– thickness measurements of formed oxide layers,

– chemical composition analysis of deposits/oxides using a Jeol JSM-6610LV scanning electron microscope (SEM) working with an Oxford EDS electron microprobe X-ray analyser,

– X-ray (XRD) measurements (studying the phase composition, crystallite sizes); the layer was subject to measurements using a Seifert 3003T/T X-ray diffractometer and the radiation originating from a tube with a cobalt anode

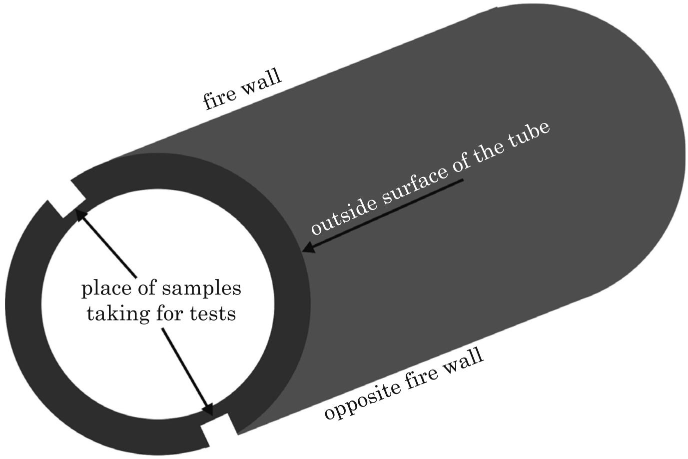

Fig. 1. Place of samples taking for tests

(λ_{Co} = 0.17902 nm). X-ray studies were performed, comprising measurements in a symmetric Bragg-Brentano geometry (XRD). A computer software and the DHN PDS, PDF4+2009 crystallographic database were used for the phase identification. X-ray studies were carried out on the outer surface of a tube, and then the layer surface was polished down and the diffraction measurements were performed again to determine individual oxide layers.

The size of crystallites of oxides was determined by the Scherrer relationship. Methods based on the analysis of diffraction line profile are used to determine the size of crystallites smaller than 100 nm and of lattice deformations (GWOŹDZIK 2016). Based on the width and the position of the main coat and substrate reflections, the size of the crystallites was determined using the Scherrer formula (1):

$$D_{hkl} = \frac{\mathrm{k} \cdot \lambda}{\beta \cdot \cos\Theta} \tag{1}$$

where:
D_{hkl} – crystallite size in the direction normal to (*hkl*) [nm],
k – constant (~1);
λ – radiation wavelength [nm],
β – reflection width depending on the crystallite size [rad],
Θ – Bragg angle [rad].

Results of examinations

The obtained results of macroscopic and microscopic studies on the oxides/deposits layer surface (Fig. 2) have shown a much greater degree of surface development on the fire side than on the counter-fire side. In addition, SEM studies (Figs. 2*c*, *d*) have shown that the formed deposits layer in certain places has a spheroidal nature. As compared with the counter-fire side the deposits formed on the fire side have larger dimensions.

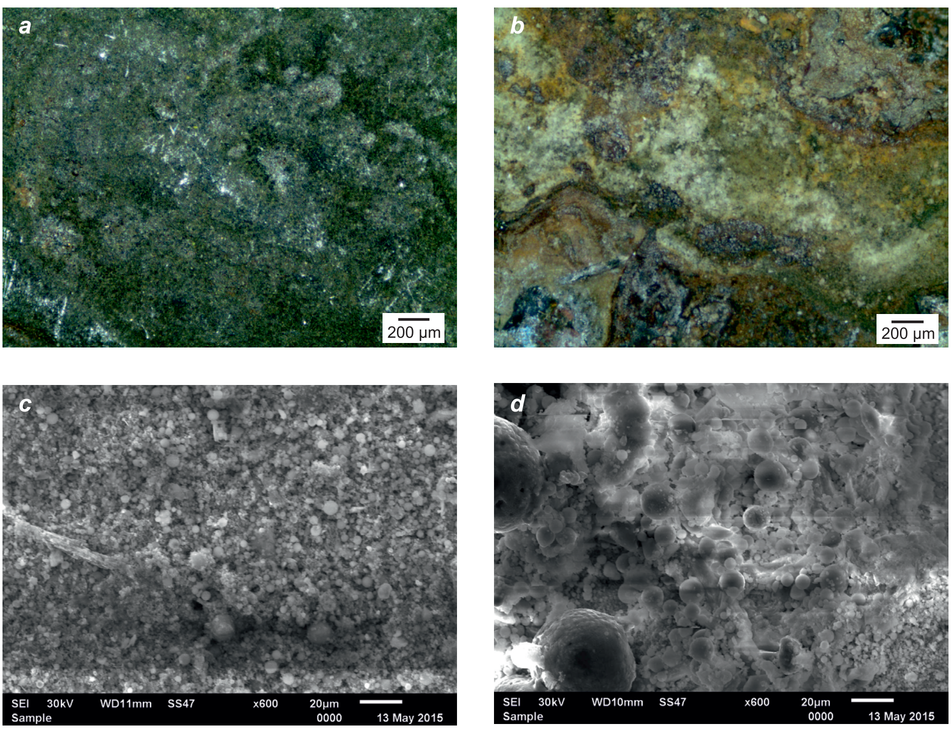

Fig. 2. Oxides formed on 10CrMo9-10 steel operated at 525°C during 200,000 hours: *a* – opposite fire wall LM (light microscopy), *b* – fire wall LM, *c* – opposite fire wall SEM (scanning electron microscopy), *d* – fire wall SEM

Microscopic examinations carried out on transverse microsections (Fig. 3) have shown that the deposits formed on the counter-fire side had a small thickness, reaching the depth of 9,83 μm. Instead, the formed oxide layer is 78.01 μm thick. On the fire side the deposits are 539 μm thick, while oxides 182,71 μm. The formed oxides/deposits layer, especially on the flue gas inflow side, is damaged to a significant extent.

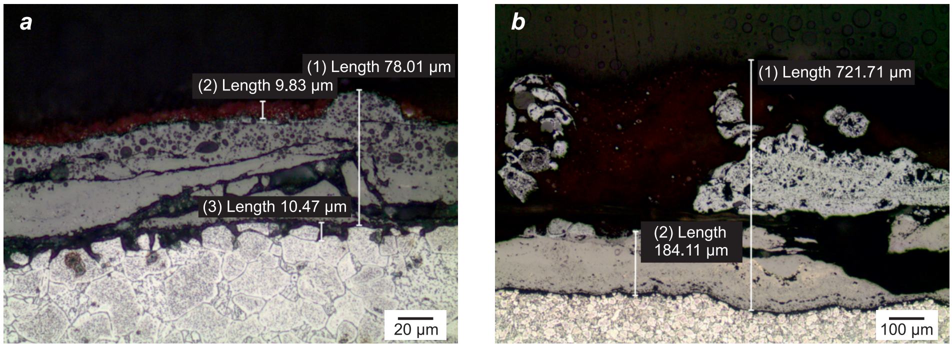

Fig. 3. The thickness of oxides layer formed on the steel examined: *a* – opposite fire wall – LM, *b* – fire wall – LM

The chemical analysis (EDS) (Fig. 4) comparison with XRD analysis on the fire side have shown that on the outside there are such deposits as: $CaSiO_2$, Al_2SiO_5 and $CaSO_4$. Fe_2O_3 and Fe_3O_4 oxides exist under this layer. Similar oxides were observed on the counter-fire side.

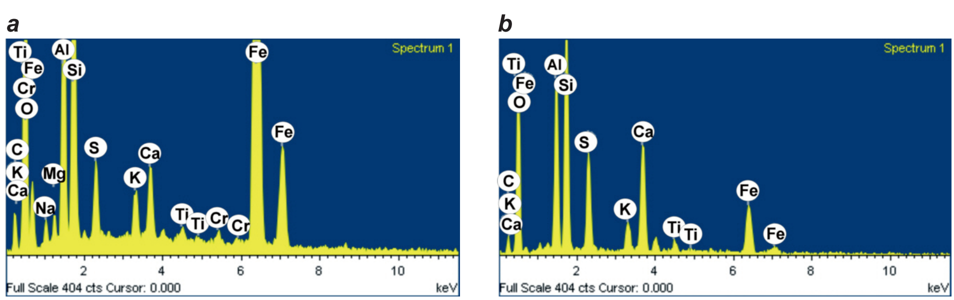

Fig. 4. EDS point microanalysis: *a* – opposite fire wall, *b* – fire wall

The size of Fe_2O_3 crystallites was determined for the (104) plane, while for Fe_3O_4 for the (311) plane. A layers of oxide 78 μm and 200 μm thick were studied (after polishing deposits), then the surface of the formed layer was polished in 11, 11, 9 and 15 cycles for Fe_2O_3 – opposite fire wall, Fe_3O_4 – opposite fire wall, Fe_2O_3 – fire wall, Fe_3O_4 – fire wall, respectively. One cycle consisted of polishing the layer to the depth of 2 μm (Fe_2O_3 – opposite fire wall), 5 μm (Fe_3O_4 – opposite fire wall), 5 μm (Fe_2O_3 – fire wall), 10 μm (Fe_3O_4 – fire wall). The exemplary of examine of XRD measurements has been shown in Figure 5.

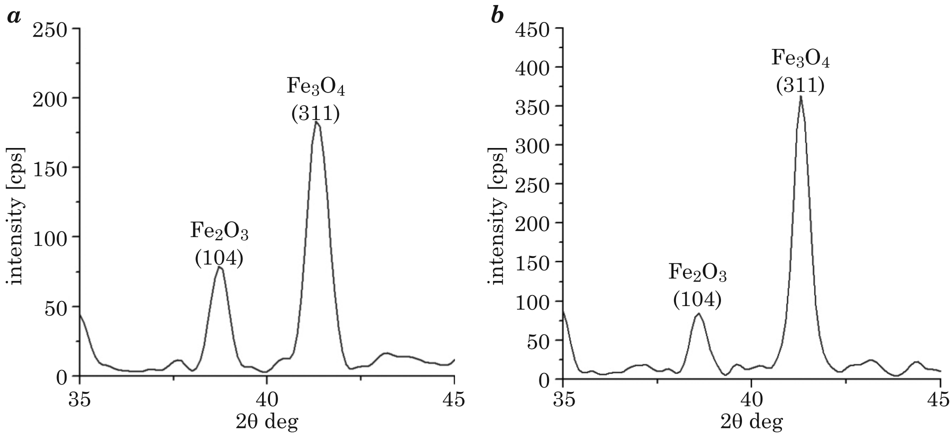

Fig. 5. X-ray diffraction patterns from the oxides layer obtained by means of XRD technique, after polishing: *a* – opposite fire wall, *b* – fire wall

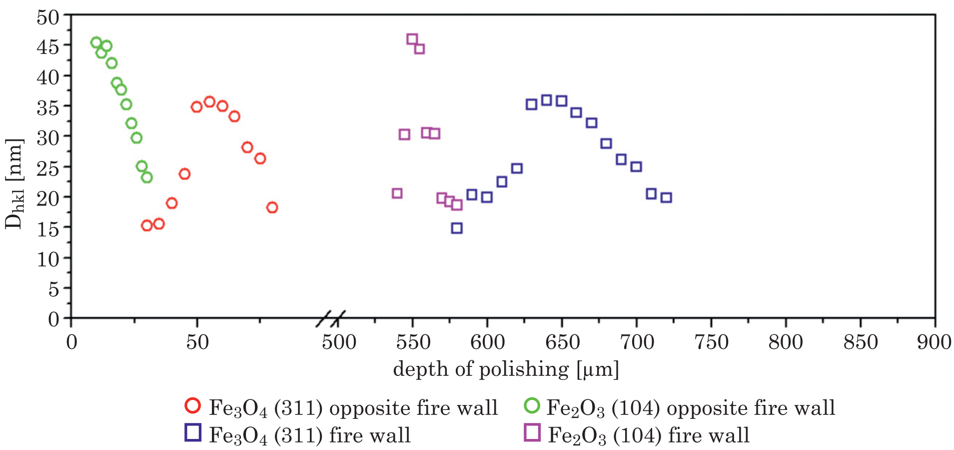

Fig. 6. Determination of crystallite size D_{hkl}

For the counter-fire side the size of hematite crystallites shows a downward trend after the next removal of the layer (Fig. 6). Fe_2O_3 crystallites at the depth of 10 µm are 45 nm in size. Instead, on the fire side the hematite peaks occur at the depth of 540 µm (Fig. 6). At this depth crystallites are 20 nm in size. A consecutive removal of the layer shows crystallites larger by 10 units, and the next two already by 15 units larger than in the previous polishing. At the depth of 560 µm the crystallites size is 30 nm. Instead, at the depth of 570–580 µm it is less than 20 nm. For magnetite in both cases (on the counter-fire as well as on the fire side) the crystallites size has a similar nature reaching the maximum of 35 nm (Fig. 6).

Summary

The paper contains assessment of hematite (Fe_2O_3) and magnetite (Fe_3O_4) formed on 10CrMo9-10 steel operated at the temperature of 525°C during 200,000 hours on the tube wall outside. Studies were carried out both for the fire and the counter-fire side. The obtained results of studies have shown that directly on the flue gas inflow side deposits are formed based on Al, Si and Ca. According paper (GAWRON, DANISZ 2012, GWOŹDZIK 2013) it has been found Al_2SiO_5 and $CaCO_3$.

The surface of deposits/oxides layer is more developed on the fire side. The deposits layer on the fire side is 539 μm thick, while on the counter-fire side only 10 μm. In both cases iron oxides Fe_2O_3 and Fe_3O_4 exist under the deposits layer. The size of hematite crystallites on the fire side at the maximum of its occurrence is D_{hkl} = 47 nm, while for the counter-fire side it is smaller by 2 units. Magnetite crystallites are smaller than those of hematite and in both cases (fire and counter-fire side) their size oscillates around 35 nm. The paper (GWOŹDZIK 2016) presents results of studies on oxides formed on the 10CrMo9-10 steel (on the flowing medium side (inside tube wall). Examinations carried out have shown that the formed layer is thicker and more degraded on the fire side. The size of crystallites on the fire side shows much larger dimensions both for hematite and magnetite. Instead, comparing the size of hematite and magnetite crystallites it is possible to state that in both cases (fire and counter-fire side) D_{hkl} is larger for hematite.

References

ANTONOV M., VEINTHAL R., HUTTUNEN-SAARIVIRTA E., HUSSAINOVA I., VALLIKIVI A., LELEIS M., PRISS J. 2013. *Effect of oxidation on erosive wear behaviour of boiler steels.* Tribology International, 68: 35–44.

BISCHOFF J., MOTTA A.T., EICHFELD C., COMSTOCK R.J., CAO G., ALLEN T.R. 2013. *Corrosion of ferritic-martensitic steels in steam and supercritical water*. Journal of Nuclear Materials, 441: 604–611.

FRANGINI S., MASCI A., MCPHAIL S.J., SOCCIO T., ZAZA F. 2014. *Degradation behavior of a commercial 13Cr ferritic stainless steel (SS405) exposed to an ambient air atmosphere for IT-SOFC interconnect applications*. Materials Chemistry and Physics, 144: 491–497.

GAWRON P., DANISZ S. 2012. *Dostosowanie zakresu badań diagnostycznych wybranych elementów kotłów pracujących w warunkach współspalania biomasy*. Energetyka, 702(12): 843–853.

GWOŹDZIK M. 2013. *Utlenianie stali 10CrMo9-10 podczas eksploatacji w wysokiej temperaturze*. Inżynieria Powierzchni, 1: 36–39.

GWOŹDZIK M. 2014. *Mechanizm degradacji warstw tlenkowych na stalach długotrwale eksploatowanych w energetyce.* Monografia, 291, Wydawnictwo Politechniki Częstochowskiej.

GWOŹDZIK M. 2016. *Analysis of Crystallite Size Changes in an Oxide Layer Formed on Steel Used in the Power Industry*. Acta Physica Polonica A, 130(4): 935–938.

KLEPACKI F., WYWROT D. 2010. *Trwałość wężownic przegrzewaczy wtórnych w warunkach niskoemisyjnego spalania*. Energetyka, 678(12): 816–820.

KLEPACKI F. 2006. *Korozja wysokotemperaturowa wężownic przegrzewaczy kotłów*. Energetyka, 621(3): 197–200.

KULESZA S., BRAMOWICZ M. 2014. *A comparative study of correlation methods for determination of fractal parameters in surface characterization*. Applied Surface Science, 293: 196–201.

LABISZ K. 2014. *Microstructure and mechanical properties of high power diode laser (HPDL) treated cast aluminium alloys*. Mat.-wiss. U. Werkstofftech, 45(4): 314–324.

LABISZ K. 2015. *Influence of Laser Feeding on Structure and Properties of Cast Aluminium Alloy Surface*. In: *Mechanical and Materials Engineering of Modern Structure and Component Design*. Eds. A. Öchsner, H. Altenbach. Advanced Structured Materials, 70. Springer, Cham, p. 317–343.

PRISS J., ROJACZ H., KLEVTSOV I., DEDOV A., WINKELMANN H., BADISCH E. 2014. *High temperature corrosion of boiler steels in hydrochloric atmosphere under oil shale ashes*. Corrosion Science, 82: 36–44.

SZAFARSKA M., IWASZKO J. 2012. *Laser remelting treatment of plasma-sprayed Cr_2O_3 oxide coatings*. Archives of Metallurgy and Materials, 57(1): 215–221.

ŢĂLU Ş., BRAMOWICZ M., KULESZA S., SHAFIEKHANI A., GHADERI A., MASHAYEKHI F., SOLAYMANI S. 2015. *Microstructure and Tribological Properties of FeNPs@a-C:H Films by Micromorphology Analysis and Fractal Geometry*. Industrial & Engineering Chemistry Research, 33 (54): 8212–8218.

Technical Sciences, 2017, 20(3), 297–309

Quarterly peer-reviewed scientific journal
ISSN 1505-4675
e-ISSN 2083-4527
TECHNICAL SCIENCES
Homepage: www.uwm.edu.pl/techsci/

BIM TECHNOLOGY IN GEOTECHNICAL ENGINEERING IN TERMS OF IMPACT HIGH BUILDING "MOGILSKA TOWER" IN CRACOW OF EXISTING BUILDING DEVELOPMENT

Dariusz Szwarkowski, Elżbieta Pilecka

Faculty of Civil Engineering
Cracow University of Technology

Received 18 March 2016, accepted 20 June 2017, available online 22 June 2017.

Key words: BIM, deep excavation, high building, settlement, influence of excavation, FEM.

Abstract

The article presents the use of BIM design method in geotechnical issues. BIM was used in the modeling of high building "Mogilska Tower" in Cracow. The object, as one of the few in Cracow, will have three underground storeys. High building with underground levels requires checking the impact of the implementation of a deep excavation on existing buildings. Analysis of settlement impact caused by deep excavation and the planned load of the building is based on the guidelines contained in the ITB (KOTLICKI, WYSOKIŃSKI 2002) standards by the simplified method and detailed method determined on the basis of numerical analysis. The article presents the results of the vertical deformation of ground adjacent to the existing object. The results of the calculations were compared with the limit values shown in ITB and PN-81/B-03020 (1985). Numerical analysis was performed in the spatial state of stress and strain model. It takes into account the spatial layout of the geotechnical subgrade and the terrain shape obtained by the measurement of terrestrial laser scanner. Subgrade was modeled elastic-plastic model of Mohr-Coulomb with linear condition of plasticity. Identified the influence and range of deep excavation and loads of the planned high building on existing development.

Correspondence: Dariusz Szwarkowski, Wydział Inżynierii Lądowej, Politechnika Krakowska im. Tadeusza Kościuszki, ul. Warszawska 24, 31-155 Kraków, phone: 12 628 25 66, e-mail: dszwarkowski@pk.edu.pl

Introductions

Building Information Modeling assumptions

The use of Building Information Modeling (BIM) in the construction industry, is currently the fastest growing new concept of obtaining and collecting data at every stage of design, modeling and implementation of buildings. The resulting data is used to update the assumptions during the construction projects. A new feature of the approach, assumptions using BIM methods, is another way of collecting data. The data are collected not only from the cycle of design and construction of the object, but also after its construction and during the exploitation until the decommissioning of buildings (TOMALA 2016). It means that, data set in the conceptof the method of BIM relate to each object lifecycle. These are not only parametric data model elements, taking into account the design, material and geometry of a particular item, for example characteristic of 3D modeling reinforced concrete beam. Also, it may be data on time execution of individual tasks on a construction site related by the stages of the object (4D models). BIM models allow to take into account cost management object (5D models). In the concept of BIM methods, deserve attention the information provided directly from the construction site (6D models), or during exploitation of a building (7D models) (TOMALA 2016). BIM is a comprehensive set of information about the building. Its containing a huge amount of data. They are made available to the various participants in the construction process: designers, engineers, managers, and contractors. The large number of entities involved in the provision of data to the model, must be based on common standards of design. This allows combine partial models developed by specialists of specific industries in a global model. The condition is compatibility model files to each other. It is important a common format for data storage, which allows the same interpretation of the models supplied by the various participants of a construction project. IFC is the basic standard for the recording format. Its used in the modeling project using BIM methods.

Building Information Modeling in geotechnical projects

Building Information Modeling is a record model in the form of elements in combination, represented in a parametric way of a specific identification number (ID). This allows explicit assignment of the properties the geometric elements, strength parameters, or material (TOMALA 2016).

In the cycle of collecting and transmitting data to the global database BIM model, data from the geotechnical industry are made available to the planning stage. These include geotechnical data layers of soil, the soil strength parameters: the angle of interior friction and cohesion. Geometric data related to course of geotechnical layers, developed on the basis of profiles of the research and prepared geotechnical sections. Application of BIM enables the acquisition of terrain data to project. It is obtained terrestrial laser scanning. Comprehensive data on the terrain shape and the course of geotechnical layers, are used to calculate the behavior of a building in the next stages of its implementation (ZHANG et al 2016). BIM data collection does not end at the design stage, but also includes, for example, data obtained from construction site. This allows update the assumptions made at the design stage.

In current practice of engineering, geotechnical project had closed source data. Modeling of the object using the assumptions of the BIM method enables connection geotechnical data and their use over the lifecycle of a building. The use of geotechnical data as part of the project BIM reduces the risk of the project, in the form of unexpected costs or extend the investment execution. Geotechnical data in the concept of BIM are not a new issue. In 1989 AGS (Association of Geotechnical and Geoenvironmental Specialists) created a data format for processing and use in other industries construction. Despite the many advantages implemented standard has not been widely used. The fundamental drawback was the inability to interpretation of the data, in the form of eg. surface course of geotechnical layers (MORIN et al. 2014). BIM solves problem with the interpretation of spatial geotechnical data. Adjustment of spatial geological models for use in the construction industry creates huge opportunities to take into account the behavior of complex object. Currently, the practice of engineering is based on the assumption that the layout of geotechnical layers is uniform along length and is not substantially changed. Hence, most of the analysis is based on the assumption of plane strain and stress state of geotechnical models. Application of BIM method in geotechnical design is necessary. Research conducted by HM Government (KESSLER et al. 2015) have shown that the construction sector, in 2025 will be dominated by the new approach BIM in 70%. In addition, in the UK since 2016 all investments in the system of public procurement (Industrial Strategy 2012), have to be aligned with existing standards BIM. Implementing BIM in the construction industry has the largest share in the US. Projects executed in this method, account for over 70% of the total number of ongoing contracts (Value of BIM in North America 2012). In Europe, the largest share of use BIM in the design focuses on three countries: Germany, France and UK. It represents a total of approximately 35% of all projects (KIVINIEMI 2010). The legal status of BIM adapting in the world is as follows (DI GIACOMO 2015):

a) Great Britain – required BIM technology in government projects. Projects implemented at BIM represent 39% of all;

b) Norway, Finland – Introduced regulations that allow BIM design;

c) Central and Southern European countries 14% of BIM projects, 60% of designers do not use this technology to design;

d) China – 5% implementation of BIM, a big upward trend;

e) Japan – almost 5% of BIM use in construction, 80% of participants in the construction process are aware of the use of this technology;

f) Austria – strong BIM adoption;

g) Singapore – 50% use BIM in construction;

h) US – largest share of the discussed technology. Special legal regulations: BIM standards, GSA & US Army BIM mandates.

In Polish conditions use of BIM method is not widely used. There are no legal solutions or standards precisely specifying the framework and extent of BIM method used in the construction industry (*Building Information Modeling. BIM in Poland* 2016).

The use of geoengineering in BIM is usually taken into account in the form of a load of pressure coming from the geotechnical layers layout. Often objects are modeled on the ground elastic behaviour. This assumptions omitting plastic properties of ground. This causes multiple errors at the stage of project design. Research conducted in the UK (KESSLER et al. 2015) have shown that more than 70% of investments in the public procurement system have exceeded the budget. The reason was poor recognition of geotechnical layers property. The article focuses on showing the use of BIM design method in geotechnical engineering. The use of that method will be presented in the context of the impact of a tall building "Mogilska Tower" in Cracow on existing buildings located in the vicinity of the planned investment. Building model was developed using Midas nGEN software based on the concept of BIM. In order to evaluate the impact of an object on the neighboring buildings, used data of geotechnical parameters (e.g strength parameters or the course of geotechnical layers). In addition, used terrestrial laser scanner in order to reflect the actual terrain shape. The resulting data were used to generate a numerical model of the area. In model used the loads results obtained from a model based on the BIM. The results were used to evaluate the influence of high building on neighboring buildings as specified (KOTLICKI, WYSOKIŃSKI 2002).

Materials and methods

Numerical analysis of high building model was carried out in the CAE/CAD Midas nGEN. Parametric building model consisted of 15 storeys above ground and 3 underground storeys. The total height of the building is equal 45 m. The object was fixed at a depth of -10 m below ground level. The building was realized in the frame construction, made of reinforced concrete load-bearing walls and partition walls from silicate blocks (PILECKA, SZWARKOWSKI 2017). Slabs, balconies, stairs were modeled as reinforced concrete elements. Figure 1 shows the visualization of the object (SEMACO INVESTMENT GROUP). The following assumptions for modeling tall building:

– the dimensions of the building plan: length: 51 m, width: 19.5 m;

– the dimensions of the underground building plan: length: 51 m, width: 19.5 m;

– the thickness of the monolithic elements, slabs and stairs: 15 cm;

– bearing walls of reinforced concrete with a thickness: 15 cm, 20 cm, 30 cm, 60 cm;

– thickness walls of silicate blocks: 10 cm and 15 cm.

Fig. 1. The concept of high building "Mogilska Tower" in Cracow
Source: www.semaco-ig.pl

Loads has been selected on the basis of standard (LENDUSZKO 2014). Adopted use loads for residential rooms, category *A*, equal to 2.0 kN m^{-2} for stairs 4.0 kN m^{-2} and balconies 2.0 kN/m^2. Material parameter of construction components and filling selected in standards (LENDUSZKO 2014). To determine the characteristic snow load on the model used standard (PAWŁOSKI, CAŁA 2013). Assumed load value equal to 0.96 kN/m^2. Detailed calculations of the load given in article (PIECKA, SZWARKOWSKI 2017). Figure 2 shows the pressure peaks of wind speed, together with the distribution of external pressure *c*pe,10 for high building.

Structural factor determined on the based on the logarithmic formula (EN 1991-1-4 2008) and the algorithm calculations presented in the article (ŻURAWSKI, GACZEK 2010). For building was chosen category 4 of the urban area. Logarithmic decrement of damping was equal to $\delta = 0.10$ for analyzed object.

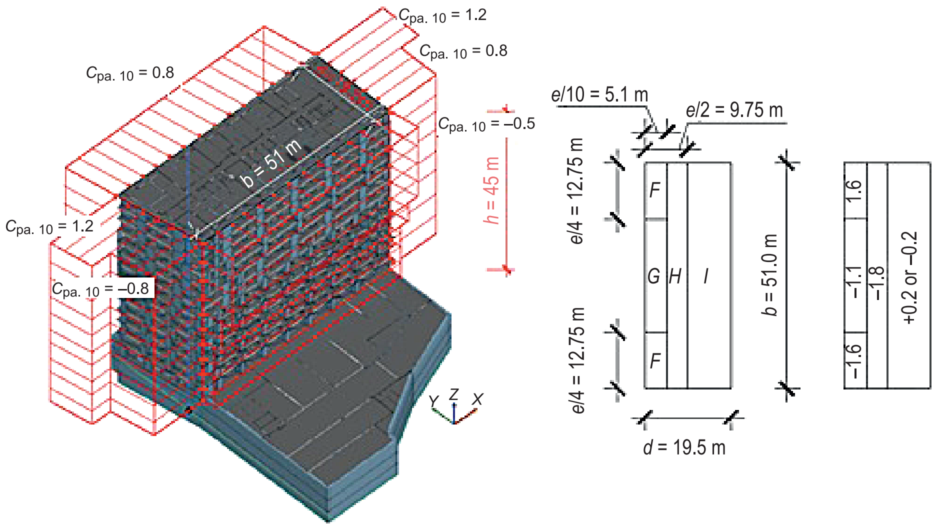

Fig. 2. Pressure peaks of wind speed, together with the distribution of external pressure $c_{pe,10}$
Source: PILECKA, SZWARKOWSKI (2017).

Eigenvalues determined in the article (PILECKA, SZWARKOWSKI 2017) were equal: for first the form of vibration f_1 = 2.70 Hz, for the second form of vibration f_2 = 3.01 Hz. Numerical model adopted on the level of detail LOD300 (TOMALA 2016). Numerical analysis was conducted based on flat finite elements. The mesh size was set equal to 0.5 m. Adopted unmovable boundary conditions at the base of the model. Numerical analysis was used to generate the reaction forces of the base model for next stages of raising the object. The individual values of the reaction forces used in the numerical model of the subgrade. It allowed to determine the impact of the implementation object to the existing buildings.

The spatial model of geotechnical layers of area in the vicinity of the planned building, made on the basis of geological engineering documentation (LENDUSZKO 2014). Linear change the course of geotechnical layers was adopted between the research profiles.

Subgrade of consider area is characterized by a complex geological structure. Anthropogenic soils occur below a depth of 1.6 m from ground level. Layer of gravel is from -1.6 m to -12 m below the ground level. Miocene clays are located at a depth of -13.3 m to -14.8 m. The numerical model of the subgrade takes into account the three layers of geotechnical. Table 1 shows the parameters of the layers included in the numerical model (SZWARKOWSKI 2017).

Geotechnical layers modeled elastic-plastic model of Mohr-Coulomb with linear plasticity condition. Area of land numerical model was generated based

Table 1

Geotechnical parameters of layers adopted in numerical modeling

Soil name	Φ [°]	c [kPa]	γ [kN/m^3]	E_0 [MPa]	ν [–]*	I_L/I_D
Ia1(saclSi)	13.00	13.50	20.50	16.50	0.25	0.30
IIa (MSa)	30.50	0.00	19.00	50.00	0.25	0.55
IIc (Gr saGr)	39.00	0.00	20.50	146.00	0.25	0.55
IIIa (Cl)	13.00	60.00	21.50	22.00	0.25	0.00

* information from CAŁA and FLISIAK (2000), GRIFFITHS and LANE (1999).

on the measurement of terrastrial laser scanning. Terrain model was created by combining triangular elements for point cloud. The cloud consists of several dozen millions of points obtained as a result of the measurement the laser beam. A detailed description of the research procedure using terrestrial laser scanning to generate the surface of the terrain for the numerical models are included in the article (SZWARKOWSKI, ZIĘBA 2017). A similar use of laser scanner in BIM was used in the modeling of a historic building in city Sondrio of Italy (BARAZZETTI et al. 2015).

Evaluation of the impact of high building "Mogilska Tower" in Cracow on existing buildings, in the context of the use BIM methods in geotechnical engineering, is based on the following stages of modeling:

– Stage I: Initial analysis model before executing the excavation. Linear static analysis;

– Stage II: Driving steel sheet piles to a depth of 16m below ground level to layer Miocene clays. Nonlinear static analysis;

– Stage III: Execution of a deep excavation to a depth of 10 m below ground level, along with the installed HP320 profiles. Nonlinear static analysis. Details in the article (SZWARKOWSKI 2017);

– Stage IV: Comparison of the results of vertical displacements obtained from numerical modeling of deep excavation with deformations obtained from measurements of terrestrial laser scanner and geodesic measurements (PILECKA, SZWARKOWSKI 2015);

– Stage V: Execution of underground storeys. Load implementation from the model of the building, to the level of the bottom of excavation. Nonlinear static analysis;

– Stage VI: The underground storeys backfilled with soil. Nonlinear static analysis;

– Stage VII: Execution of 6 floors above ground building. Nonlinear static analysis;

– Stage VIII: The loads from the self weight of the building model includes all 14 floors above ground. Nonlinear static analysis;

– Stage IX: Full load building model: loads: self weight, use load, weight of snow, wind pressure. Nonlinear static analysis;

– Stage X: Comparison of the results of vertical displacements in the vicinity of the existing building with the limit values set out in the specifications ITB (KOTLICKI, WYSOKIŃSKI 2002, PN-81/B-03020 1985).

Numerical model of the subgrade located in a deep excavation. It was modeled hexagonal finite elements of size 1 m. Subgrade close to excavation divided of finite elements mesh of size 2 m. Steel sheet, constituting the casing of excavation was modeled quadrangular finite elements of type shell. The size of shell elements is 1 m. Elements for the top beam and steel profiles matched the size of the finite elements of type beam equal to 1 m. Movements of the soil model is blocked at the horizontal direction, allowing freedom of displacement in the vertical direction. The basis of the model immobilized in three directions. Between elements of shell casing excavation and subgrade modeled contact, based on the Coulomb law (SZWARKOWSKI 2017). Results of vertical displacements, compared with the limit values for existing buildings situated in the vicinity of a deep excavation (KOTLICKI, WYSOKIŃSKI 2002). On the basis of the guidelines drawn up zone of direct influence of deep excavation on existing buildings and the zone of secondary impact, including the maximum range of influence of deep excavation. Figure 3 shows the range of impact zones of deep excavation on the existing building. Zone *S*I refers to the immediate effect of deep excavation on the existing development building and its range is 7 m. *S*II zone is associated with a secondary impact of the deep excavation and the proposed high building on the existing construction. Its range is not more than 20 m from the edge of the excavation.

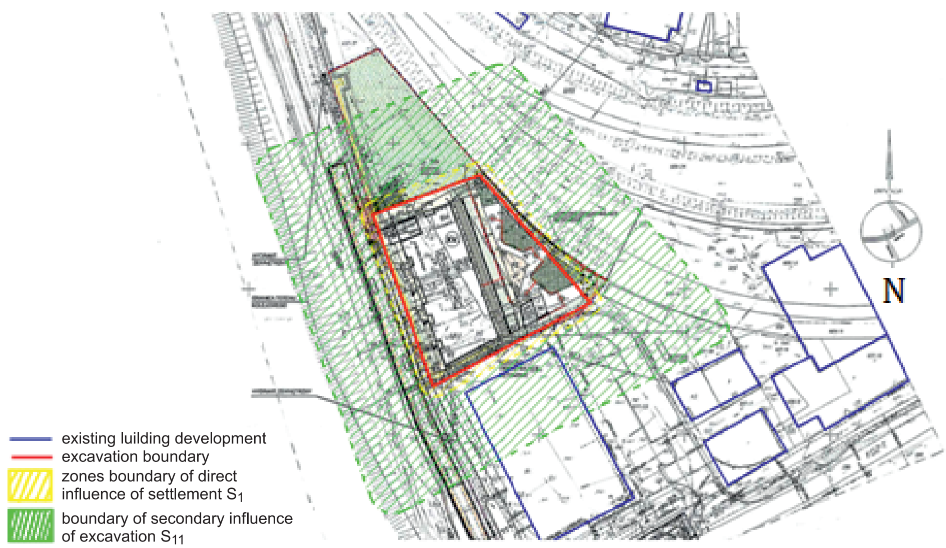

Fig. 3. The development plan with marked zones of influence of deep excavation
Source: SZWARKOWSKI (2017).

Maximum allowable settlement for the existing building structure should not exceed 8 cm, according to norm PN-81/B-03020 (1985). Figure 4 shows the procedure for assessing the impact of a tall building on existing development.

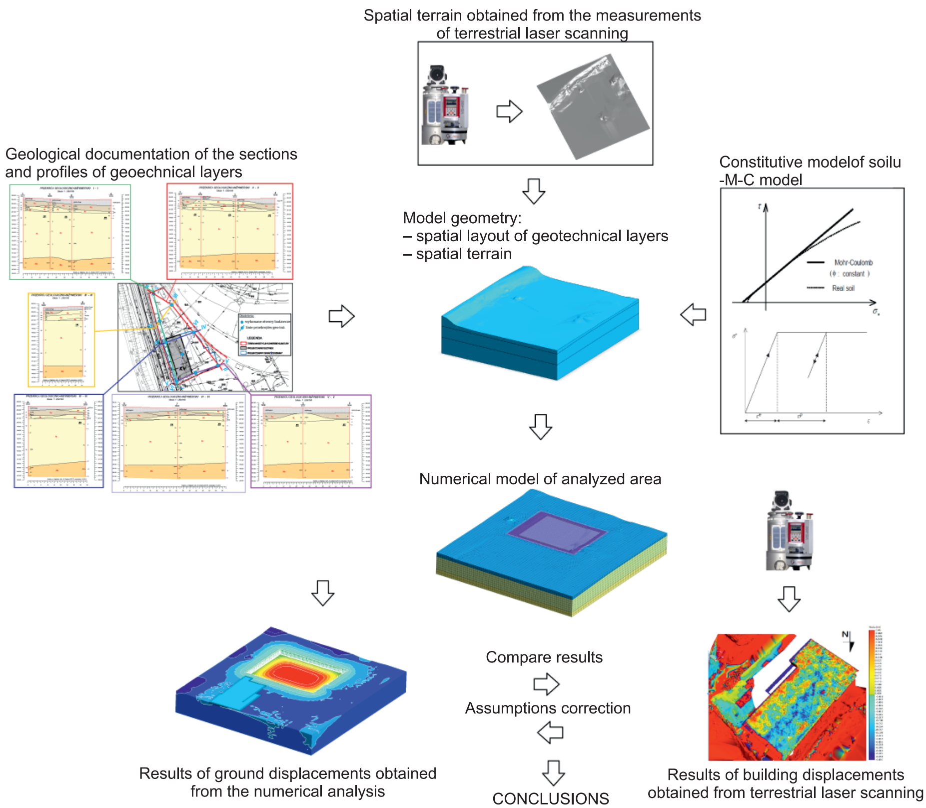

Fig. 4. Algorithm for determination of the impact the execution deep excavation on settlement neighboring building

Source: SZWARKOWSKI (2017).

Results and discussion

The impact of high building “Mogilska Tower” in Krakow was determined on the basis of numerical analysis of the subsoil, made of deep excavation in the neighbor of the existing buildings. The numerical model determined areas corresponding to the zone of direct impact of building settlements S_{I}, and to change the vertical displacements in the area S_{II} of secondary impact on building development. The analysis took into account total loads of building model in fundation level of excavation. Figure 5 and Figure 6 shows the vertical displacements obtained in step IX with marked zones of influence of S_{I} and S_{II}. Displacements determined using the simplified method given in the specification ITB (KOTLICKI, WYSOKIŃSKI 2002). Vertical displacements determined for 18 measuring points spaced every 4 m (Fig. 5).

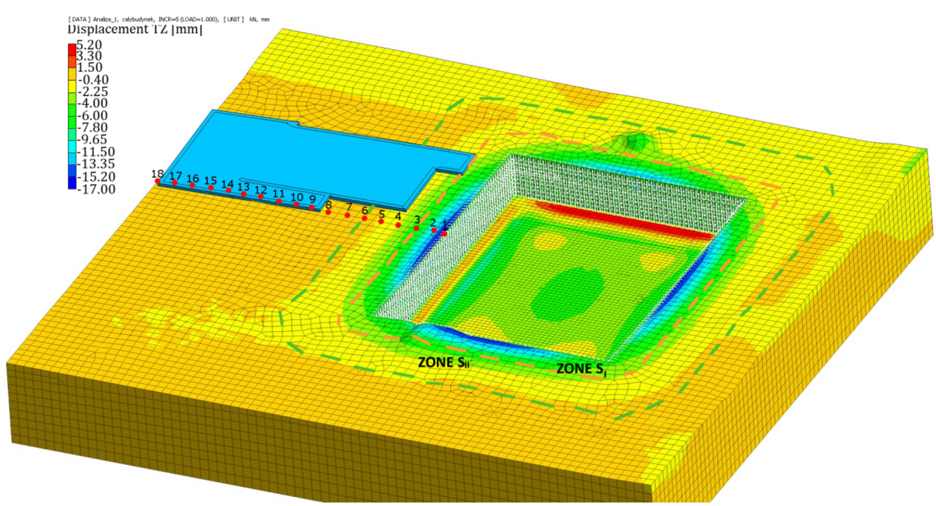

Fig. 5. Vertical displacements in the vicinity of the existing building for stage IX of numerical analysis
Source: SZWARKOWSKI (2017).

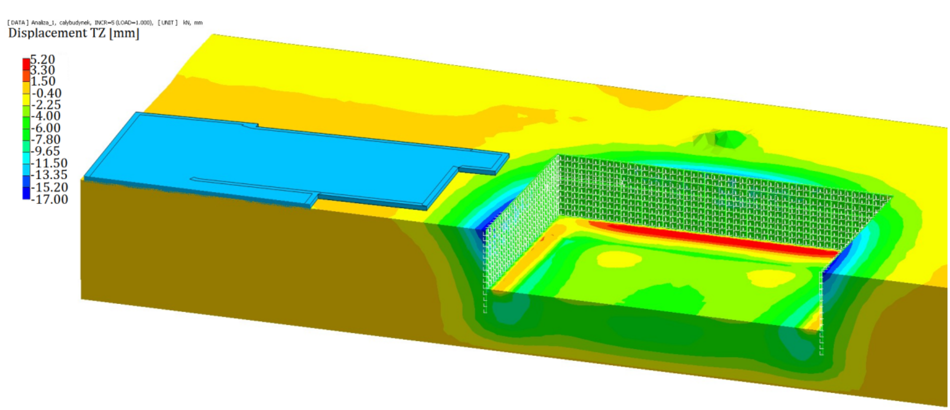

Fig. 6. Vertical displacements in the vicinity of the existing building in deep excavation section; stage IX numerical analysis
Source: SZWARKOWSKI (2017).

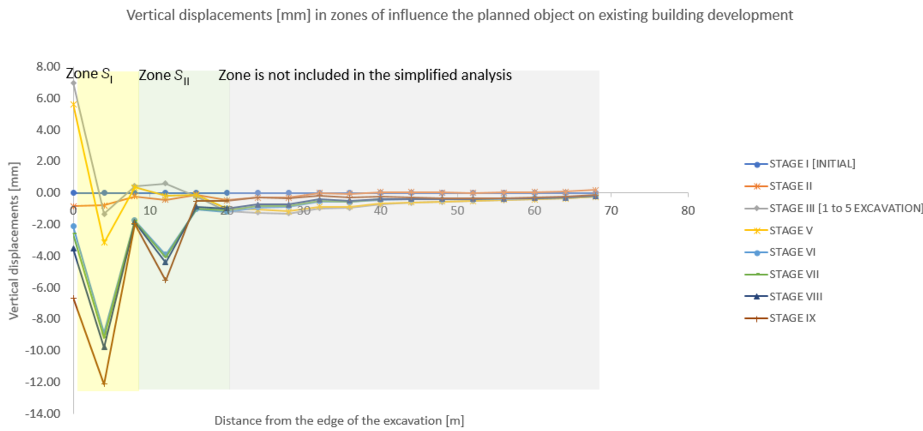

Fig. 7. Vertical displacements in zones of influence the planned object on existing building development
Source: SZWARKOWSKI (2017).

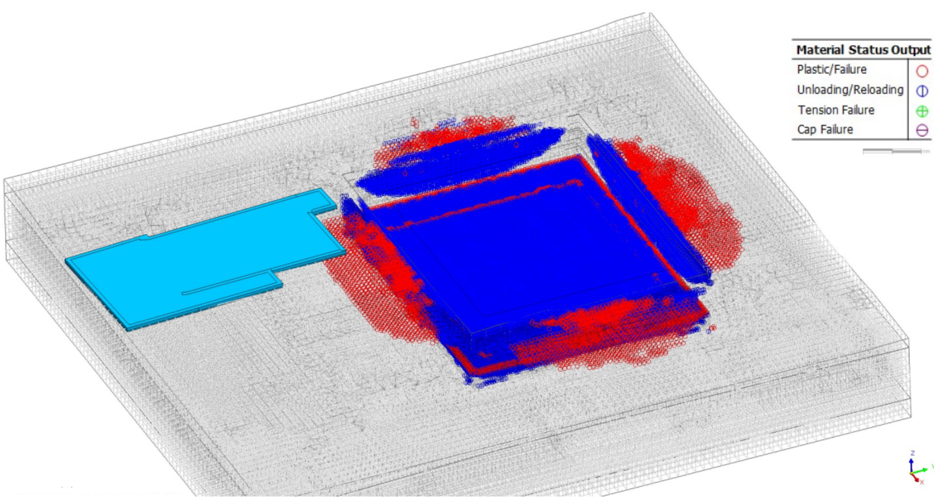

Fig. 8. Plasticity zones of ground in the vicinity of deep excavation
Source: SZWARKOWSKI (2017).

Displacement obtained for each affected zones of high building on neighboring buildings, for the last numerical analysis (stage IX), are equal: zone S_{I} direct impact of deep excavation for building S_{I} = 12 mm, zone S_{II} is equal to almost 6 mm. The largest displacements are located at distance no greater than 4 m from the edge of excavation. Beginning edge of the building is located 8 m from the edge excavation. It corresponds to the vertical displacements of the order of 4–6 mm. For the building portion, it located in the zone of vertical deformation S_{II} and not exceed 3 mm. The remaining part of the building is sited on area where not required simplified analysis. The maximum displacement does not exceed 1 mm. Figure 8 shows a plastic deformation area of ground in the vicinity of deep excavation.

Figure 8 shows regions exceeding the maximum soil shear strength give rise the formation of zones plasticity of ground, according to Mohr-Coulomb model with linear plasticity condition. Maximum effects of the impact of the deep excavation loaded with forces of the planned building on existing building development shows in Figure 8.

Conslusions

The values obtained for the maximum deformation numerical model of the subgrade subjected to the influence of a deep excavation loaded high building, showed that the vertical displacements do not exceed the limit specified in the specification ITB and standard PN-81/B-03020. Displacement values do not exceed the limit values 8cm. The deep excavation with a planned investment in the form of a 15-storeys high building "Mogilska Tower" will not adversely affect the work of construction of the existing building. Measurement conducted using terrestrial laser scanning and geodesic measurements showed displacements of the building equal 3 mm. In article summarizes the results of soils deformation only due execution of deep excavation. The obtained data have been developed for the typical model of the soil based on the Mohr-Coulomb hypothesis with linear plasticity condition. The proximity of the location of the object with the existing buildings would require to carry out detailed numerical calculations, taking into account the full model the plastic behavior of ground, eg. using a model Cam-Clay for layers of Miocene clays. However, this requires additional, time-consuming laboratory tests using triaxial or oedometer apparatures. This is related to a problem to increase spending on geotechnical researches and a better recognition of the subsoil. Obtained additional parameters can be used to model the soil, taking into account the full plasticity of the considered medium (eg. mentioned earlier Cam Clay model or Modified Mohr-Coulomb model). This is particularly important for modeling the behavior of plastic soils: clays, silits. As mentioned in the introduction of article, the better recognition and numerical analysis with the use of numerical modeling based on the method of BIM enables probably reduce the negative effects, which may occur during implementation of the investment. They can have an impact on the increase in investment costs. BIM technology in geotechnical engineering, use of complex data from field studies, laboratory and numerical modeling of the planned investments, allows more accurate way to predict the behavior of the planned investments and reduce costs.

References

BARAZZETTI L., BANFI F., BRUMANA R., GUSMEROLI G., PREVITALI M., SCHIANTARELLI G. 2015. *Cloud-to-BIM-to-FEM: Structural simulation with accurate historic BIM from laser scans.* Simulation Modelling Practice and Theory, 57: 71–87.

Value of BIM in North America. Multi-Year trend Analysis and User Rating. 2012. SmartMarket Report. McGraw-Hill Construction. Online: http://www.bimformasonry.org/pdf/the-business-value-of-bim-in-north-america.pdf (access:open source)

CAŁA M., FLISIAK J. 2000. *Analiza stateczności skarp i zboczy w świetle obliczeń analitycznych i numerycznych*. XXIII Zimowa Szkoła Mechaniki Górotworu, Bukowina Tatrzańska.

DI GIACOMO E. 2015. *BIM, trends from all around the world*. European BIM Summit, February 13th, Barcelona.

EN 1991-1-4:2008. *Eurocode 1: Actions on structures-Part 1–4: General actions-Wind actions*.

GRIFFITHS D.V., LANE P.A. 1999. *Slope stability analysis by finite elements*. Geotechnique, 49(3): 387-403.

Industrial Strategy: government and industry in partnership. 2012. Building Information Modeling, HM Government, London.

KIVINIEMI A. 2010. *Proprietary vs open BIM-demand public project*. SCRI BIM Forum, School of the Built Environment.

KESSLER H., WOOD B., MORI G., GAKIS A., MCARDLE G., DABSON O., FITZGERALD R., DEARDEN R. 2015. *Building Information Modeling (BIM) – A Route for Geological Models to Have Real World Impact.* AER/AGS Special Report 101, p. 13-18.

KOTLICKI W., WYSOKIŃSKI L. 2002. *Ochrona zabudowy w sąsiedztwie głębokich wykopów*. Instrukcje, Wytyczne, Poradniki, 376, ITB, Warszawa.

LENDUSZKO P. 2014. *Dokumentacja geologiczno-inżynierska dla projektowanej inwestycji: budowa budynku mieszkalnego wielorodzinnego z usługami w parterze wraz z infrastrukturą techniczną i garażem podziemnym oraz zagospodarowaniem terenu w zakresie kubatury zlokalizowanej na działce nr 657/31 obr. 4 Śródmieście w rejonie ul. Mogilskiej w Krakowie*. Firma Usług Projektowych Paweł Lenduszko, Kraków.

MORIN G., HASSALL S., CHANLER R. 2014. *Case study – The real life benefits of Geotechnical Information Modelling*. Information Technology in Geo-Engineering, Durham, p. 95–102.

PAWŁOSKI A.Z., CAŁA I. 2013. *Budynki wysokie*. Oficyna Wydawnictwa Politechniki Warszawskiej, Warszawa.

PILECKA E., SZWARKOWSKI D. 2015. *Wykorzystanie skanera laserowego RIEGL VZ-400 do badania deformacji na terenach górniczych GZW.* Budownictwo Górnicze i Tunelowe, 4.

Building Information Modeling. Ekspertyza dotycząca możliwości wdrożenia metodyki BIM w Polce. 2016. Polish Ministry of Infrastructure and Construction, KPMG Advisory sp. z o.o., sp.k., Warszawa.

PN-81/B-03020. 1985. *Grunty budowlane. Posadowienie bezpośrednie budowli. Obliczenia statyczne i projektowanie.* ITB, Warszawa.

SZWARKOWSKI D., ZIĘBA J. 2016. *Monitoring osiadań budynków w sąsiedztwie głębokiego wykopu budynku „Mogilska Tower" w Krakowie przy zastosowaniu naziemnego skaningu laserowego Riegl VZ-400*. Episteme, Kraków, p. 149–160.

SZWARKOWSKI D. 2017. *Wpływ wykonania głębokiego wykopu pod budynek wysoki Mogilska Tower w Krakowie na istniejącą zabudowę w ujęciu modelu przestrzennego opartego na metodzie elementów skończonych.* Współczesne budownictwo w badaniach młodych naukowców, Gdańsk.

SZWARKOWSKI D., ZIĘBA J. 2017. *Slope stability analysis of an open-pit mine as a prospective S-7 and S-52 road intersection.* Transaction 11/2017. Cracow.

TOMALA A. 2016. *BIM. Innowacyjna technologia w budownictwie. Podstawy, standardy, narzędzia*. PWB MEDIA, Kraków.

Semaco Invest Group. Mogilska Tower. www.semaco-ig.pl/inwestycje/mogilska-tower/.

ZHANG J., WU CH., WANG L., MAO X., WU Y. 2016. *The Work Flow and Operational Model for Geotechnical Investigation Based on BIM*. IEEE Access. Digital Object Identifier 10.1109/ACCESS.2016.2606158.

ŻURAWSKI J.A, GACZEK M. 2010. *Obciążenie wiatrem budynków w ujęciu normy PN-EN 1991-1-4:2008.* Inżynieria i Budownictwo, 9: 494–501.

Guide for Autors

Introduction

Technical Sciences is a peer-reviewed research Journal published in English by the Publishing House of the University of Warmia and Mazury in Olsztyn (Poland). Journal is published continually since 1998. Until 2010 Journal was published as a yearbook, in 2011 and 2012 it was published semiyearly. From 2013, the Journal is published quarterly in the spring, summer, fall, and winter.

The Journal covers basic and applied researches in the field of engineering and the physical sciences that represent advances in understanding or modeling of the performance of technical and/or biological systems. The Journal covers most branches of engineering science including biosystems engineering, civil engineering, environmental engineering, food engineering, geodesy and cartography, information technology, mechanical engineering, materials science, production engineering etc.

Papers may report the results of experiments, theoretical analyses, design of machines and mechanization systems, processes or processing methods, new materials, new measurements methods or new ideas in information technology.

The submitted manuscripts should have clear science content in methodology, results and discussion. Appropriate scientific and statistically sound experimental designs must be included in methodology and statistics must be employed in analyzing data to discuss the impact of test variables. Moreover there should be clear evidence provided on how the given results advance the area of engineering science. Mere confirmation of existing published data is not acceptable. Manuscripts should present results of completed works.

There are three types of papers: a) research papers (full length articles); b) short communications; c) review papers.

The Journal is published in the printed and electronic version. The electronic version is published on the website ahead of printed version of Technical Sciences.

Technical Sciences does not charge submission or page fees.

Types of paper

The following articles are accepted for publication:

Reviews

Reviews should present a focused aspect on a topic of current interest in the area of biosystems engineering, civil engineering, environmental engineering, food engineering, geodesy and cartography, information technology, mechanical engineering, materials science, production engineering etc. They should include all major findings and bring together reports from a number of sources. These critical reviews should draw out comparisons and conflicts between work, and provide an overview of the 'state of the art'. They should give objective assessments of the topic by citing relevant published work, and not merely present the opinions of individual authors or summarize only work carried out by the authors or by those with whom the authors agree. Undue speculations should also be avoided. Reviews generally should not exceed 6,000 words.

Research Papers

Research Papers are reports of complete, scientifically sound, original research which contributes new knowledge to its field. Papers should not exceed 5,000 words, including figures and tables.

Short Communications

Short Communications are research papers constituting a concise description of a limited investigation. They should be completely documented, both by reference list, and description of the experimental procedures. Short Communications should not occupy more than 2,000 words, including figures and tables.

Letters to the Editor

Letters to the Editor should concern with issues raised by articles recently published in scientific journals or by recent developments in the engineering area.

Contact details for submission

The paper should be sent to the Editorial Office, as a Microsoft Word file, by e-mail: techsci@uwm.edu.pl

Referees

Author/authors should suggest, the names, addresses and e-mail addresses of at least three potential referees. The editor retains the sole right to decide whether or not the suggested reviewers are used.

Submission declaration

After final acceptance of the manuscript, the corresponding author should send to the Editorial Office the author's declaration. Submission of an article implies that the work has not been published previously (except in the form of an abstract or as part of a published lecture or academic thesis or as an electronic preprint), that it is not under consideration for publication elsewhere, that publication is approved by all authors and tacitly or explicitly by the responsible authorities where the work was carried out, and that, if accepted, it will not be published elsewhere in the same form, in English or in any other language.

To prevent cases of ghostwriting and guest authorship, the author/authors of manuscripts is/are obliged to: (i) disclose the input of each author to the text (specifying their affiliations and contributions, i.e. who is the author of the concept, assumptions, methods, protocol, etc. used during the preparation of the text); (ii) disclose information about the funding sources for the article, the contribution of research institutions, associations and other entities.

Language

Authors should prepare the full manuscript i.e. title, abstract and the main text in English (American or British usage is accepted). Polish version of the manuscript is not required.

The file type

Text should be prepared in a word processor and saved in doc or docx file (MS Office).

Article structure

Suggested structure of the manuscript is as follows:

Title
Authors and affiliations
Corresponding author
Abstract
Keywords
Introduction
Material and Methods
Results and Discussion
Conclusions

Acknowledgements (*optional*)
References
Tables
Figures

Subdivision – numbered sections

Text should be organized into clearly defined and numbered sections and subsections (optionally). Sections and subsections should be numbered as 1. 2. 3. then 1.1 1.2 1.3 (then 1.1.1, 1.1.2, ...). The abstract should not be included in numbering section. A brief heading may be given to any subsection. Each heading should appear on its own separate line. A single line should separate paragraphs. Indentation should be used in each paragraph.

Font guidelines are as follows:
– Title: 14 pt. Times New Roman, bold, centered, with caps
– Author names and affiliations:12 pt. Times New Roman, bold, centered, italic, two blank line above
– Abstract: 10 pt. Times New Roman, full justified, one and a half space. Abstract should begin with the word Abstract immediately following the title block with one blank line in between. The word Abstract: 10 pt. Times New Roman, centered, indentation should be used
– Section Headings: Not numbered, 12 pt. Times New Roman, bold, centered; one blank line above
– Section Sub-headings: Numbered, 12 pt. Times New Roman, bold, italic, centered; one blank line above
– Regular text: 12 pt. Times New Roman, one and a half space,full justified, indentation should be used in each paragraph

Title page information

The following information should be placed at the first page:

Title

Concise and informative. If possible, authors should not use abbreviations and formulae.

Authors and affiliations

Author/authors' names should be presented below the title. The authors' affiliation addresses (department or college; university or company; city, state and zip code, country) should be placed below the names. Authors with the same affiliation must be grouped together on the same line with affiliation information following in a single block. Authors should indicate all affiliations with a lower-case superscript letter immediately after the author's name and in front of the appropriate address.

Corresponding author

It should be clearly indicated who will handle correspondence at all stages of refereeing and publication, also post-publication process. The e-mail address should be provided (footer, first page). Contact details must be kept up to date by the corresponding author.

Abstract

The abstract should have up to 100-150 words in length. A concise abstract is required. The abstract should state briefly the aim of the research, the principal results and major conclusions. Abstract must be able to stand alone. Only abbreviations firmly established in the field may be eligible. Non-standard or uncommon abbreviations should be avoided, but if essential they must be defined at their first mention in the abstract itself.

Keywords

Immediately after the abstract, author/authors should provide a maximum of 6 keywords avoiding general, plural terms and multiple concepts (avoid, for example, 'and', 'of'). Author/authors should be sparing with abbreviations: only abbreviations firmly established in the field may be eligible.

Abbreviations

Author/authors should define abbreviations that are not standard in this field. Abbreviations must be defined at their first mention there. Author/authors should ensure consistency of abbreviations throughout the article.

Units

All units used in the paper should be consistent with the SI system of measurement. If other units are mentioned, author/authors should give their equivalent in SI.

Introduction

Literature sources should be appropriately selected and cited. A literature review should discuss published information in a particular subject area. Introduction should identify, describe and analyze related research that has already been done and summarize the state of art in the topic area. Author/authors should state clearly the objectives of the work and provide an adequate background.

Material and Methods

Author/authors should provide sufficient details to allow the work to be reproduced by other researchers. Methods already published should be indicated by a reference. A theory should extend, not repeat, the background to the article already dealt within the Introduction and lay the foundation for further work. Calculations should represent a practical development from a theoretical basis.

Results and Discussion

Results should be clear and concise. Discussion should explore the significance of the results of the work, not repeat them. A combined Results and Discussion section is often appropriate.

Conclusions

The main conclusions of the study may be presented in a Conclusions section, which may stand alone or form a subsection of a Results and Discussion section.

Acknowledgements

Author/authors should include acknowledgements in a separate section at the end of the manuscript before the references. Author/authors should not include them on the title page, as a footnote to the title or otherwise. Individuals who provided help during the research study should be listed in this section.

Artwork
General points

– Make sure you use uniform lettering and sizing of your original artwork
– Embed the used fonts if the application provides that option

– Aim to use the following fonts in your illustrations: Arial, Courier, Times New Roman, Symbol
– Number equations, tables and figures according to their sequence in the text
– Size the illustrations close to the desired dimensions of the printed version

Formats

If your electronic artwork is created in a Microsoft Office application (Word, PowerPoint, Excel) then please supply 'as is' in the native document format

Regardless of the application used other than Microsoft Office, when your electronic artwork is finalized, please 'Save as' or convert the images to one of the following formats (note the resolution requirements given below):

EPS (or PDF): Vector drawings, embed all used fonts

JPEG: Color or grayscale photographs (halftones), keep to a minimum of 300 dpi

JPEG: Bitmapped (pure black & white pixels) line drawings, keep to a minimum of 1000 dpi or combinations bitmapped line/half-tone (color or grayscale), keep to a minimum of 500 dpi

Please **do not**:
– Supply files that are optimized for screen use (e.g., GIF, BMP, PICT, WPG); these typically have a low number of pixels and limited set of colors
– Supply files that are too low in resolution
– Submit graphics that are disproportionately large for the content

Color artwork

Author/authors should make sure that artwork files are in an acceptable format (JPEG, EPS PDF, or MS Office files) and with the correct resolution. If, together with manuscript, author/authors submit color figures then Technical Sciences will ensure that these figures will appear in color on the web as well as in the printed version at no additional charge.

Tables, figures, and equations

Tables, figures, and equations/formulae should be identified and numbered consecutively in accordance with their appearance in the text.

Equations/mathematical and physical formulae should be presented in the main text, while tables and figures should be presented at the end of file (after References section). Mathematical and physical formulae should be presented in the MS Word formula editor.

All types of figures can be black/white or color. Author/authors should ensure that each figure is numbered and has a caption. A caption should be placed below the figure. Figure must be able to stand alone (explanation of all symbols and abbreviations used in figure is required). Units must be always included. It is noted that figure and table numbering should be independent.

Tables should be numbered consecutively in accordance with their appearance in the text. Table caption should be placed above the table. Footnotes to tables should be placed below the table body and indicated with superscript lowercase letters. Vertical rules should be avoided. Author/authors should ensure that the data presented in tables do not duplicate results described in figures, diagrams, schemes, etc. Table must be able to stand alone (explanation of all symbols and abbreviations used in table is required). Units must be always included. As above, figure and table numbering should be independent.

References

References: All publications cited in the text should be presented in a list of references following the text of the manuscript. The manuscript should be carefully checked to ensure that the spelling of authors' names and dates of publications are exactly the same in the text as in the reference list. Authors should ensure that each reference cited in the text is also present in the reference list (and vice versa).

Citations may be made directly (or parenthetically). All citations in the text should refer to:

1. Single author

The author's name (without initials, with caps, unless there is ambiguity) and the year of publication should appear in the text

2. Two authors

Both authors' names (without initials, with caps) and the year of publication should appear in the text

3. Three or more authors

First author's name followed by et al. and the year of publication should appear in the text

Groups of references should be listed first alphabetically, then chronologically.

Examples:

"... have been reported recently (ALLAN, 1996a, 1996b, 1999; ALLAN and JONES, 1995). KRAMER et al. (2000) have recently shown..."

The list of references should be arranged alphabetically by authors' names, then further sorted chronologically if necessary. More than once reference from the same author(s) in the same year must be identified by the letters "a", "b", "c" etc., placed after the year of publication.

References should be given in the following form:

KUMBHAR B.K., AGARVAL R.S., DAS K. 1981. *Thermal properties of fresh and frozen fish*. International Journal of Refrigeration, 4(3), 143–146.

MACHADO M.F., OLIVEIRA F.A.R., GEKAS V. 1997. *Modelling water uptake and soluble solids losses by puffed breakfast cereal immersed in water or milk*. In Proceedings of the Seventh International Congress on Engineering and Food, Brighton, UK.

NETER J., KUTNER M.H., NACHTSCHEIM C.J., WASSERMAN W. 1966. *Applied linear statistical models* (4th ed., pp. 1289–1293). Irwin, Chicago.

THOMSON F.M. 1984. *Storage of particulate solids*. In M. E. Fayed, L. Otten (Eds.), Handbook of Powder Science and Technology (pp. 365–463). Van Nostrand Reinhold, New York.

Citation of a reference as 'in press' implies that the item has been accepted for publication.

Note that the full names of Journals should appear in reference list.

Submission checklist

The following list will be useful during the final checking of an article prior to the submission. Before sending the manuscript to the Journal for review, author/authors should ensure that the following items are present:

– Text is prepared with a word processor and saved in DOC or DOCX file (MS Office). One author has been designated as the corresponding author with contact details: e-mail address

– Manuscript has been 'spell-checked' and 'grammar-checked'

– References are in the correct format for this Journal

– All references mentioned in the Reference list are cited in the text, and vice versa

– Author/authors does/do not supply files that are too low in resolution

– Author/authors does/do not submit graphics that are disproportionately large for the content